Heat Flow, Uplift and Maturity Model of the Jan Mayen Microcontinent during Breakup and Rifting

Project Summary Report

Karthik Iyer (GMS)
Anett Blischke (ÍSOR)
John M. Millett (VPBR)
Daniel W. Schmid (GMS)

ÍSOR ICELAND GEOSURVEY

GEOMODELLING SOLUTIONS

Volcanic Basin Petroleum Research

Heat Flow, Uplift and Maturity Model of the Jan Mayen Microcontinent during Breakup and Rifting

Project Summary Report

Karthik Iyer (GMS)
Anett Blischke (ÍSOR)
John M. Millett (VPBR)
Daniel W. Schmid (GMS)

Prepared for Orkustofnun (OS)

Note

This report layout is for duplex printing
and occasional white pages are intentional.

June 2018

This report is the result of the
Jan Mayen study
commissioned by ÍSOR

Authors:
Karthik Iyer, Anett Blischke, John M. Millett & Daniel W. Schmid

ÍSOR ICELAND GEOSURVEY

Report no.	Date	Distribution
ÍSOR-2018/036	July 2018	☐ Open ☒ Closed for 2 years

Report name / Main and subheadings	Number of copies
Heat Flow, Uplift and Maturity Model of the Jan Mayen Microcontinent during Breakup and Rifting. Project Summary Report.	3
	Number of pages
	81 + 2 Appendices

Authors	Project manager
Karthik Iyer, Anett Blischke, John M. Millett & Daniel W. Schmid	Anett Blischke

Classification of report	Project no.
Confidential for a period of 2 years	16-0211

Prepared for

Prepared for Orkustofnun (OS)

Cooperators

Geomodelling Solutions GmbH & Volcanic Basin Petroleum Research AS

Abstract

The project´s main goal was to develop a heat-flow, uplift, and maturity model for the Jan Mayen microcontinent (JMMC) for the time of the Northeast Atlantic breakup and the forming of the North Atlantic igneous province (NAIP), through the separation of the microcontinent area from the East Greenland margin. This model will serve as a basic tool for future frontier basin maturity modelling and hydrocarbon system predictions for the JMMC, specifically the northern Dreki exploration area. Modelled input data and assumptions had to be considered in regards to the maximum mantle potential temperatures (Tp) of 1550 °C for this study. The thermal uplift history during breakup and rifting was reviewed in relation to evidence from reflection seismic interpretation and modelling that have revealed transient uplift events during the main phases of NAIP volcanism and the pulsing of the proto-Icelandic plume that also effects frequency and magnitude of the regions of uplift and igneous activity. Relatively similar present-day heat flow patterns are modelled, but large variations are observed in the heat flow values in the southern JMMC block of the Dreki area that result from the amount of rifting experienced. The modelled internal variation of topography of sub-regions may be largely controlled by thermal input from the ridges and not just due to regional tectonic processes and changes in sea level, which is supported by a high-resolution sequence stratigraphy mapping study as well. Hydrocarbon maturity at the northern, eastern and western edges of the northern JMMC is elevated and affected by ridge processes. Maturity levels in the southern JMMC block are affected by ridge processes at the eastern and western edges, while rifting of the SJMMC affects the entire block, raising the oil and gas windows with respect to the northern block. The models show that hydrocarbons may be best preserved in the south central area of the northern block (NJMMC) just north of the Dreki area. A full hydrocarbon maturation model could not be obtained for the JMMC region, as the project was funded for only half of its proposed work phases. Completion is strongly recommended for a valid risk assessment input parameter in regards to hydrocarbon maturity.

Key words	ISBN-number
Heat flow, Jan Mayen microcontinent, maturation, modelling, uplift, Orkustofnun, ÍSOR, Geomodelling Solutions GmbH & Volcanic Basin Petroleum Research AS	
	Project manager's signature
	[signature]
	Reviewed by
	Guðni Axelsson

Table of contents

List of tables

List of figures

1   Introduction

At present there is well-developed understanding of the tectonostratigraphic setting of the JMMC from breakup time to present (e.g. Gaina et al., 2009; 2017; Peron-Pinvidic et al., 2012a, b; Blischke and Erlendsson, 2014; Blischke et al., 2016). However, the thermal and uplift history has not been investigated in detail. Therefore, the objective of this project was to quantify the thermal maturation state of potentially prospective areas of the underexplored Jan Mayen microcontinent (JMMC) region. The JMMC has a complex history including the combined effects of uplift and subsidence processes with time constrained crustal heating and cooling related to the rift jump and dual rift system development (Blischke et al., 2016). The main goal of such a multifaceted model was to enable the generation of a frontier basin maturity model for the Jan Mayen microcontinent, specifically the northern Dreki exploration area, for the time of the Northeast Atlantic breakup through the separation of the microcontinent area from the East Greenland margin. It aims to establish a basic tool for hydrocarbon system predictions for the exploration areas within a mid-oceanic rift environment, and an important tool for future decision making of exploration activities for the North-Dreki area (Figure 1).
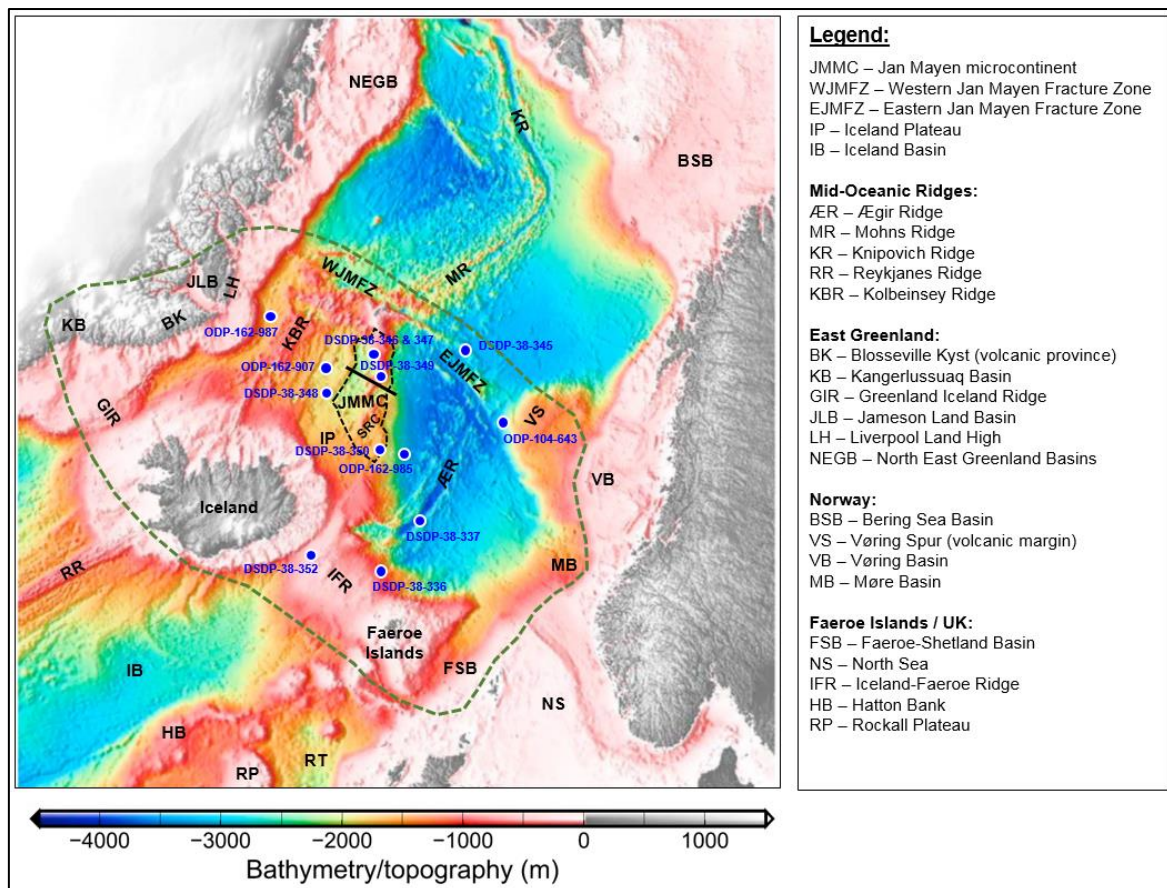
Figure 1. *Regional location map of the central NE Atlantic region based on ETOPO-2 bathymetry and topography (Smith & Sandwell 1997), and borehole location in the central East Greenland – Jan Mayen micro-continent (JMMC, dashed black line) – Norwegian shelf corridor. The area of investigation is marked with a dark green dashed line.*

The project was conducted in collaboration between:

1. **Iceland GeoSurvey,**
   which provided the tectonostratigraphic and geodynamic data input,

2. **Volcanic Petroleum Basin Research AS (VPBR),**
   which provided detailed input on heat flow estimates, processes and magmatic systems modelling, and

3. **Geomodelling Solutions GmbH (GMS),**

   Which designed, built and executed the numerical modelling of rifting, uplift, thermal history and maturation within the project.

The original project proposal to the Icelandic hydrocarbon research fund (IHCRF) included a complete exploration maturity model phase, however, only the data compilation and regional thermodynamic and uplift modelling was funded by the IHCRF in fall 2016. Therefore, this study comprises only the first 2 phases of the original project (see timeline in Table 1 and original project proposal in Appendix 1) that included:

1. **Initial maturation phase – pre-breakup (*literature study)***
   Compilation of regional data from analogue areas including central East Greenland, the Faroe Shetland basin and the Vøring basin to constrain realistic data inputs for modelling.

2. **Secondary maturation – *(funded by the IHCRF)***

   Quantification of the thermal history of the JMMC region related to the complex tectonic development from the onset of rifting at ca. 56 Ma to the present day, with a particular focus on the effects of ridge jumps. This provides integral insights into the first order thermal history of the JMMC.

Permission has been obtained to use an initial base model for the JMMC within this project that was originally developed by Geomodelling Solutions GmbH (GMS) (Schmid et al., 2017). This model was developed further during the study by combining known research results of the tectonostratigraphic framework into a spatially more complex thermal model.

In particular, a review of modelling input considerations relating to the southern extent of the JMMC addresses major questions in regards to the magmatic evolution in this area due to the interplay of different rifting and magmatic episodes on the thermal state of the JMMC crust. Information regarding the thermodynamic processes is lacking for this region, information which is essential to model detailed source rock maturation history in later projects. The study aimed to quantify the magnitudes and spatial distribution of major thermal influences as a response to the complex tectonic evolution of the JMMC and its location throughout the breakup history of the northeast Atlantic.

Table 1. *Project time table status as of March 2018.*

Year	2016		2017				2018	
Quarter	3	4	1	2	3	4	1	2
Project start meeting in Oslo		M						
PHASE 1: Model input database completed								
Skype meeting			M					
Tectonostratigraphic input JMMC		X						
Source rock data compilation			X					
Heat flow, or geothermal gradient data compilation		X	X					
Analogue area (JLB, FSB, central Norwegian Shelf) data compilation		X	X					
Project status meeting in Iceland				M				
PHASE 2: Large scale thermal model								
Data implementation and process setup final			X	X				
Model build and iterations				X	X			
Final project presentation					M			
Submit final project report							X	

The following project summary report introduces the study area and the central Northeast Atlantic geodynamic development in connection with mid-oceanic ridge developments and the role of the JMMC and the ridge jumps across the Iceland Plateau area. This is followed by the compilation and justification of heat flow, uplift, and maturation model input data and model setup parameters, followed by a detailed documentation of the model build and model run results. At the end the modelling results are discussed and necessary future project steps are listed and recommended.

2   The Jan Mayen microcontinent domain

The JMMC is a distinct structural entity located between the volcanic complex of the Jan Mayen Island (Svellingen & Pedersen, 2003), which is part of the Jan Mayen Fracture Zone system, and the NE coastal shelf area of Iceland, between the Norway basin to the East, and the Iceland Plateau to the south-southwest (Figure 2). Based on numerous studies since the 1970´s (e.g. Vogt et al., 1970; Talwani & Eldholm, 1977; Gunnarsson et al., 1989; Johansen, 1992; Doré et al., 1999; Lundin and Doré, 2002; Scott et al., 2005; Gaina et al., 2009; Blischke et al., 2011, 2016; Gernigon et al., 2015; Peron-Pinvidic et al., 2012a, b; Gernigon et al., 2012) the JMMC has been interpreted as a fragment of continental origin. The boundaries of the micro-continent itself have been defined based on magnetic, gravity, refraction and reflection seismic data (Talwani & Eldholm 1977; Johansen, 1992; Gaina et al., 2009; Peron-Pinvidic et al., 2012a). The micro-continent is interpreted as a ~100 km wide crustal fragment of the East Greenland central coast-line (Gaina et al., 2009), with stratigraphic and crustal structures corresponding to the conjugate central East Greenland coast. The southern extent of the micro-continent is underexplored but has recently been described as a rift transition zone. This transfer zone comprising of several rift segments, also referred to as the Iceland Plateau rift segments I – IV in Blischke et al. (2016), formed from Mid-Eocene though Early Oligocene (Blischke et al., 2018), thus forming a volcanic margin from the Norway basin across the Iceland plateau to the south-western margin of the JMMC (Blischke et al., 2016; 2018) (Figures 1–3).

The JMMC contains several major unconformities and structures, such as listric faults, rotated fault blocks, and small-scale reverse faults. These structures appear to be related to the complex opening processes on either side of the micro-continent, which formed the volcanic passive margins of the JMMC. The opening process comprises several major events, which started with the opening of the Ægir Ridge, east of the micro-continent, during the first primary phase of extensional processes (rift to drift) affecting the JMMC during Early Eocene (Ypresian 55.9–47.9 Ma). This process was not gradual and coincided with major volcanic activity forming a distinct volcanic margin (Blischke et al., 2016) with igneous complexes and sill intrusions that are recorded in particular along the eastern flank and close to the ridge crests, primarily intruded into Eocene to Early Oligocene sediment strata (Peron-Pinvidic et al., 2012a; Blischke and Erlendsson, 2014; Blischke et al., 2018).

The second main phase is described as a rifting transition and uplift along the south-eastern and southern flanks of the micro-continent from the Mid-Eocene to Early Miocene Oligocene. However, very little is known on that stage of transition. The third, and final stage is associated with the formation of the Kolbeinsey Ridge system along the western flank of the micro-continent during the Early Miocene, separating the JMMC from East Greenland (Gunnarsson et al., 1989). During that stage the youngest large-scale igneous event is identified as a flat laying, opaque reflection seismic marker, the so called "F-Reflector" (Gunnarsson et al., 1989), covering an area of approximately 18400 km^2 of the "low-lands" between the micro-continent´s ridges, along the western and southern flank of the Jan Mayen Ridges, and within the Jan Mayen Trough area, west of the Jan Mayen Southern Ridge Complex (SRC, Figure 1).
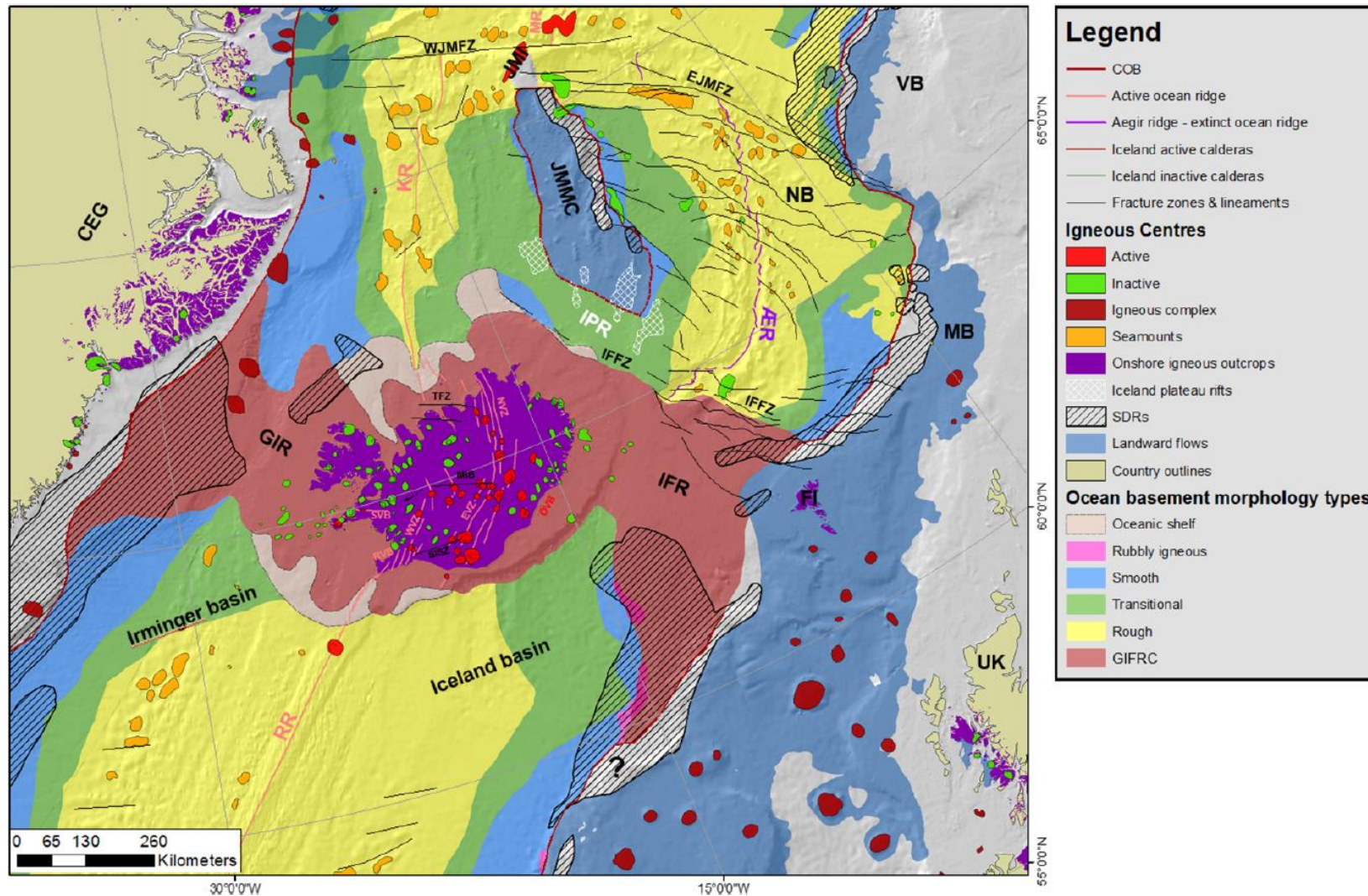
Figure 2. *Regional setting map showing the main volcanic facies elements (á Horni et al., 2017), major structural lineaments (Funck et al., 2014), the Iceland Plateau Rift system (Blischke et al. 2016), ocean basin morphology type map (Funck et al. 2014; Gaina et al., 2017; Geissler et al., 2016) and bathymetry data (Hopper et al., 2014) of the GIFRC, surrounding oceanic basins and continental margins. This compilation illustrates the complex segmentation of the central NE Atlantic region with its active and extinct volcanic systems (e.g. SDRs, igneous complexes and rift systems, and major boundary structural elements, such as fracture zones), for abbreviations see List of abbreviations (Einarsson, 2008; Gaina et al., 2009; Gernigon et al., 2015; Blischke et al., 2016).*
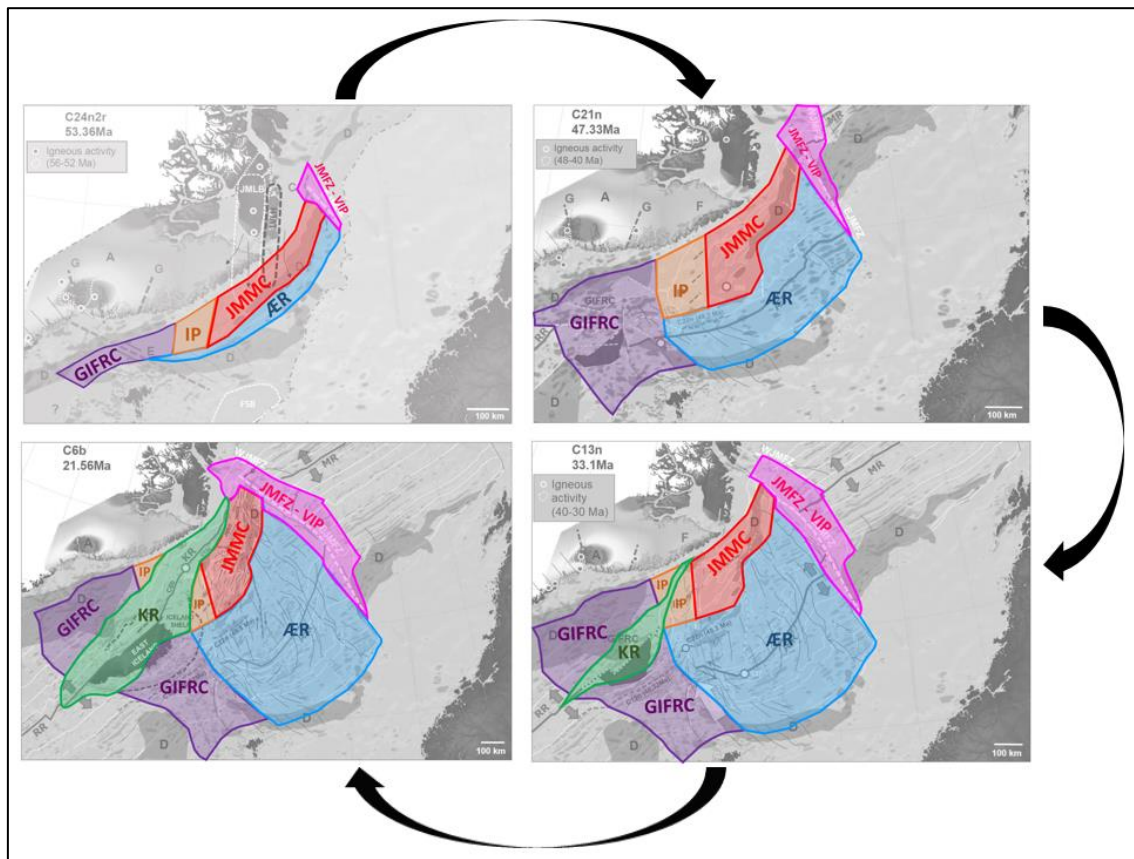
Figure 3. *Evolution of the JMMC and nearby regions and simplified structural elements for the heat flow – maturity model, modified from Blischke et al. (2016).*

However, the actual age and composition of those igneous formations are not known, as geophysical records can only give indirect evidence of the igneous activity. The igneous formations were most likely emplaced during the period of the JMMC - Mid-East-Greenland breakup volcanism (~C7-C6) and the establishment of the Kolbeinsey Ridge system.

The evolution of the micro-continent appears to be controlled by deep structures, which are interpreted to be linked to the development of the Greenland-Iceland-Faroe Islands ridge complex (GIFRC), a part of the North Atlantic igneous province (NAIP) (Hopper et al., 2014; Hjartarson et al., 2017). The micro-continent forms a complex WNW-ESE striking ridge structure, including the Greenland-Iceland Ridge (GIR), the entire Iceland shelf, and the Iceland-Faeroe Ridge (IFR), which is inferred to result from increased magmatic activity associated with the Iceland plume (Morgan, 1971; Holbrook & Keleman, 1993; Lawver & Müller, 1994; Torsvik et al., 2001) (Figure 3).

The main rifting phases from the initial breakup situation at around 53 Ma ago can be described as follows (Figure 3):

(1) <u>Initial breakup phase ca. 53-47 Ma:</u> During the uppermost Palaeocene to Middle Eocene, extensive magmatism affected the JMMC, forming escarpments, sills, and larger-scale intrusive sections, especially along the East Ridge Flank of the JMMC (Gunnarsson et al., 1989). Several stages of activity along the SE edges of the micro-continent during the separation from the Norwegian margin can be described, including observations in two

key wells (DSDP 38-348 & 350; Figure 1) that reached through the entire overlying sediment cover into the basalt section. Well DSDP 38-350 reaches through the Tertiary sediment section into an Eocene basalt sill intrusion.

(2) <u>Rift transition phase ca. 47-33 Ma:</u> The geological period from the Late Eocene to Early Oligocene is also associated with intensive magmatic activity along the flanks of the JMMC, with numerous sills, larger scale intrusive sections, and probably large-scale lava flows (F-Marker). The origin of the large-scale lava flows is unknown. One hypothesis postulates that these lava flows originally came from an elevated area to the south of the JMMC, as a result of a major volcanic eruption, or a series of eruptions that covered large stretches of the land into the low areas between the elevated ridges of the JMMC (Blischke et al., 2016). However, only indirect data exists (refraction-/reflection seismic, gravity, and magnetic data) for this hypothesis, and the observed igneous activities in the strata can only be described with no direct compositional or available age data.

(3) <u>Final breakup phase ca. 33-21 Ma:</u> Between the Early to Middle Miocene, extensive shallow intrusions are emplaced regionally along and over the western and south-western areas of the micro-continent, which occurred most likely simultaneously with the opening of the Kolbeinsey Ridge. This sub-region of the JMMC margin also includes a calibration well, DSDP 38-348, as a borehole that reached through the Neogene sediment section into the Miocene basalt cover but has not been analysed for its reported tephra layers. The majority of the offshore cores, located west of the micro-continent, include tephra layers of Miocene age. Here a connection of igneous activities in age can be observed along the easternmost edge of the Blosseville Kyst (Larsen et al., 2013).

3 Model input data, assumptions & methods

This section includes the listing and brief description of reviewed and considered input parameters and assumptions to build into the geo-chronological heat-flow, uplift, and maturation model runs.

This data review included a detailed review of available offshore boreholes along with existing geothermal and heat-flow data estimates for the Northeast Atlantic region. A simplified version of the most recent high-resolution tectonostratigraphic model and stratigraphic framework of the JMMC has been included as well (Blischke et al., 2016), see Figure 3. This includes a review of structural elements and igneous domains, crustal fabric evolution and parameters, geo-chronologic reconstruction, uplift and unconformity data, available heat flow data, formation thermal conductivity, and the geothermal gradient database for the micro-continent and surrounding areas (Hopper et al., 2014).

As the thermal effects of rifting and magmatism proximal to continental crust is of key importance to thermal evolution, a detailed review of estimates of mantle temperature in the Northeast Atlantic Igneous Province (NAIP) (Saunders et al., 2007; Hole & Millett, 2016) was undertaken. The impact of increased temperatures, where the crust becomes thinner and mantle upwelling occurs, forms a major thermal influence. Furthermore, the presence of significant temperature fluctuations inferred from transient uplift and variations in petrologically derived mantle potential temperatures (T_P) during the evolution of the NAIP

spanning ~60 Ma (Nadin et al., 1997; Parnell-Turner et al., 2014; Millett et al., 2015), were also identified (Figures 4–6). To test model sensitivity of these temperature fluctuations, a range of temperature estimates were implemented into the model setup, which are based largely on the review and compilation by Hole & Millett (2016).

The model has also been appraised by comparing the results with published studies in regards to the regions thermal and general uplift history for both margin areas (Larsen et al., 2013; 2014; Hopper et al., 2014; Japsen et al., 2014; Hartley et al., 2011; Millett et al., 2015). The thermal uplift history during breakup and rifting was reviewed in relation to pulsing of the proto-Icelandic plume (Holbrook et al., 2001; Rudge et al., 2008; Hartley et al., 2011; Parnell-Turner et al., 2014) that also effects frequency and magnitude of the regions of uplift and igneous activity. These were then compared to the geo-chronological reconstructions (Torsvik et al., 2015; Blischke et al., 2016; Gaina et al., 2017; Geissler et al., 2016), which guided the selection of the thermal model stages and segmentations to model the best case JMMC thermal model history.

Table 2. *Input datasets, model input purpose, and references.*

Year	Data type	Model input purpose	Reference
1997, 2014 & 2015	Petrologically derived mantle potential temperatures (Tp)	Mantle potential temperature ranges	Nadin et al. 1997; Parnell-Turner et al., 2014; Millett et al., 2015
2000-2003	Present day heat flow seafloor data and maps for the JMMC	Heat flow calibration, formation thermal conductivity for present day	Sundvor et al. 2000 & Rey et al., 2003.
2007 & 2016	Mantle potential temperature of the NAIP	Mantle potential temperature ranges	Saunders et al., 2007; Hole & Millett, 2016
2009, 2016	Geochronological model	Model time steps	Gaina et al., 2009 & Blischke et al., 2016
2011-2015	Conjugate margin thermal and general uplift history	Heat flow & Uplift	Jones et al., 2012; Larsen et al., 2013; 2014; Hopper et al., 2014; Japsen et al., 2014; Hartley et al., 2011; Millett et al., 2015
2013	Mantle tomography	Crustal	Rickers et al., 2013
2014	Depth to Moho & crustal type and thickness maps	Crustal	Hopper et al., 2014
2014	Heat flow map of the Northeast Atlantic	Heat flow calibration for present day; geothermal gradients	Hopper et al., 2014
2014	Structural elements map, uplift and unconformity model		Hopper et al., 2014
2015	Iceland plateau crustal thickness	Crustal	Brandsdóttir et al., 2015
2016	JMMC crustal structure	Crustal	Blischke et al., 2016
2016	Stratigraphic framework model	Model segmentation and layers	Blischke et al., 2016

3.1 Heat flow data input parameters & assumptions

Present day heat-flow of the greater JMMC area (Figure 5) does not reflect the heat-flow history of the area, which has experienced widespread volcanism during the late Palaeocene to early Eocene and a completely different aerial variation of heat-flow affecting the microcontinent. Therefore, it is important to understand the origin of the widespread pre-, syn- and post-breakup volcanism that has been influenced by both additional heat and material sourced from the proto-Icelandic thermal anomaly or plume (e.g. Saunders et al., 1997). Other hypotheses including the presence of fertile mantle derived from subduction of Iapetus oceanic crust have been used to explain e.g. the lack of a continuous tomographic thermal anomaly down to the lower mantle (Foulger & Andersen, 2005). For the purposes of this study we support a model whereby increased temperature was involved in the formation of the NAIP.

The temperature of the mantle, in general referred to as the mantle potential temperature (Putirka, 2009) that forms a first order parameter for any large scale thermal model such as the model developed within this project (Hole and Millett, 2016). Within this section we address the question:

"Do mantle potential temperature variations inferred from the NAIP have significant potential to alter the thermal history of the JMMC away from the ambient mantle temperature state?"

A range of methods exist for estimating paleo-temperatures including fluid inclusions, vitrinite reflectance (VR) and spore colouration for sediments, and petrological methods based on measurements of crystallized volcanic rocks (e.g. whole rock and mineral chemistry). A range of geophysical methods which interpret e.g. past land surface movements, residual basement depths, melt production volumes or tomography etc. also exist. Many models give different results and therefore, no 'level playing field' exists from which to base models that incorporate thermal modelling results. A combination of petrological and geophysical inference from recent publications gives insights into the possible first order temperature ranges that may have affected the JMMC continental block (Hole & Millett, 2016; Hartley et al., 2011).

Hole & Millett (2016) compiled a comprehensive database of primary magma composition and modelled mantle temperature estimates for the entire NAIP. The modelling was carried out using the PRIMELT3 software (Herzberg & Asimow, 2015), which incorporates both forward and inverse modelling to constrain a unique solution for primary magma compositions. This is achieved by computing a melt fraction that is common to both partial melts of mantle peridotite and to the primitive magmas from which the lava in question was derived.

Any study of magmatism associated with a thermal anomaly necessarily requires knowledge of mantle potential temperature (T_P) that expresses the mantle temperature projected along the solid-state adiabatic to surface pressure. Mantle T_P equates to the temperature at the base-lithosphere (thermal boundary layer) boundary condition in the JMMC model (Figure 6).

The sensitivity of temperature estimates from a range of other models was tested by Hole et al. (2015) (Figure 4), with the result that all petrological methods return hotter than ambient results for the NAIP. The conclusion is that the NAIP was produced by dominantly hotter than ambient (ca. 1350 °C) mantle temperatures in between 1450 and 1550 °C.

Temperatures fluctuate geographically and temporally throughout the NAIP province (Hole et al., 2015). Age dating of Palaeogene NAIP magmas remains controversial at the 1-2 Ma scale due to disagreements between isotopic and bio-stratigraphic determinations (Passey & Jolley, 2009). It has previously been proposed that the proto-Icelandic plume cooled temporally from ca. 60 Ma to present by ca. 50-150 °C (Herzberg & Gazel, 2009), which appears a broadly robust estimate, albeit with significant scatter from the available data (Hole & Millett, 2016).
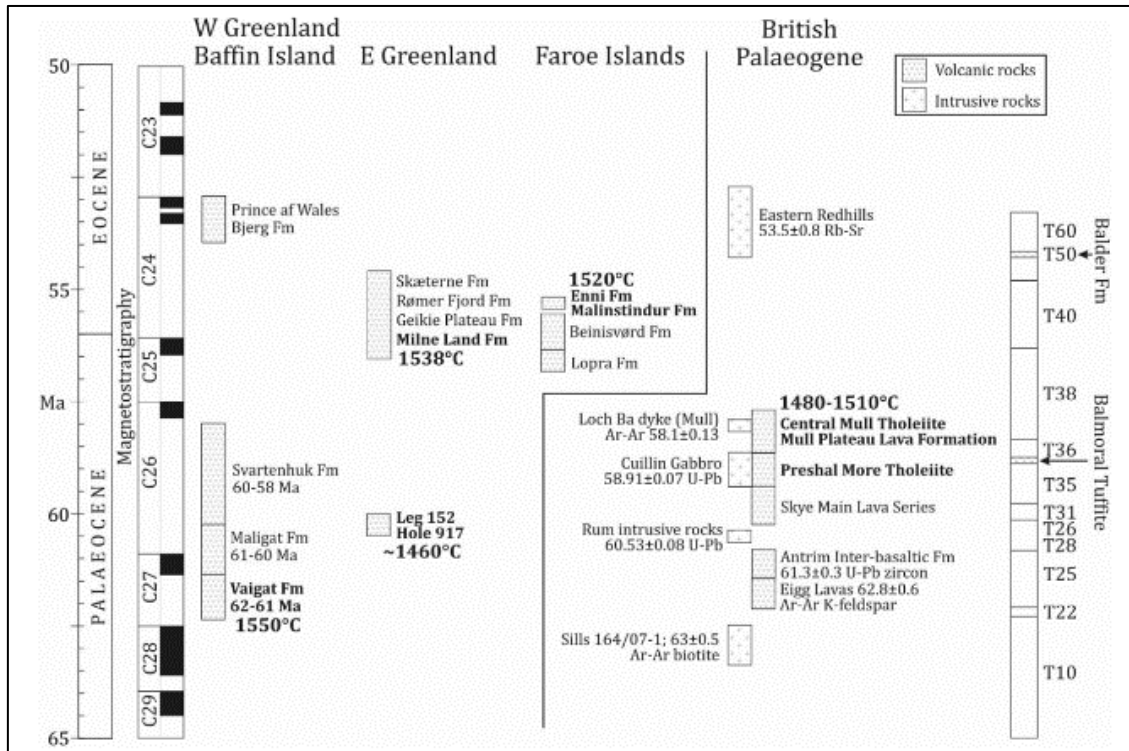
Figure 4. *Compilation of calculated mantle potential temperatures and ages from across the NAIP (Hole & Millett, 2016).*

For the Palaeogene aged lavas, a mantle T_P value of around 1500-1550 °C ca. 150-200 °C above ambient, is supported by all the studied areas within error. It is important to note that modelled temperatures can only be derived from primary magmas that crystallize only olivine during ascent through the lithosphere and crust. The majority of magmas that reach the surface and shallow crust undergo additional modification (crustal contamination, cpx crystallization, mixing etc.) and therefore cannot be modelled as primary magmas. The results for the province therefore give an indication of the ranges of temperatures but never the whole story. A temperature of 1550 °C will therefore be used as the maximum T_P for this study, with an 'ambient' plume temperature of ca. 1400 °C (Figure 6).
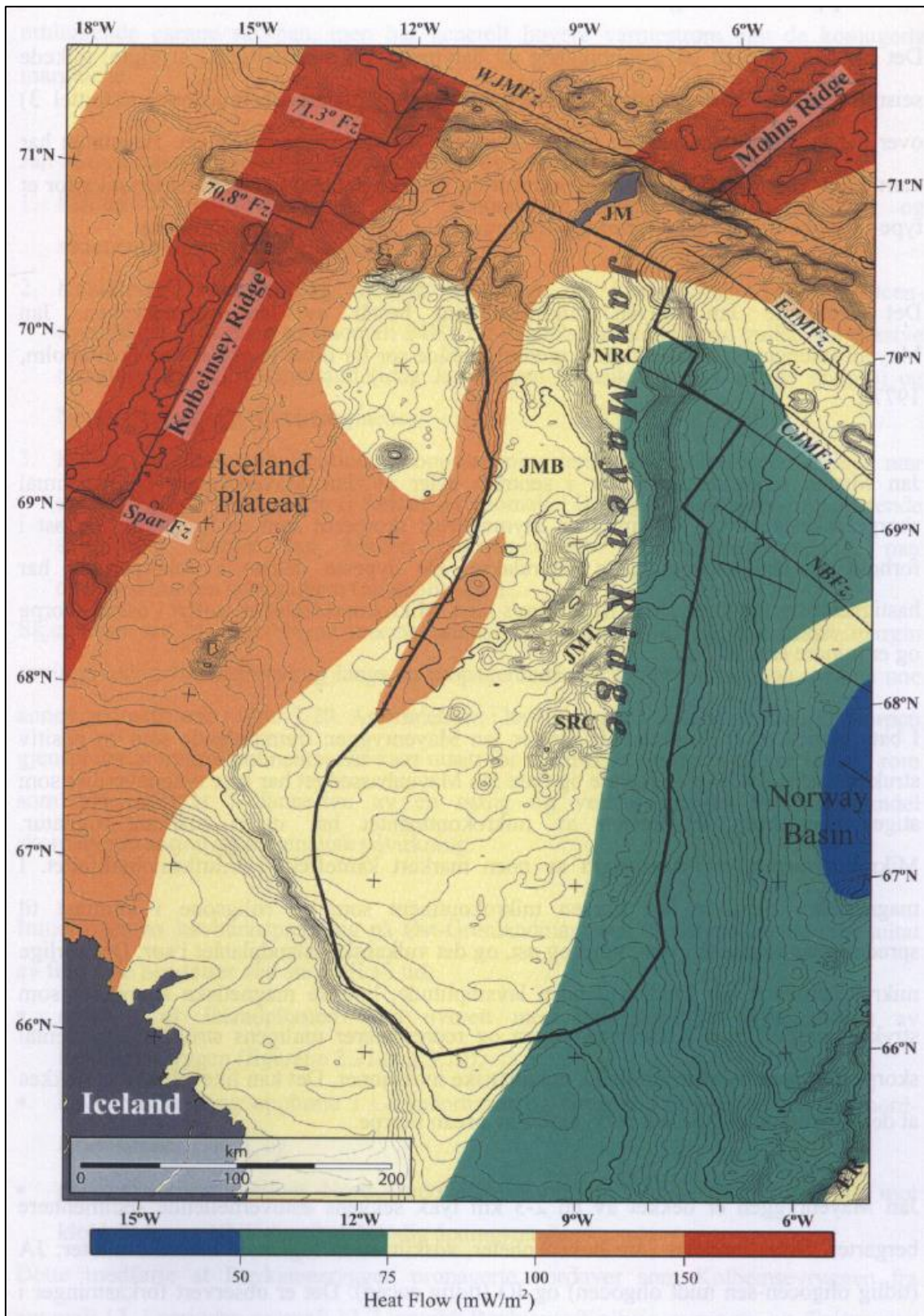
Figure 5. *Present day heat flow map of the greater JMMC area, compiled by Rey, (2013) from seafloor heat-flow data by Sundvor et al. (2000).*

Age (Ma)	Ambient Tp model (°C)	High Tp initial pulse (°C)	High Tp waning model (°C)
0	1333	1330	1400
3	1333	1330	1408
6	1333	1355	1417
9	1333	1331	1425
12	1333	1340	1433
15	1333	1353	1442
18	1333	1330	1450
21	1333	1337	1458
24	1333	1327	1467
27	1333	1330	1475
30	1333	1335	1483
33	1333	1340	1492
36	1333	1330	1500
39	1333	1322	1508
42	1333	1323	1517
45	1333	1317	1525
48	1333	1326	1533
51	1333	1340	1542
54	1333	1550	1550
56.5	1333	1550	1550
57	1333	1450	1450
59	1333	1450	1450
60	1333	1550	1550
61	1333	1550	1550

Figure 6. *Simplified mantle potential temperature models for beneath the JMMC.*

The distribution of higher temperatures appears to have been more restricted post break-up, likely as a combination of a minor decrease in plume temperatures alongside the focusing of melting beneath the thinning lithosphere and a reduction in plume head spreading. All models are generally focused either on uplift history or melt production and the implications of pulses of hotter than ambient mantle on the thermal history of the overlying lithosphere are generally ignored (e.g. zero heat flux boundary condition at the LAB).

Recent modelling (Parnell-Turner et al., 2014) predicts conservative variations of 5-10 °C (55-35 Ma on 3 Ma cycles) and 25-30 °C (35 Ma to the present on 8 Ma cycles) above ambient temperature spreading away from Iceland. Interestingly enough this cyclicity is similar to rift jump processes observed for Iceland, where rift zones tend to stay stable for 8-10 Ma, before relocating closer to the plume location (Harðarson et al., 2008; Hjartarson et al., 2017).

These temperatures are significantly lower than those inferred beneath the present-day Iceland neo-volcanic zone (e.g. 1400-1500 °C), which are thought to be related directly to the centre of the present-day Iceland plume conduit.

Based on the discussion and assumptions in this section, three simple temperature models for the JMMC over the past ca. 60 Ma have been made to test the 1st order impacts of elevated temperatures on the JMMC thermal model including (Figure 6):

1. *Constant ambient T_p.*

2. *Initial short lived High T_p pulse followed by low amplitude variations around ambient (based on Parnell-Turner et al., 2014).*

3. *High initial T_p pulse decaying gradually over time (broadly based on Hole & Millett, 2016).*

The location of the plume centre through time, its diameter and channelling of any convective pulses may all have had important influences on the JMMC. Constraints on these factors are, however, poor and therefore we opt for a uniform temperature distribution model across the study area to test the first order effects. It should also be noted that the modelling does not incorporate convective mantle flow or melt generation, both of which will impart variations on the thermal structure of the rifting corridors described below. Incorporation of dynamic melting models and mantle flow are possible, but out of the scope of this project.

3.2 Uplift input parameters & assumptions

Additional to petrological arguments, evidence from reflection seismic interpretation and modelling have revealed transient uplift events during the main phases of NAIP volcanism. Estimated uplift during the Eocene was estimated and is displayed in Figure 7, showing the inferred uplift associated with the 'Eocene swell' phases, which is based on literature estimates (Jones et al., 2012).

The main phases of modelled uplift are associated with:

- **Phase 1** of the NAIP e.g. at ca. 62-59 Ma is limited to <200 m and is highly localized (Saunders et al., 2007). Thermal perturbations associated with Phase 1 appear to be very restricted, however, the plume head may have been close to JMMC at this time based on the estimates of Torsvik et al. (2015).

- **Phase 2** ca. 56.5-54 Ma is where the majority of the magmatism and uplift occurred.

Evidence for repeated uplift and subsidence events occurring approximately in 0.4 Ma time intervals, have also now been identified from the stratigraphic records (Hartley et al., 2011) and combined stratigraphic and chemical records of the NAIP (Millett et al., 2015; Millett, 2014).

The plume pulsing hypothesis was recently expanded to include evidence from V-shaped ridges along the Reykjanes Ridge from ca. 55 Ma to the present (Parnell-Turner et al., 2014). These models include assessments of melt productivity from combined gravity and reflection seismic data to interpret residual basement heights (e.g. White, 1997).
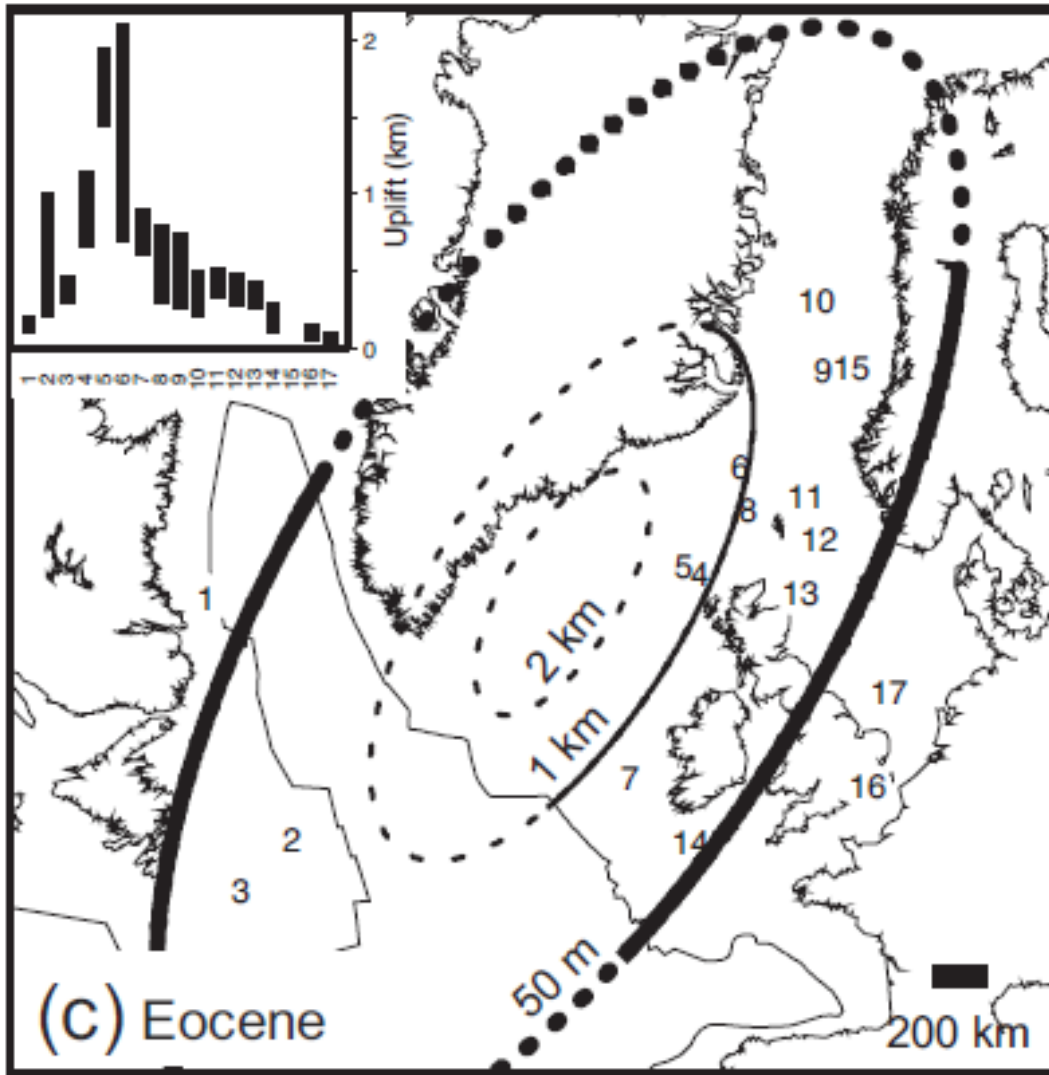
Figure 7. *Map highlighting the proposed uplift associated with the Early Eocene Northeast Atlantic breakup event, associated with the emplacement of the NAIP (Jones et al., 2012). This is used as a background control and reference to the JMMC model´s uplift results.*

3.3 Crustal thickness input parameters & assumptions

Crustal thickness input parameters were selected based on today´s measurable crustal thicknesses of the central East Greenland coast and the seismic refraction thickness estimates for the JMMC, IP, and Iceland areas. Present day crustal thickness estimates are based on gravity inversions and seismic refraction data calculations of OBS, ESP & SB datasets (Hopper et al., 2014; Brandsdóttir et al., 2015; Blischke et al., 2016) (Figure 8; Table 3).

Table 3. *Crustal thickness variations for the different sub-areas of the JMMC and the Iceland plateau for model input considerations (Hopper et al., 2014; Brandsdóttir et al., 2015; Blischke et al., 2016).*

Layer	Unit type	Thickness range (km)
JMMC Main ridge		
1	Sediments (stratigraphic and igneous)	0.5 – 6
2	Continental crust	8 – 27
JMMC ridge flanks		
1	Sediments (stratigraphic and igneous)	0.5 – 7.5
2	Continental crust	4 – 12
Iceland Plateau		
1	Sediments (stratigraphic and igneous)	0.2 – 2.4
2	Transitional crust *(slivers of continental crust and igneous domain / centres)*	8 – 21
Greenland – Iceland – Faroe – Ridge Complex (GIFRC)		
1	Sediments (stratigraphic and igneous) *(generally, no more than 0.5 km for most of the complex area offshore)*	0 – 3
2	Composite crust	11 – 40
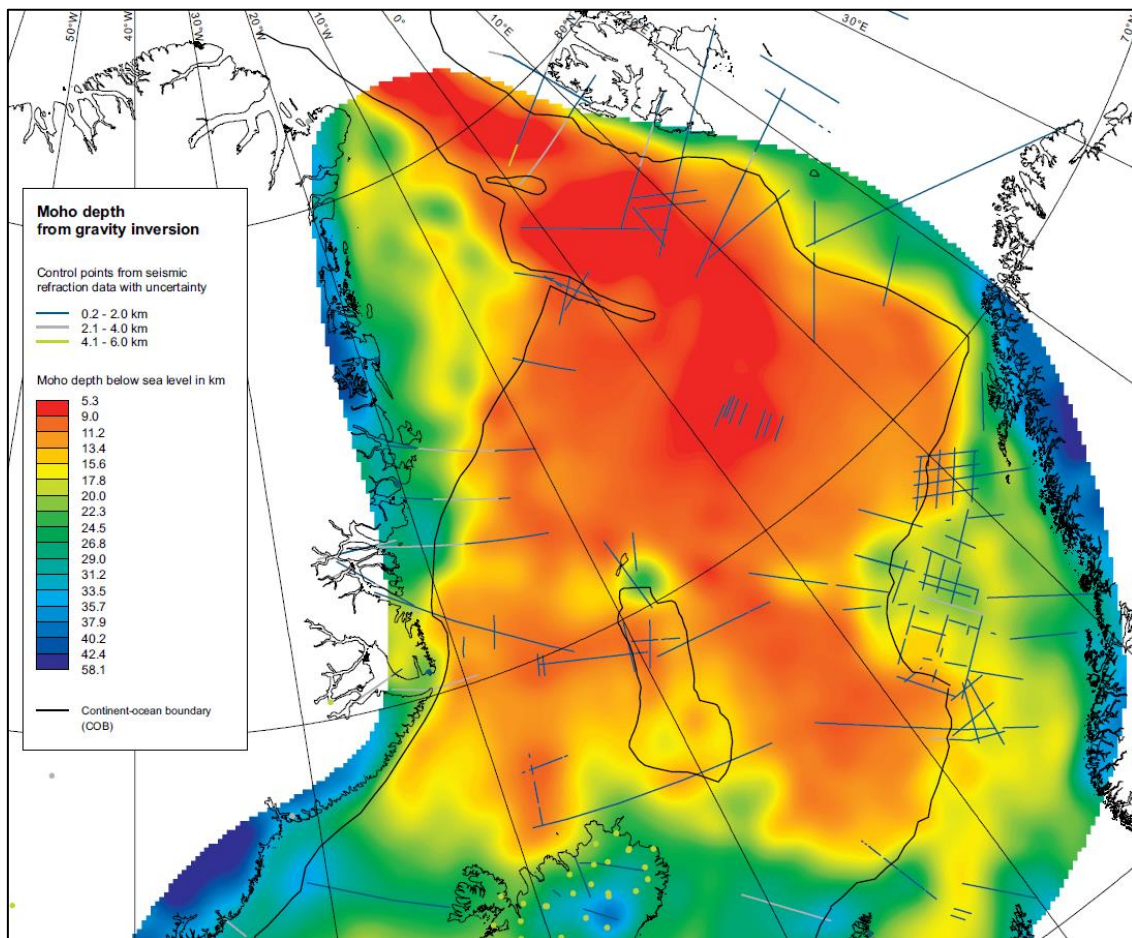
Figure 8. *Moho depth from gravity inversion, tied to seismic refraction data profiles (Hopper et al., 2014).*

As can be seen in Table 3 these ranges reflect heterogeneity of the area at present day conditions. The highest value for JMMC are in the northern part of the main ridge and present the most undisturbed / faulted or stretched sections of the microcontinent that is more or less still intact, and can serve as a point of original state, before the flank sub-basin areas of the JMMC were thinned due to the rifting processes to either side of the microcontinent. The flank areas of the JMMC are stretched and altered by intruded igneous rock formations.

Deep crustal and mantel variations are just as heterogeneous, as the Iceland Plume – Kolbeinsey Ridge – Jan Mayen igneous centre system that are a-typical in regards to mid-oceanic rift systems. These complex systems show lateral and vertical in-homogeneities and low-velocity intervals and areas that are possibly sourced by the lower mantle system, e.g. for the Iceland and the Jan Mayen igneous systems (Bjarnason & Schmeling, 2009; Rickers et al., 2013). The high-resolution S-velocity model of the North Atlantic region by Rickers et al., 2013 indicates the presence of two separate hot-spot areas, one beneath Iceland and one beneath the northern part of the Kolbeinsey Ridge – Jan Mayen igneous system. Rickers et al. (2013) model transects across the Kolbeinsey ridge – JMMC corridor indicate an upper mantle thickness range of around 100 – 150 km close to the JMMC area, and an average thickness of the heat-flow model z-axis is set to 125 km.

The existence of a possible dual hot-spot system is important for the heat-flow model input assumptions, as these two areas form the northern and southern boundaries of the microcontinent, literally surrounding the JMMC by active igneous areas.
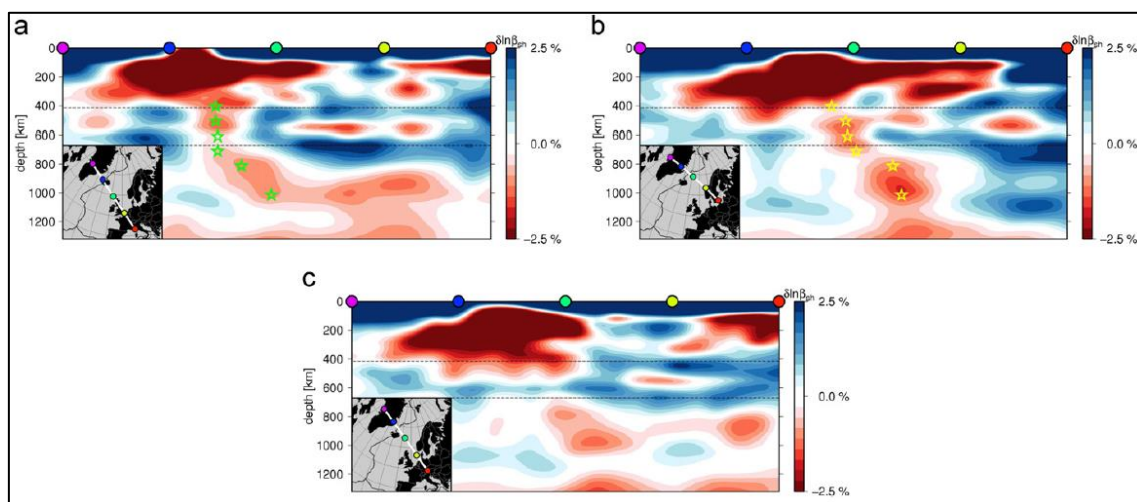
Figure 9. *Vertical slices through the S-wave model by Rickers et al. (2013).*

4 Heat flow, uplift and maturity model setup

The heat flow, uplift and maturity model has been calibrated and built using the in chapter 3 described input parameters and a previously constructed generic model used to study transform margins (Schmid et al., 2017). The complexity of the model geometry was increased in phases to assure that the model parameter calculations and iterations functioned properly. The phases are separated into four runs steps (Appendix 2):

✓ *Model 1: Simplified geometry*

  Base orthogonal model – simple rifting scenario.

✓ *Model 2: Complex geometry - reference model*

  JMMC with 2 blocks, oblique rifting & simplified Iceland plateau rift (IPR)

✓ *Model 3: Complex geometry - reduced rifting*

  JMMC with 2 blocks, oblique rifting & IPR & varied crustal thickness

✓ *Model 4: Reduced rifting & increased mantle potential temperature*

  JMMC with 2 blocks & oblique rifting, simplified IPR, & variable mantle potential temperature T_P)

4.1 Model Stages

Each model run is developed for three distinct time spans, here referred to as stages, which correspond to the main tectonic phases based on the geochronology work described. Stage 1 starts at initial breakup time of the Ægir MOR from the eastern flank of JMMC at 53 Ma and ending at 33.25 Ma with the cessation of the Ægir MOR and the rift transfer across the Iceland plateau region and the IPR, which starts Stage 2 of the modelling. Stage 2 ends at 23.25 Ma with the forming of the proto-Kolbeinsey MOR and marks the beginning of the last Stage 3 to the present (Appendix 2).

> ✓ *Stage 1 - Initial Configuration (53 Ma)*
>   *Stage 1– End Configuration (33.25 Ma)*
>
> ✓ *Stage 2 - Initial Configuration (33 Ma)*
>   *Stage 2 – End Configuration (23.25 Ma)*
>
> ✓ *Stage 3 - Initial Configuration (23 Ma)*
>   *Stage 3 – End Configuration (23.25 Ma)*

Temperature, maturity, differential maturity, hydrocarbon maturity windows (HC windows), effective heat flow and uplift are calculated within the modelled domain through time.

All model runs are also compared to each other and published work that describe the present status in regards to changes of heat flow, uplift, resulting bathymetry, and hydrocarbon maturation windows for the 2 JMMC blocks (JMMC-N & JMMC-S).

4.2 3D Model input settings

The 3D models use a simplified setup to explore the opening of the North Atlantic and the formation of the JMMC. The modelled domain in all models is:

- *X-axis (E-W orientation)* : 1600 km
- *Y-axis (N-S orientation)* : 800 km
- *Z-axis (depth)* : 125 km

The reference frame of the model is static with respect to the spreading ridges, i.e. oceanic crust is formed on both sides of the spreading centres pushing continental crust away with the half-spreading rate on either side. Additionally, the thermal evolution and associated processes are separately tracked for the JMMC and the Vøring and Møre basins. The temperature within active spreading centres is set to 1333 °C. The model contains different layers with unique material properties given in Table 4.

Table 4. *Material properties used in the 3D models. Note that a high thermal conductivity for ocean water is used to simulate fast heat transfer across the sediment-water interface.*

Lithology	Density [kg/m³]	Heat Capacity [J/kg/K]	Conductivity [W/m/K]
Water	1000	3000	420
Sediments	2700	854	1.7
Oceanic Crust	3000	854	2.82
Continental Crust	2800	854	2.13
Mantle	3300	853	2.82

Please note that heat capacity and conductivity values for water are different from average values for water, i.e. 4200 J/kg/K or 0.5 W/m/K. Natural processes, such as convection, in the water column would quickly remove heat from the sediment-water interface. As such processes are not modelled, artificially high conductivity and low heat capacity values are used to simulate this effect in the lithospheric column for water (Gadd, S., Scrutton, R., 1997).

4.2.1 Model 1 (Simplified geometry)

The first and simplest 3D model uses a block model setup where the Mohn's (MR), Ægir (AR) and Kolbeinsey Ridges (KR) are simplified with ridge axes aligned along the Y-axis (N-S orientation) and symmetrical spreading around the axes. Note that for clarity, parts of the Kolbeinsey Ridge to the south of the JMMC are separated and relabelled as the Icelandic Plateau (IPR) and Greenland–Iceland–Faroe Ridge Complex Ridges (GIFRCR). The ridge axes are 5 km wide. The model results are separated into three stages defined by the initiation of

spreading at the different ridges. The timeframe for the model extends from 53 Ma when spreading in the region initiated to the present.

4.2.2 Model 2 (Reference model)

The second 3D model builds on the first and is closer to the observed structural framework of the JMMC. It also investigates the thermal effects of rifting of the JMMC. The JMMC is split into two parts: the northern (NJMMC) and southern (SJMMC). The Mohn's Ridge and the northern part of the Ægir Ridge spread symmetrically at 1 cm/yr. (half-spreading rate). The southern part of the Ægir ridge spreads asymmetrically; 1 cm/yr. to the east and 0.25 cm/yr. to the west. The SJMMC undergoes rifting at the same time such that it widens at a rate of 0.75 cm/yr. taking up the difference resulting from the asymmetrical spreading. The western edge of the N and SJMMC are therefore aligned with each other at all times. The thinned SJMMC extends from an initial width of 100 km to a final width of 250 km volumetrically balancing the thinning. The final configuration of the SJMMC is an interlayered cover of basalt flows and sediments overlying transitional / highly intruded crust that are ~ 3 and 11 km deep, respectively. Additionally, when active, the IPR south of the JMMC extends diagonally across the extent of SJMMC connecting the KR above and the GIFRCR below.

4.2.3 Model 3 (Reduced rifting)

The third model is similar to the second model, the reference model, and explores the effect of reduced rifting within the SJMMC. Here, the crust of the SJMMC is thinned from an initial 27 km thickness to 20 km. The final configuration of the SJMMC is an interlayered cover of basalt flows and sediments overlying transitional / highly intruded crust that are ~ 4.5 and 20 km deep, respectively. Note that, in this case, volume is not conserved as the extension of the SJMMC remains the same. The rest of the model setup with respect to spreading centres and rates is identical to the reference model. The timeframe for the model is from 53 Ma when spreading in the region initiated to the present.

4.2.4 Model 4 (Increased mantle potential temperature)

The fourth and last model is another variation of the second, reference model, where an increase in mantle potential temperature simulating the impingement of a mantle plume is also considered (Torsvik et al., 2015). This variation is implemented by changing the bottom boundary temperature with time based on the temperature curve for the region (Figure 5). The rift corridor temperatures were kept at ambient mantle temperature in this model run and further model iterations were required in order to quantify a more complex dynamic heat-flow model incorporating time-dependent upwelling and melting within these corridors. The timeframe of the model is extended to 61 Ma to account for bottom boundary temperature variations prior to seafloor spreading at 53 Ma. The rest of the model setup with respect to rifting of the SJMMC, activation of spreading centres and rates are identical to the second reference model.

5 Modelling results

The JMMC dual breakup scenario is modelled using a three-dimensional heat conduction model that also gives insights and estimates with respect to maturity and potential uplift of the modelled area. The thermal input is assumed to result mostly from the emplacement of new oceanic ridges (ÆR, RR, MR, IPR & KBR in Figures 1–3) against the JMMC and its conjugate margins since the initial breakup around 55 Ma. The models also explore the thermal effects of JMMC rifting and increased mantle potential temperature.

This chapter documents the main results for each model setup showing the modelled thermal structure (Temperature - T [°C]), thermal maturity (Vitrinite Reflectance - VR [%Ro]), heat-flow [mW/m^2], and uplift (Elevation [m]) for each modelled setup and time interval.

The *thermal structure* refers to the modelled temperature (T °C) fluctuation spatially and temporally in the lithosphere throughout the rifting process, including base assumptions for mid-oceanic rift zones and crustal segments (chapters 3 & 4) and model algorithms documented by Schmid et al. (2017).

Vitrinite reflectance, referred to as %Ro, is a widely used indicator of thermal maturity and can be readily measured in the field. These values are obtained by measuring the percentage of incident light reflected from the surface of vitrinite particles in a sedimentary rock (Tissot & Welte, 1984) (Figure 10), and can be related to the degree of maturation, e.g. for kerogen type I-II (*marine to lacustrine organic material source*) from immature VR (%Ro) < 0.5-0.7; oil window VR (%Ro) 0.5-0.7 to 1.2-1.4; wet gas window VR (%Ro) 1.2-1.4 to 2.0; dry gas VR (%Ro) 2.0 - 4.0; and over-mature VR (%Ro) > 4.0.
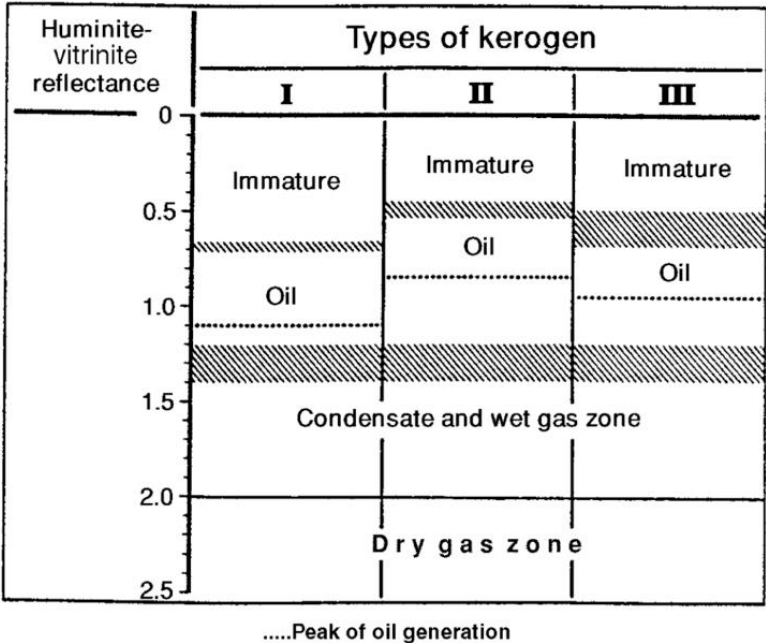

Figure 10. *Approximate maturity boundaries for kerogen types I, II, and III (Tissot & Welte, 1984).*

The model calculates *synthetic thermal maturity* of the source rock using the EASY%Ro method put forward by Sweeney and Burnham (1990). This model uses 20 parallel Arrhenius-type first order reactions to describe the process of kerogen breakdown due to temperature increase and the reacted fraction of kerogen and corresponding vitrinite reflectance (%Ro) can be determined.

Heat-flow refers to the calculated heat transferred at the modelled lithospheric surface (see chapters 3 & 4).

The *uplift models* are directly linked to the temperature and heat-flow models and reflect the local isostatic response in elevation (m).

All model setup results (sections 4.2.1 to 4.2.4) are presented for each time stage (section 4.1) t. This is accompanied by model evolution videos in Appendix 2 for better understanding and visualization.

Note that the associated modelled time at each stage is displayed in the upper left corner of each figure. Furthermore, unless the vertical scale is specified, are all three-dimensional displays without a vertical scale bar show the entire lithosphere except for the maturity (VR) figures that only show the uppermost 10 km of the JMMC at a vertical exaggeration of 10. Heat flow and subsidence values are not calculated for oceanic lithosphere, and therefore are shown as white regions in the model display figures. As a final note, uplift contour values are displayed as positive elevation change values and subsidence as negative elevation changes for all model display figures.

5.1 Model 1 (Simplified geometry)

The simplified model (see 4.2.1) addresses the first stage calibration of the model and is subdivided into three stages defined by the initiation of spreading at the different ridges.

5.1.1 Stage 1: 53 to 33 Ma

The model is initialized as continental lithosphere with the crustal Moho at a depth of 27 km. The continental lithosphere has a sediment thickness of 6 km. Oceanic crust is formed at the ridges with a water depth of 2.5 km and an oceanic Moho at a depth of 8 km. The model has a 5 and 1333 °C surface and bottom boundary condition, respectively, at both the continental and oceanic regions. The thermal structure of the model is initialized to its steady-state before ridge spreading occurs (Figure 11).

The first stage is marked by the establishment of the Ægir ridge system separating the mid-Norwegian Vøring and Møre basins from the Central East Greenland margin. The MR and AR are both active during this stage, spreading symmetrically with a half-spreading rate of 1 cm/yr. The temperature within active spreading centres is 1333 °C. The MR is centred 100 km west of model centre and extends 100 km south from the northern edge of the box. The southern tip of the MR initially lies at the north-western tip of the JMMC. The Vøring basin extends 400 km east of the MR and lies to the north of the JMMC. The AR is initially placed at the left flank of the JMMC and the Møre basin extends a further 100 km east of the AR and is 400 km long along the N-S direction. The JMMC is 200 km wide and 400 km long.
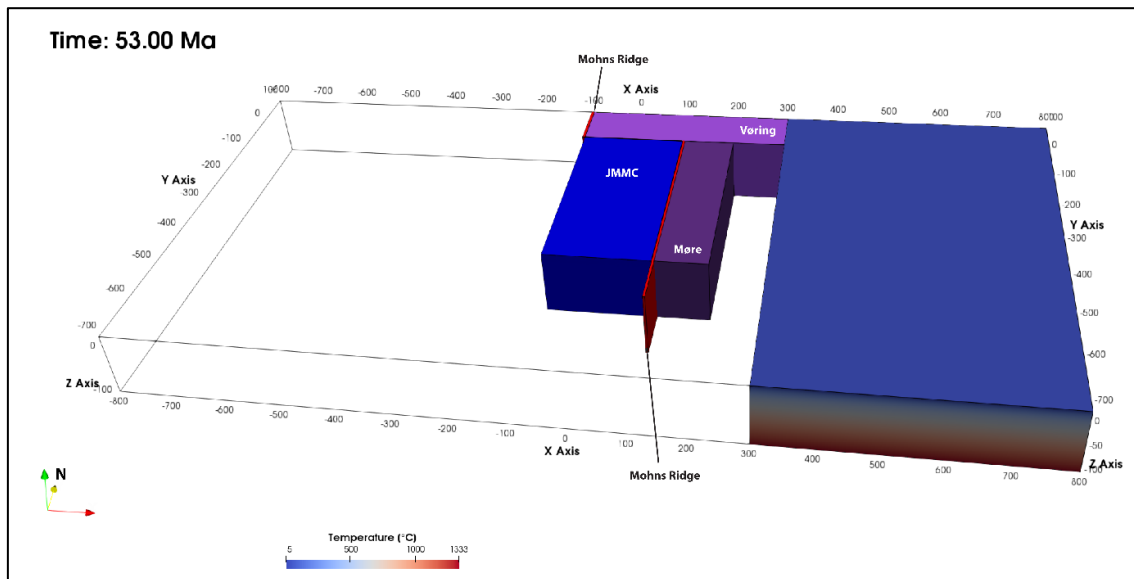
Figure 11. *Setup of Model 1 around 53Ma, showing the initial temperature field in the continental lithosphere. The Mohn's and Ægir Ridges start spreading symmetrically. Spreading at the Mohn´s Ridge pushes the Vøring basin eastwards due to formation of new oceanic lithosphere while the spreading of the Ægir Ridge pushes the JMMC and More Basin west and east, respectively.*

The JMMC receives heat from two sources during this first stage. It initially receives significant heat directly from the AR at its eastern boundary as spreading commences which then decreases as the eastern boundary is only in contact with aging oceanic lithosphere as spreading continues till the end of Stage 1. It also receives heat via its northern edge from the MR and associated oceanic lithosphere as the JMMC is pushed further westwards. At the end of Stage 1, temperature isotherms at the eastern boundary (AR influence) have almost returned to background values due to the retreat of the AR by spreading, while the isotherms are uplifted towards the north-eastern edge where the MR is present (Figure 12). Thermal maturity increases concurrently as temperature increases and follows the same pattern within the JMMC, as the thermal input from the edges, i.e. highest maturity is observed at the eastern and northern edges adjacent to the spreading centres at the end of Stage 1 with maturity levels falling back towards background levels towards the interior of the JMMC (Figure 13). Deviations of maturity levels w.r.t. to background values ($\Delta VR = 0.1 \%$ Ro) in the JMMC, are observed ~56 km inwards from both the eastern and northern edges. Note that maturity levels are calculated within the entire crustal section and not limited to the sediments.

Figure 12. *Thermal structure of the JMMC and the relative positions of the Mohn's and Ægir Ridges at the end of Stage 1 around 33.25 Ma. Temperature isotherms at the eastern edge of the JMMC have almost fallen back to background values while the position of the Mohn's Ridge at the north-eastern edge of the JMMC results in uplifted isotherms there.*
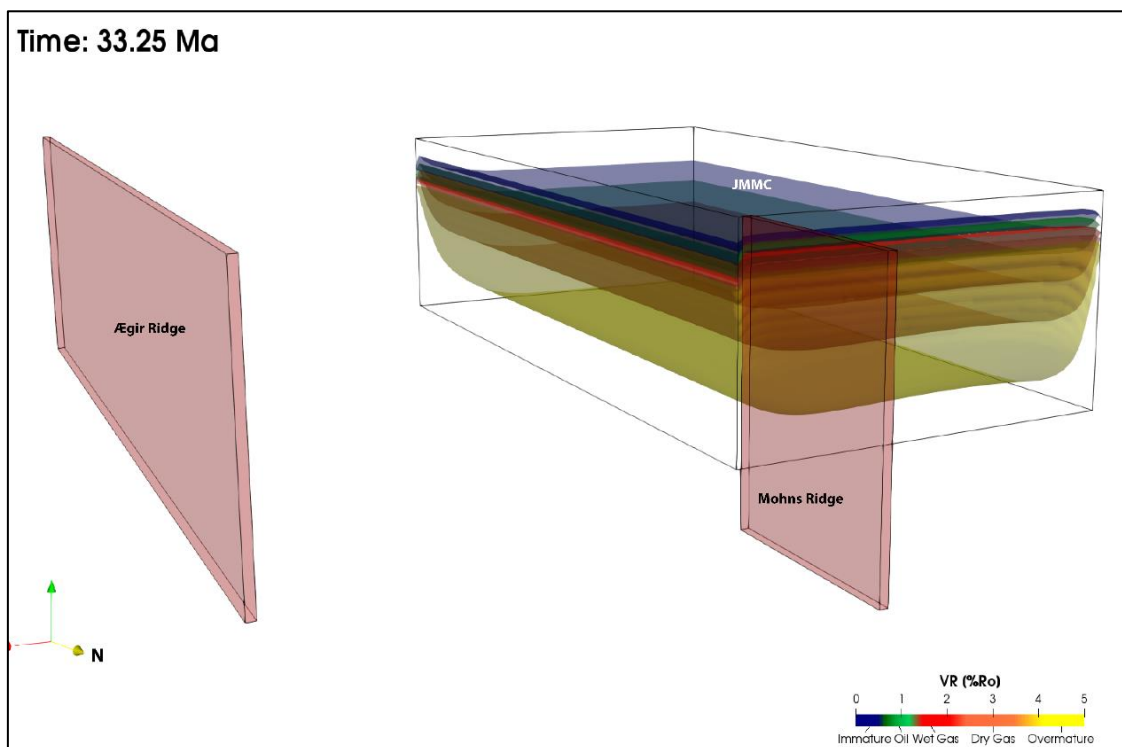
Figure 13. *Thermal maturity of the JMMC and the relative positions of the Mohn's and Ægir Ridges at the end of Stage 1 around 33.25 Ma. Maturity levels are highest at the eastern and northern boundaries through which heat from the ridges enters the JMMC.*

Maximum heat flow values (~200 mW/m²) occur within the JMMC close to the contact with the ridge where it is the hottest and spreads out away from there. Heat flow values then decrease as the JMMC moves away from the spreading centres. An asymmetry develops in the regions with increased heat flow as they move away from the ridges during ocean spreading.

Figure 14. *Heat flow within the JMMC and the relative positions of the Mohn's and Ægir Ridges at the end of Stage 1 around 33.25 Ma. Contour values are between 50 and 200 mW/m² in steps of 25 mW/m².*

Figure 15. *Uplift within the JMMC and the relative positions of the Mohn's and Ægir Ridges at the end of Stage 1 around 33.25 Ma. Contour values are between 200 and 1600 m in steps of 200 m with an additional contour at 50 m.*

An increase in heat flow (~65 mW/m²) relative to the background value (59 mW/m²) is measured ~40 and 30 km into the JMMC from the northern and eastern edges, respectively, at the end of Stage 1 (Figure 14). Highest values are present near the MR at the north-eastern corner.

Maximum uplift (~1600 m) occurs within the JMMC close to the contact with the ridge where it is the hottest and spreads out away from there (Figure 15). Uplift decreases as the JMMC moves away from the spreading centres and cools. An asymmetry develops in the uplifted continental lithosphere as they move away from the ridges during ocean spreading. Uplift (50 m) is modelled ~60 km into the JMMC, from both the eastern and northern edges, respectively, at the end of Stage 1.

5.1.2 Stage 2: 33 to 23 Ma

The second stage is marked by the establishment of the IPR and GIFRCR with a half-spreading rate of 1 cm/yr. to the south of the JMMC and the simultaneous extinction of the Ægir ridge system (Figure 16). As a result, the JMMC does not move during this stage. The temperature within active spreading centres is 1333 °C. The IPR is centred in the middle of the southern edge of the JMMC and extends 100 km south. The GIFRCR is centred along the MR axis. Both ridge axes have a N-S orientation.

The JMMC does not move with respect to the spreading centres during this stage. It is heated constantly from the north-eastern edge by the MR and the centre of the southern edge by the IPR (Figure 17). Temperature rapidly increases at this contact and diffuses away from it. Similarly, sediment maturity increases where the JMMC is in contact with the IPR and increases gradually around it as the microcontinent is further heated (Figure 18). Deviations of maturity levels w.r.t. to background values (ΔVR = 0.1 % Ro) has not moved much further into the JMMC at the northern and eastern edges during this stage. There is a slight perturbation at the southern edge where the IPR is present.

Figure 16. *Setup of Model 1 around 33 Ma, showing the positions of the JMMC and Vøring and Møre basins with respect to the active ridges. The JMMC does not move during this stage.*
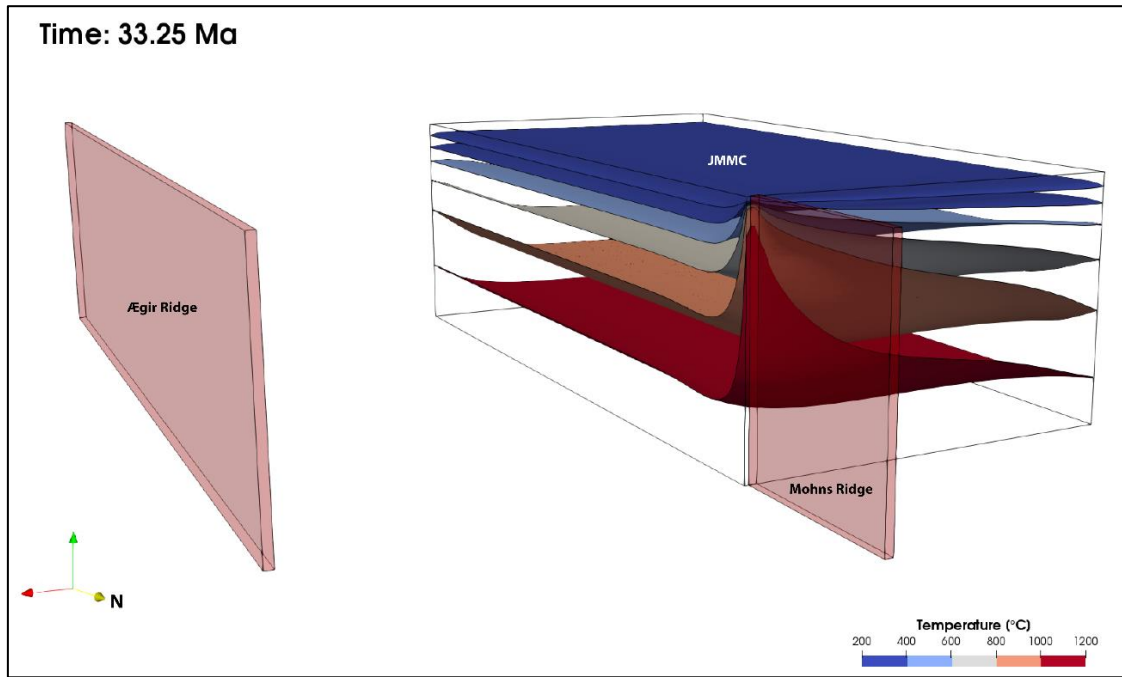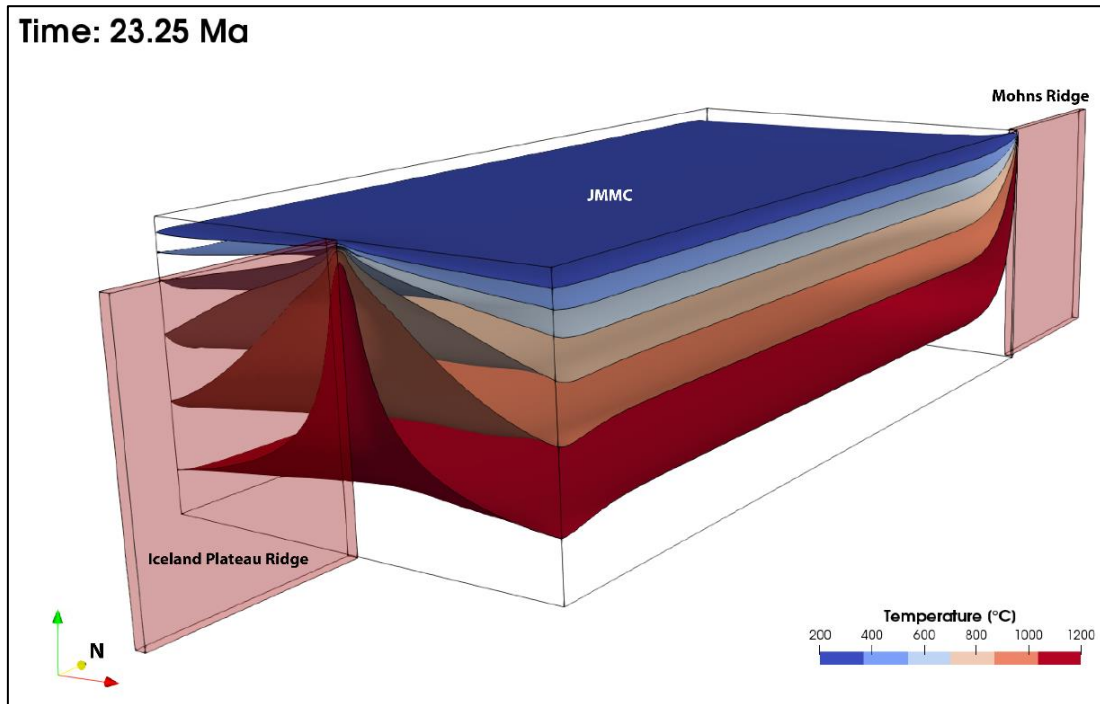
Figure 17. *Thermal structure of the JMMC and the relative positions of the Mohn's and Iceland Plateau Ridges at the end of Stage 2 around 23.25 Ma. Temperature increases rapidly at the contact between the JMMC and the IPR and the isotherms spread out from there. The GIFRCR is not shown for visual clarity.*
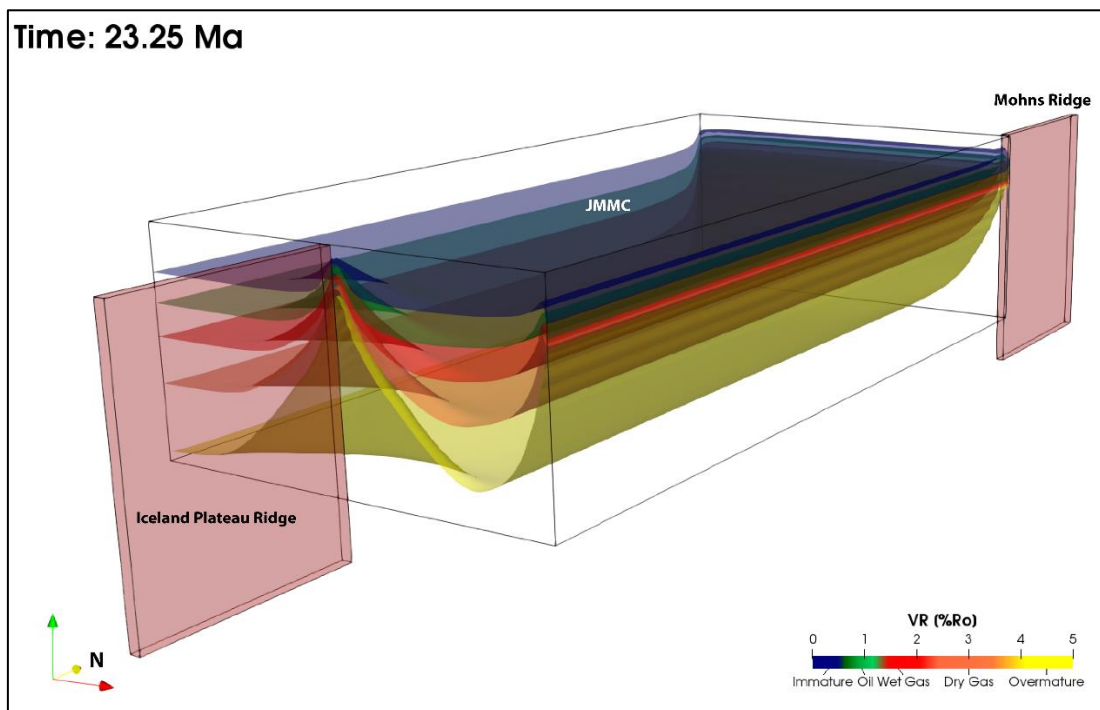
Figure 18. *Thermal maturity of the JMMC and the relative positions of the Mohn's and Iceland Plateau Ridges at the end of Stage 2 around 23.25 Ma. Maturity levels increases rapidly at the contact between the IPR and JMMC and the region near it. The GIFRCR is not shown for visual clarity.*

Heat flow values decrease at the eastern edge of the JMMC as there is no further influence of the AR on the microcontinent (Figure 19). Heat flow values in the north-western part of the JMMC also gradually decrease as the MR is relatively far away at the north-eastern edge.
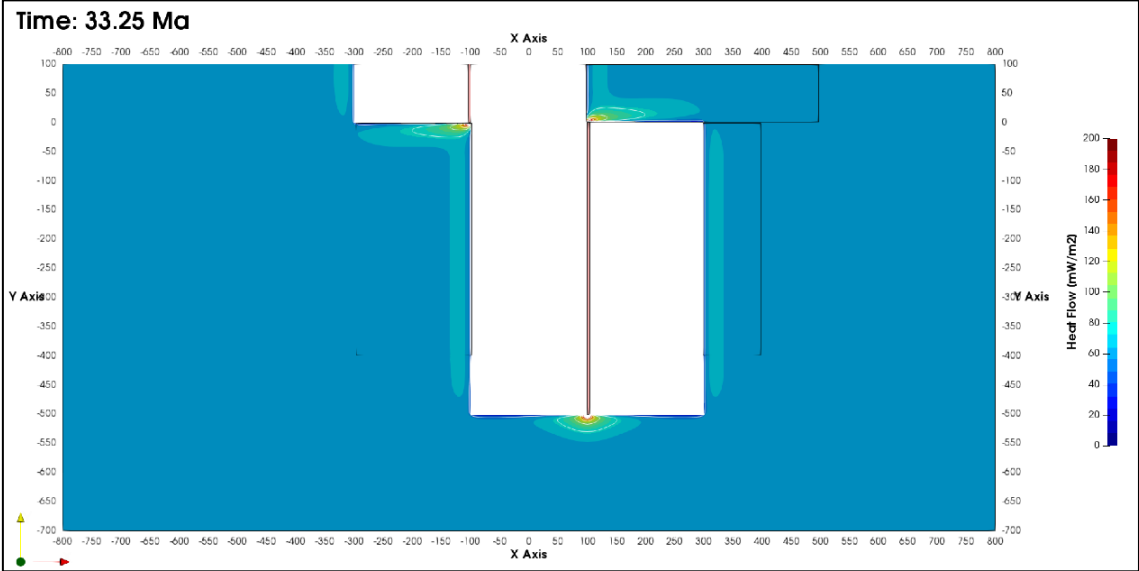

Figure 19. *Heat flow within the JMMC and the relative positions of the MR, IPR and GIFRCR at the end of Stage 2 around 23.25 Ma. Contour values are between 50 and 200 mW/m² in steps of 25 mW/m².*
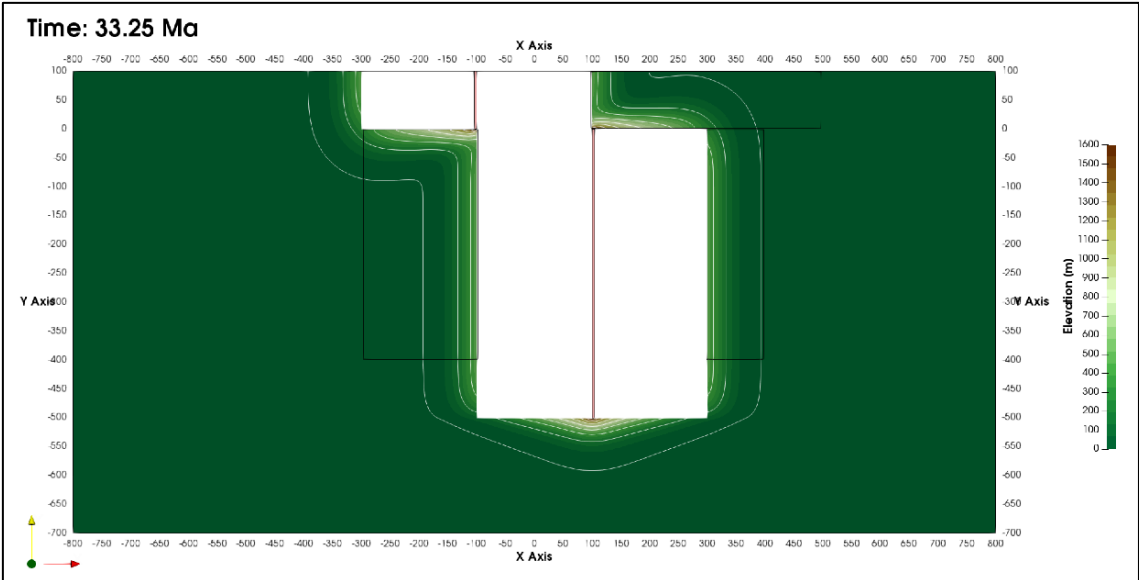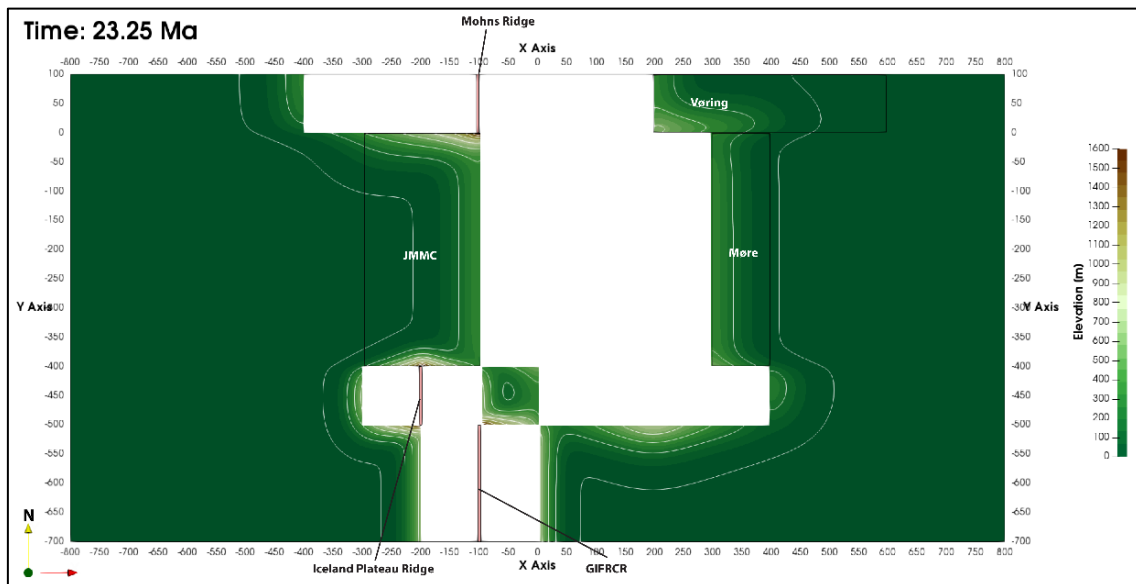

Figure 20. *Uplift within the JMMC and the relative positions of the MR, IPR and GIFRCR at the end of Stage 2 around 23.25 Ma. Contour values are between 200 and 1600 m in steps of 200 m with an additional contour at 50 m.*

Heat flow values increase outwards from the centre of the southern edge due to the IPR. An increase in heat flow (~65 mW/m²) relative to the background value (59 mW/m²) is measured ~52 and 41 km into the JMMC from the northern and eastern edges, respectively, at the end of Stage 2. Maximum values are present near the MR and the IPR in the northeast and southcentral regions, respectively.

More of the interior part of the JMMC is uplifted as the thermal perturbation moves inwards (Figure 20). Severe uplift is also experienced by the JMMC where the IPR is in contact at the southern edge. Uplift (5 m) is predicted ~72 km into the JMMC from, both the eastern and northern edges, respectively, and ~50 km into the JMMC from the southern edge at the end of Stage 2.

5.1.3 Stage 3: 23 to 0 Ma

The third and final stage is marked by the establishment of the Kolbeinsey Ridge with a half-spreading rate of 1 cm/yr. to the west of the JMMC which moves the microcontinent eastwards (Figure 21). The KR runs along the entire western margin of the JMMC and has N-S orientation.
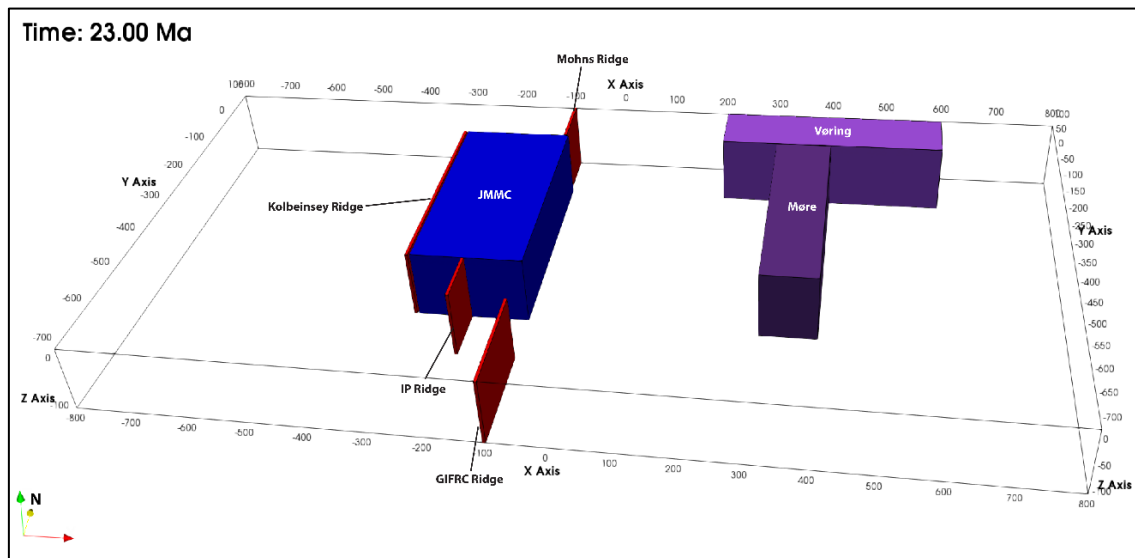
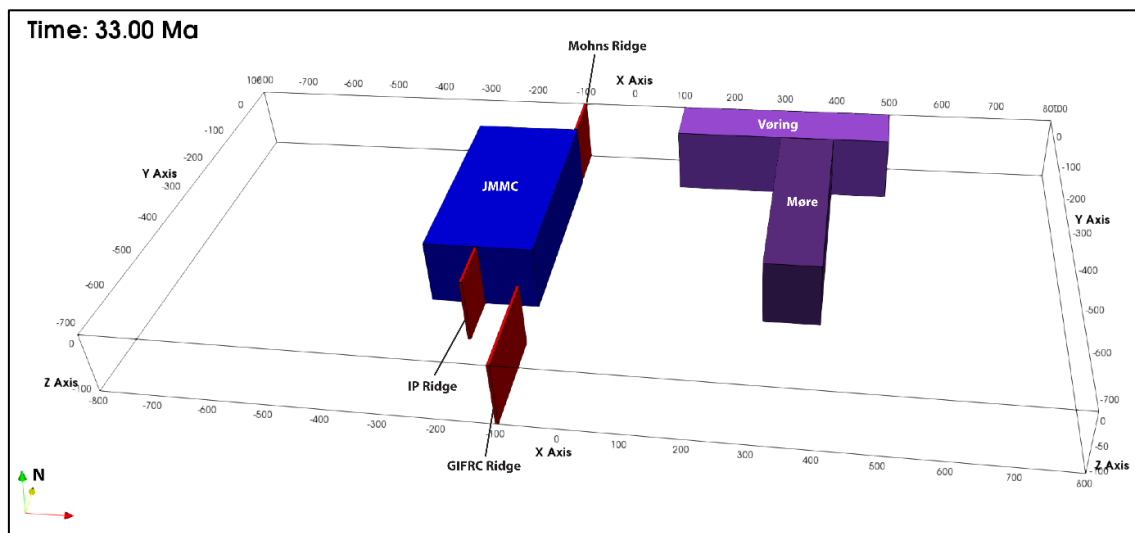**Figure 21.** *Setup of Model 1 at the start of Stage 3 around 23.25 Ma, showing the positions of the JMMC and Vøring and Møre basins with respect to the active ridges. The JMMC moves eastwards due to the generation of oceanic lithosphere at the Kolbeinsey Ridge during this stage.*

The JMMC moves eastwards as oceanic lithosphere is formed at the KR. As a result, the MR and IPR traverse the northern and southern edges of the JMMC, respectively. The JMMC is heated from the northern, western and southern edges by the MR, KR and IPR, respectively. It later cools down as it moves away from the influence of the spreading centres. The predicted present-day thermal structure has returned to background values in most of the interior of the JMMC with remnants of the ridge thermal input only present at the north- and south-western edges (Figure 22). Maturity increases dramatically where the JMMC is in contact with the KR and also at the western part of the southern edge as the IPR moves across it (Figure 23). Deviations of maturity levels w.r.t. to background values ($\Delta VR = 0.1$ % Ro) has moved further

into the JMMC during this stage. It is ~65 km away from the northern and eastern edges and ~41 km from the southern edge.
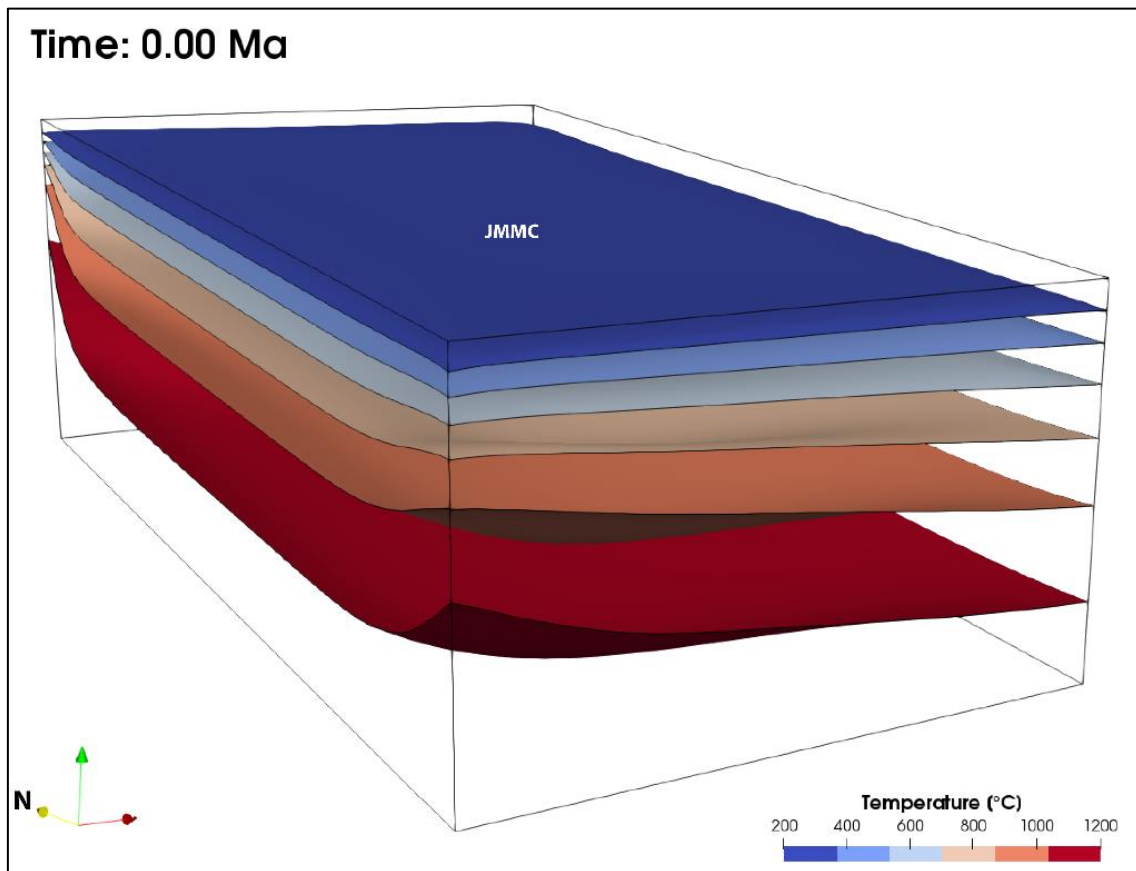
Figure 22. *Thermal structure of the JMMC at the end of Stage 3 at present day. Temperature isotherms in the interior have returned to background values with elevated values present only at the north- and south-western edges. The ridges are not shown for visual clarity.*

Heat flow values increase from the western edge of the JMMC inwards due to the influence of the KR (Figure 24). Heat flow values in the northern part of the JMMC also increase as the MR traverses the northern edge again but in the opposite direction. Similarly, heat flow values during this stage increase in the western part of the southern JMMC edge as the IPR moves across it. Heat flow values in the JMMC gradually decrease as the microcontinent moves away from the ridges with elevated values predicted along the northern, western and southern edges to the present. The highest heat flow values (~90 mW/m²) are predicted at the north-western edge of the JMMC at present day. An increase in heat flow (~65 mW/m²) relative to the background value (59 mW/m²) is modelled ~60 km from the northern and southern edges and ~20 km into the JMMC from the western edge at present day. Maximum values (~90 mW/m²) are observed at the north-western corner of the JMMC.
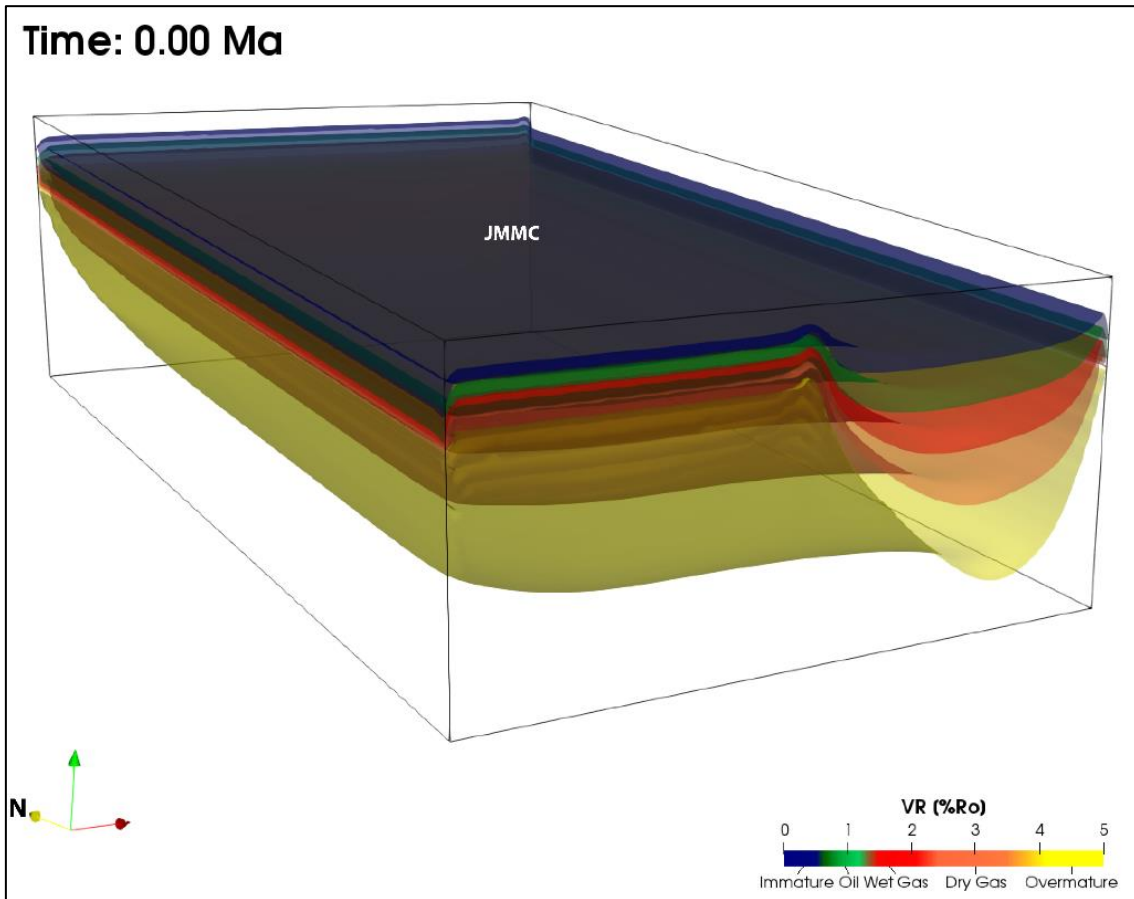
Figure 23. *Thermal maturity of the JMMC at the end of Stage 3 at present day. Maturity levels increase rapidly at the western and western part of the southern JMMC margins due to the KR and IPR, respectively. The ridges are not shown for visual clarity.*
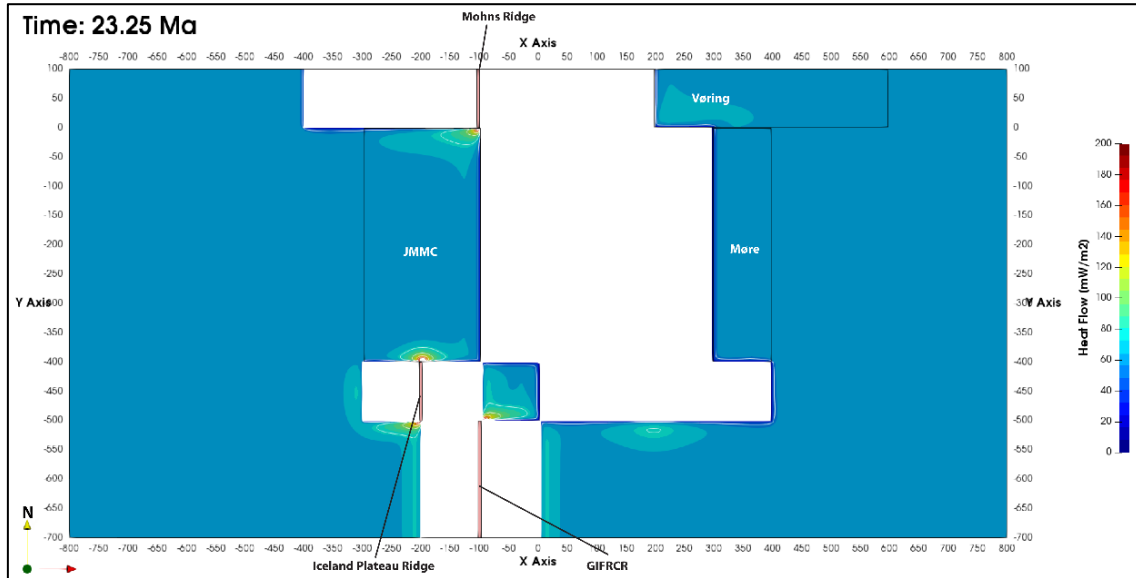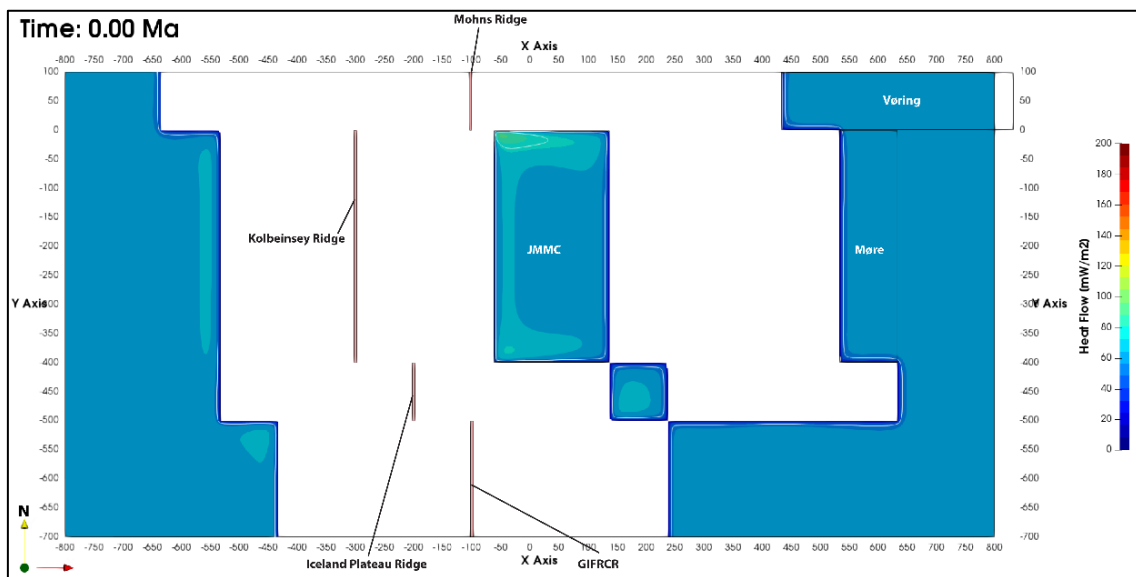

Figure 24. *Heat flow within the JMMC and the relative positions of the MR, KR, IPR and GIFRCR at the end of Stage 3 at present day. Contour values are between 50 and 200 mW/m² in steps of 25 mW/m².*

Uplift is also generated by heat input from the KR along the western edge of the JMMC during Stage 3 (Figure 25). Heat input from the MR and IPR at the northern and southern edges also generates uplift. The microcontinent gradually subsides as the ridges move away from it. The entire microcontinent is uplifted at present day with high values at the north- and south-western edges (~1200 and 800 m, respectively) and lowest values in the centre.
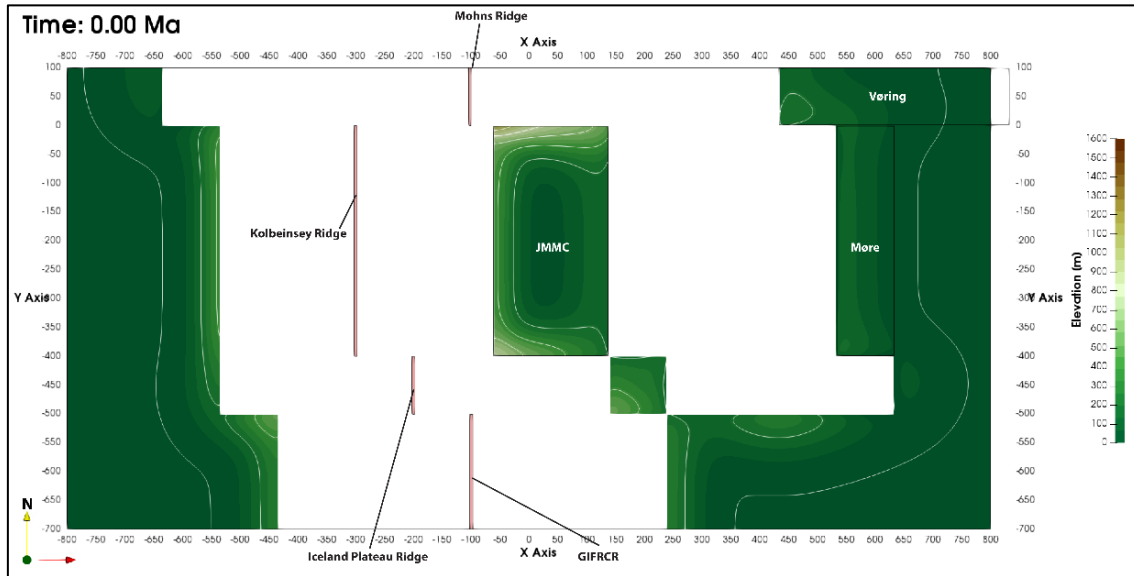
Figure 25. *Uplift within the JMMC and the relative positions of the MR, KR, IPR and GIFRCR at the end of Stage 3 at present day. Contour values are between 200 and 1600 m in steps of 200 m with an additional contour at 50 m.*

5.2   Model 2 (Reference Model)

The reference model (see 4.2.2) addresses the second stage calibration of the model and subdivision into the northern and southern JMMC blocks. It also accounts for a more complex IPR geometry and rifting of the JMMC. This model is sub-divided into three stages defined by the initiation of spreading at the different ridges. The model iteration stages are listed in section 4.1.

5.2.1   Stage 1: 53 to 33 Ma

Similar to the first model, the second model is initialized to continental lithosphere with the crustal Moho at a depth of 27 km. The continental lithosphere has a sediment thickness of 6 km. Oceanic crust is formed at the ridges with a water depth of 2.5 km and an oceanic Moho at a depth of 8 km. The model has 5 and 1333 °C surface and bottom boundary condition, respectively, at both the continental and oceanic regions. The thermal structure of the model is initialized to its steady-state before ridge spreading occurs (Figure 26).

The first stage is marked by the establishment of the Ægir ridge system separating the mid-Norwegian Vøring and Møre basins from the Central East Greenland margin. The MR and AR are both active during this stage. The MR spreads symmetrically with a half-spreading rate of 1 cm/yr. The northern part of the AR in contact with the NJMMC spreads symmetrically with

a half-spreading rate of 1 cm/yr. while the southern part of the AR in contact with the SJMMC spreads asymmetrically with half-spreading rate of 1 and 0.25 cm/yr. towards the east and west, respectively. The MR is centred 50 km west of model centre and extends 100 km south from the northern edge of the box. The southern tip of the MR initially lies at the north-western tip of the JMMC. The Vøring basin extends 300 km east of the MR and lies to the north of the JMMC. The AR is initially placed at the left flank of the JMMC and the Møre basin extends a further 100 km east of the AR and is 400 km long in the N-S direction. The northern and southern JMMC are initially 100 km wide and 200 km long each. The crust of the SJMMC is thinned from an initial thickness of 27 km to ~11 km during this stage and is extended in the EW direction from an initial 100 km width to 250 km. The thinning and extension of the SJMMC per time step is done such that its western edge is always in line with that of the NJMMC.

The entire JMMC receives heat from the Ægir Ridge at its eastern edge, the influence of which decreases as the JMMC moves away and is influenced by increasingly colder and older oceanic lithosphere. The temperature in the SJMMC further increases as rifting progresses and hot mantle is brought up to shallower depths. The NJMMC also receives heat via its northern edge as it passes the Mohn's Ridge. Maturity increases significantly and quickly to the maximum at the edges of the JMMC that are in contact with the hot ridge. Maturity of sediments inwards from the edges increases gradually as the thermal effects of the ridges propagates into the microcontinent.
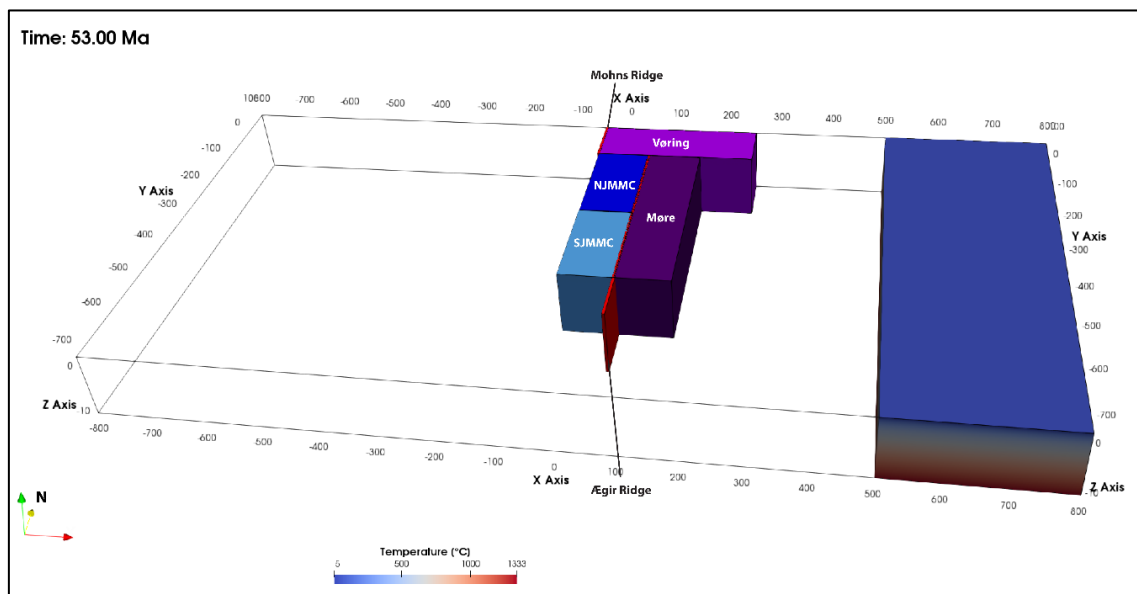
Figure 26. *Setup of Model 2 at the first step of Stage 1 around 53 Ma, showing the initial temperature field in the continental lithosphere. The Mohn's and northern Ægir Ridges start spreading symmetrically while the southern Ægir Ridge spreads asymmetrically.*

At the end of Stage 1, temperature isotherms at the eastern boundary of the entire JMMC (AR influence) are almost flat due to the retreat of the AR by spreading while the isotherms are more uplifted towards the north-eastern edge of the NJMMC where the MR is closer (Figure 27). The isotherms in the SJMMC are much shallower than those in the NJMMC due to rifting which also results in somewhat increased temperatures at the boundary between the two regions of the JMMC. Thermal maturity increases as temperature within the JMMC increases and follows the same pattern as the thermal input from the edges, i.e. highest maturity is observed at the eastern and northern edges adjacent to the spreading centres at the end of Stage 1 with maturity levels falling back towards background levels towards the interior of the JMMC (Figure 28). Note that the maturity level at depth in the SJMMC in this case is much higher than the NJMMC due to heat input from rifting. Deviations of maturity levels w.r.t. to background values ($\Delta VR = 0.1 \% Ro$) in the NJMMC, are observed ~60 km inwards from the eastern edge and the northern edge. The perturbation has also moved inwards from the southern edge of the NJMMC by ~20 km due to rifting in the SJMMC. The SJMMC shows a perturbation in maturity levels ~65 km away from the eastern edge. Note that maturity levels are calculated within the entire crustal section and not limited to the sediments.

Figure 27. *Thermal structure of the JMMC and the relative positions of the Mohn's and Ægir Ridges at the end of Stage 1 around 33.25 Ma.*
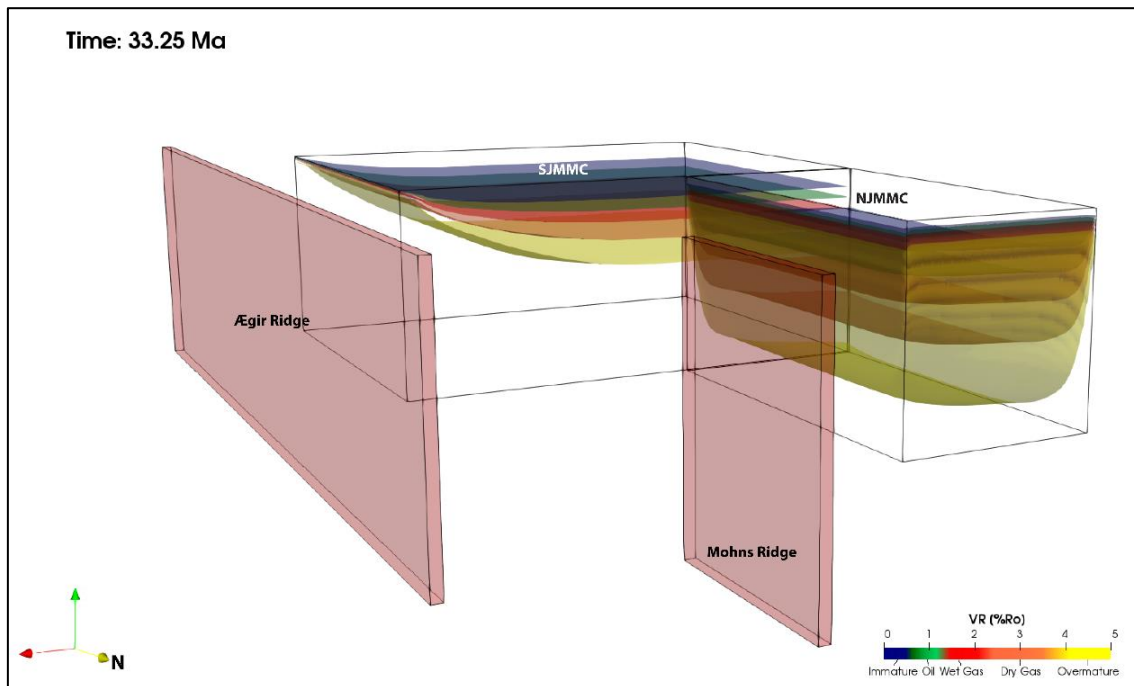
Figure 28. *Thermal maturity of the JMMC and the relative positions of the Mohn's and Ægir Ridges at the end of Stage 1 around 33.25 Ma. Maturity levels are highest at the eastern and northern boundaries through which heat from the ridges enters the JMMC. Additionally, the maturity isotherms are shallower in the SJMMC due to rifting.*

Maximum heat flow values (~200 mW/m²) occur within the continent close to the contact with the ridge where it is the hottest and spreads away from there (Figure 29). Heat flow values decrease as the continent moves away from the spreading centres. An asymmetry develops in the regions with increased heat flow as they move away from the ridges during ocean spreading. The SJMMC shows heat flow values higher than the NJMMC due to rifting. An increase in heat flow (~75 mW/m²) relative to the background value (59 mW/m²) is observed in the region around the north-eastern corner of the NJMMC and in most of the SJMMC where it reaches a maximum of ~100 mW/m² at the end of Stage 1.

Figure 29. *Heat flow within the JMMC and the relative positions of the Mohn's and Ægir Ridges at the end of Stage 1 around 33.25 Ma. Contour values are between 50 and 200 mW/m² in steps of 25 mW/m².*

Maximum uplift (~2000 m) occurs within the continent close to the contact with the ridge where it is the hottest and spreads out away from there (Figure 30). Uplift decreases as the continents move away from the spreading centres and cool with an asymmetry developing in the uplifted continental lithosphere as they move away from the ridges during ocean spreading. The SJMMC subsides significantly (>3000 m) as it thins bringing up hot mantle upwards resulting in a dense lithospheric column relative to the initial continental configuration. Most of the NJMMC has experienced uplift by the end of Stage 1, except for a small region at the western edge.

Figure 30. *Uplift/subsidence within the JMMC and the relative positions of the Mohn's and Ægir Ridges at the end of Stage 1 around 33.25 Ma. Contour values for uplift are between 250 and 1750 m with a contour increment of 250 m and an additional contour at 50 m. Contour values for subsidence are between -500 and -3000 m with a contour increment of -500 m.*

5.2.2   Stage 2: 33 to 23 Ma

The second stage is marked by the establishment of the IPR and GIFRCR with a half-spreading rate of 1 cm/yr. to the south of the JMMC and the simultaneous extinction of the Ægir ridge system (Figure 31). Rifting of the SJMMC ceases during this stage. The GIFRCR is centred along the MR axis and extends 200 km north from the southern box edge with N-S orientation. As opposed to the first model with simplified geometry the IPR extends diagonally from then south-western tip of the SJMMC to the northern tip of the GIFRCR diagonally splitting the Iceland Plateau.

The JMMC does not move with respect to the spreading centres during this stage. Only the SJMMC receives heat directly from the IPR from its south-western corner bringing up isotherms in the region (Figure 32). The NJMMC receives some heat from its northern edge as relatively hot oceanic lithosphere formed at the Mohn's Ridge moves past it. Maturity levels increase rapidly at and immediately around the south-western corner of SJMMC in contact with the northern tip of the IPR (Figure 33). Deviations of maturity levels w.r.t. to background values ($\Delta VR = 0.1$ % Ro) move into the JMMC with time. This covers most of the NJMMC during this stage. There is a small perturbation in maturity levels at the south-western corner of the JMMC. The perturbation extends ~62 km from the eastern edge of the SJMMC showing a slight reduction in extent as compared to Stage 1.

Figure 31. *Setup of Model 2 at the start of Stage 2 around 33 Ma, showing the positions of the JMMC and Vøring and Møre basins with respect to the active ridges. The JMMC does not move during this stage.*
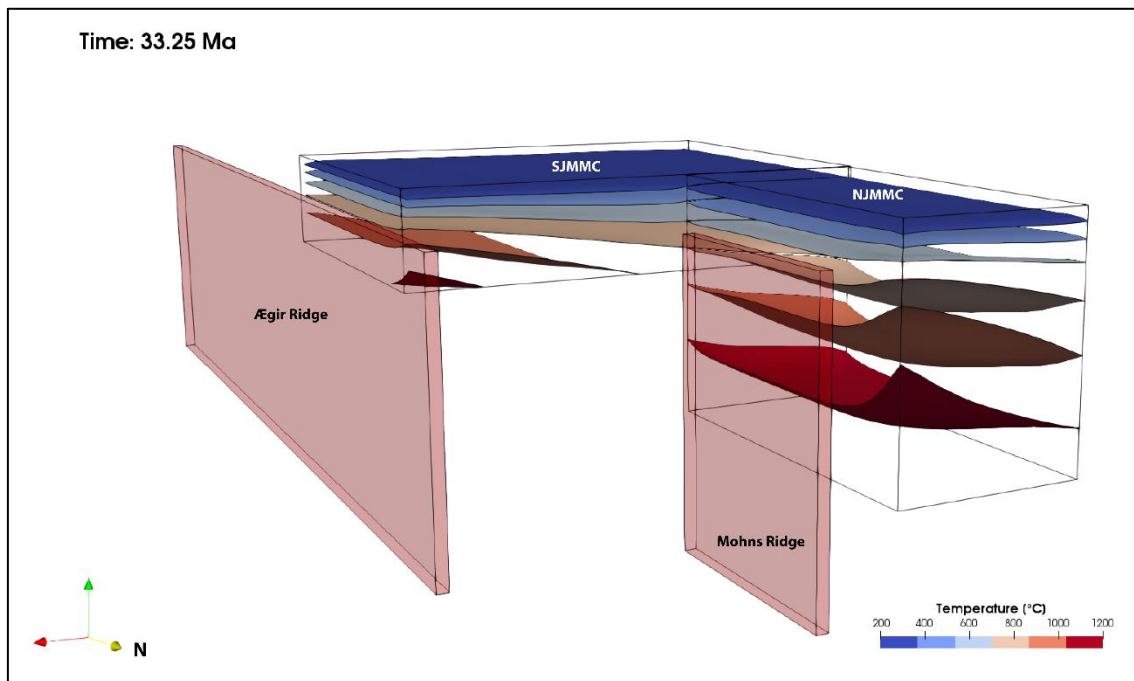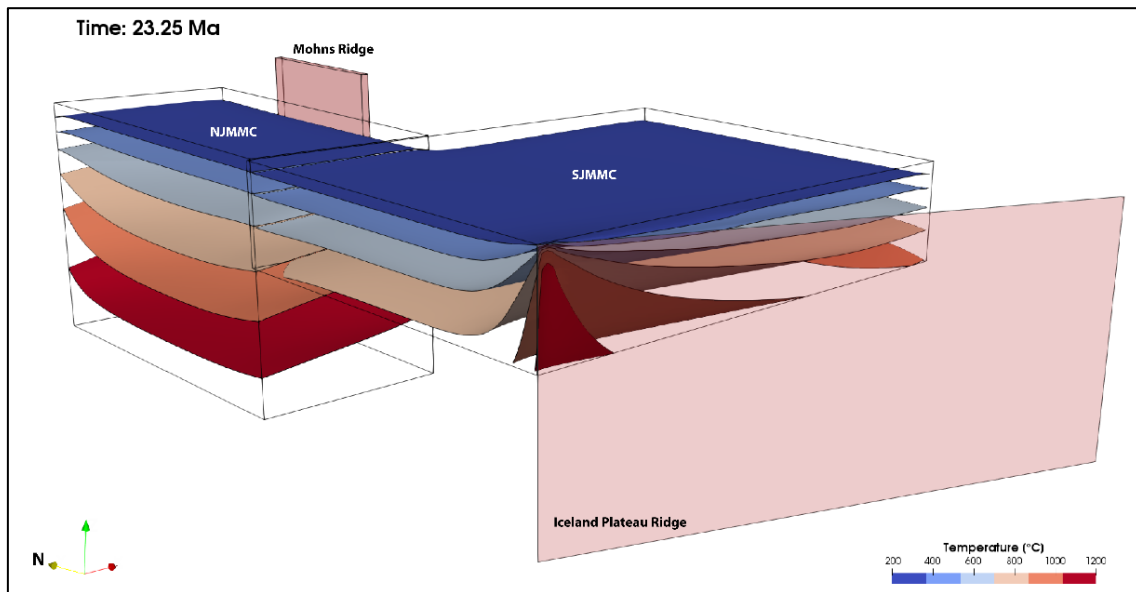
**Figure 32.** *Thermal structure of the JMMC and the relative positions of the Mohn's and Iceland Plateau Ridges at the end of Stage 2 around 23.25 Ma. Temperature increases rapidly at the contact between the SJMMC and the IPR and the isotherms spread out from there. The GIFRCR is not shown for visual clarity.*
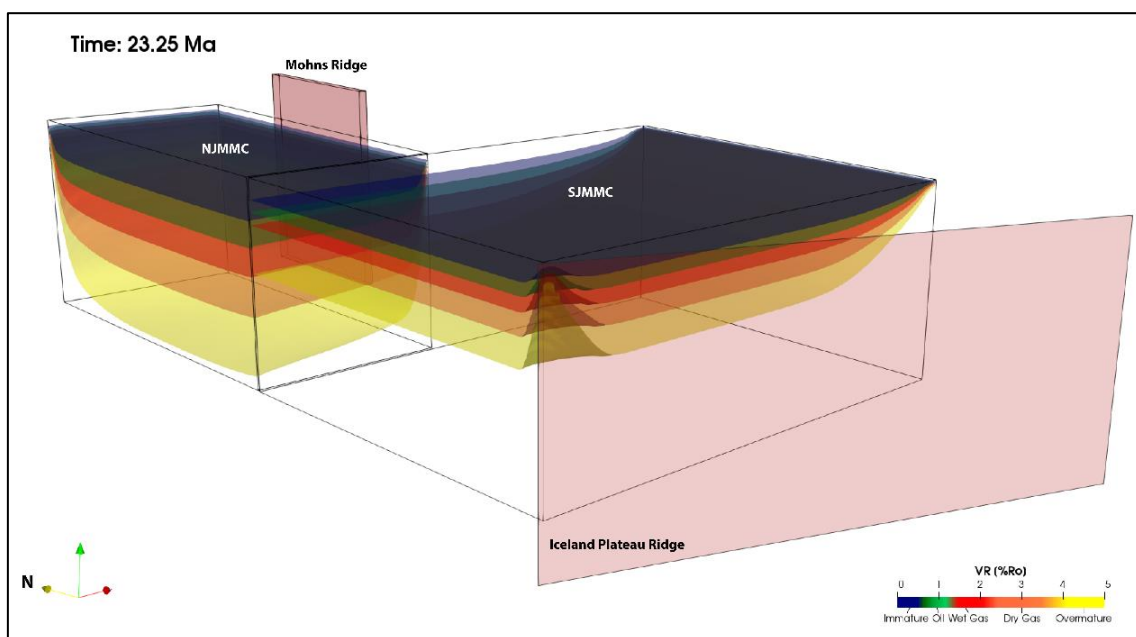
Figure 33. *Thermal maturity of the JMMC and the relative positions of the Mohn's and Iceland Plateau Ridges at the end of Stage 2 around 23.25 Ma. Maturity levels increases rapidly at the contact between the IPR and SJMMC and the region near it. The GIFRCR is not shown for visual clarity.*

Heat flow values in the NJMMC are slightly lower when compared to the previous stage but do not return to background values as it receives some heat from oceanic lithosphere generated by the MR (Figure 34). Maximum heat flow values are recorded at the north-eastern region and are only slightly higher (~68 mW/m^2) than the background value at the end of this stage. Heat flow values in most of the SJMMC decrease as it cools after rifting. Values close to the south-western corner increase due to heat input from the IPR but do not propagate significantly inwards due to the short time frame of this stage. Values of ~80 mW/m^2 are recorded close to the eastern edge.

The entire NJMMC has experienced uplift at the end of this stage with most of the region experiencing more than 50 m uplift (Figure 35). The highest amount of uplift (~800 m) is modelled at the north-eastern corner. Uplift decreases from east to west. The SJMMC subsides further as most of it cools during this stage. Only the south-western edge of the SJMMC experiences relative uplift as it is heated by the IPR.
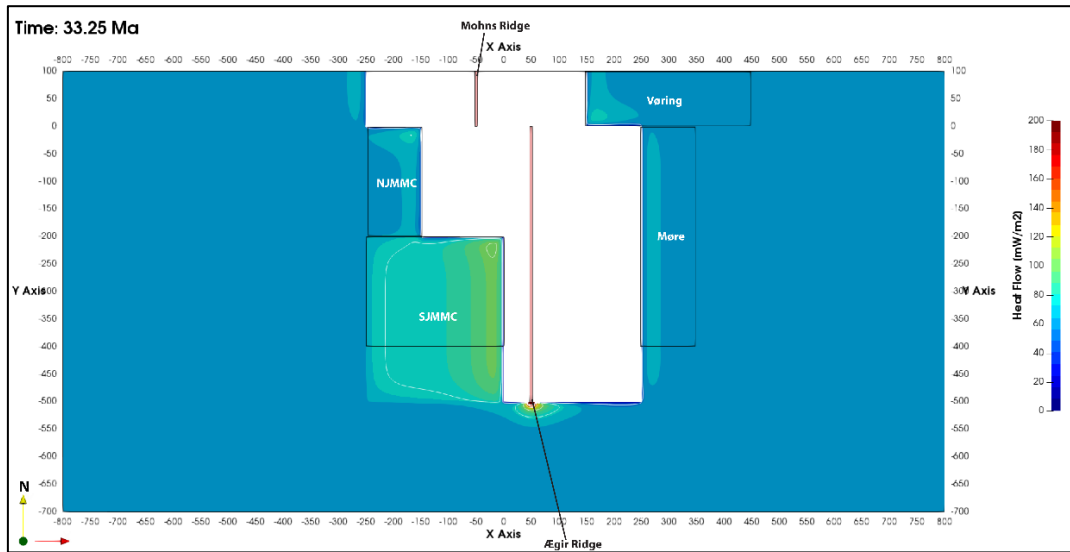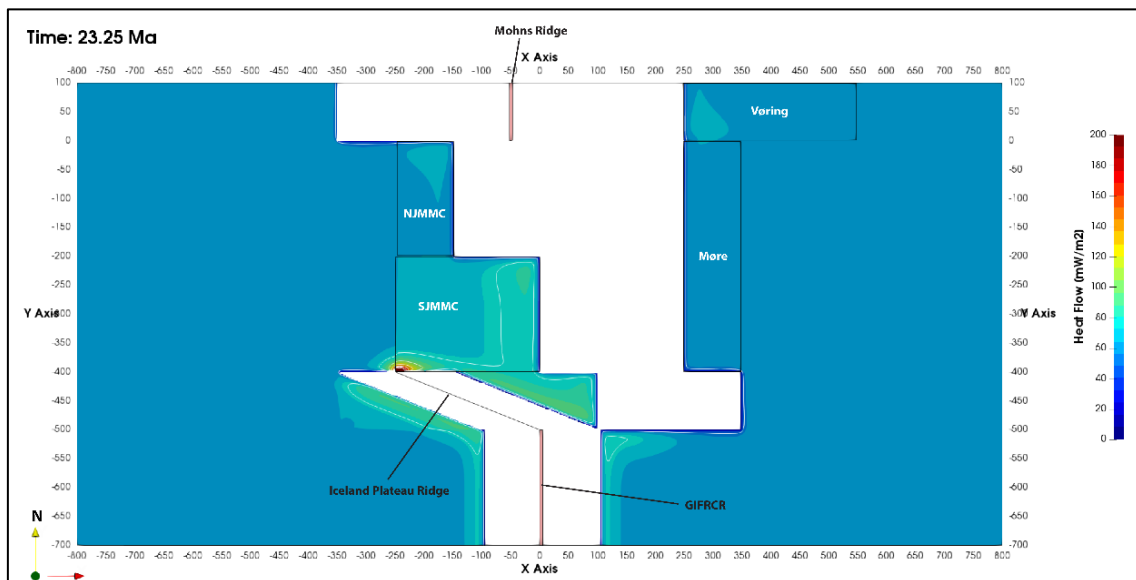

Figure 34. *Heat flow within the JMMC and the relative positions of the MR, IPR and GIFRCR at the end of Stage 2 around 23.25 Ma. Contour values are between 50 and 200 mW/m^2 in steps of 25 mW/m^2.*
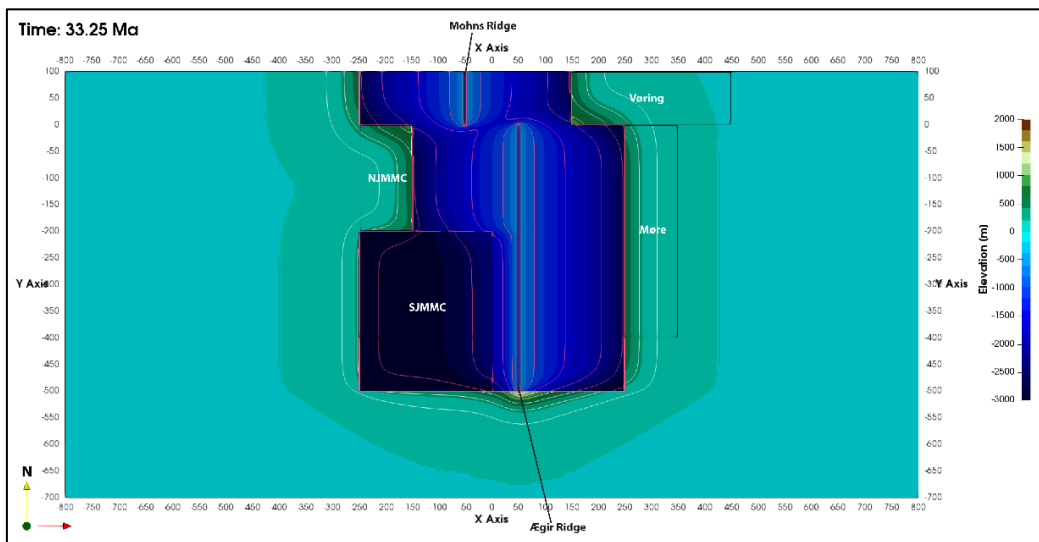
Figure 35. *Uplift/subsidence within the JMMC and the relative positions of the MR, IPR and GIFRCR at the end of Stage 2 around 23.25 Ma. Contour values for uplift are between 200 and 1600 m in steps of 200 m with an additional contour at 50 m. Contour values for subsidence are between -500 and -3000 m with a contour interval of -500 m.*

5.2.3 Stage 3: 23 to 0 Ma

The third and final stage is marked by the establishment of the Kolbeinsey Ridge with a half-spreading rate of 1 cm/yr. to the west of the JMMC which moves the microcontinent eastwards (Figure 36). The KR runs along the entire western margin of the JMMC and has N-S orientation.
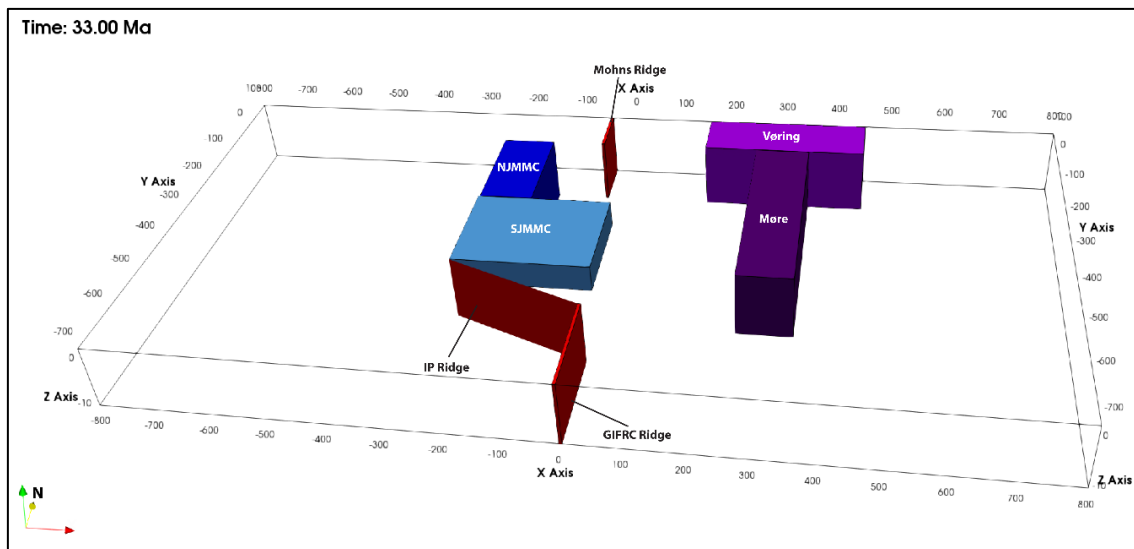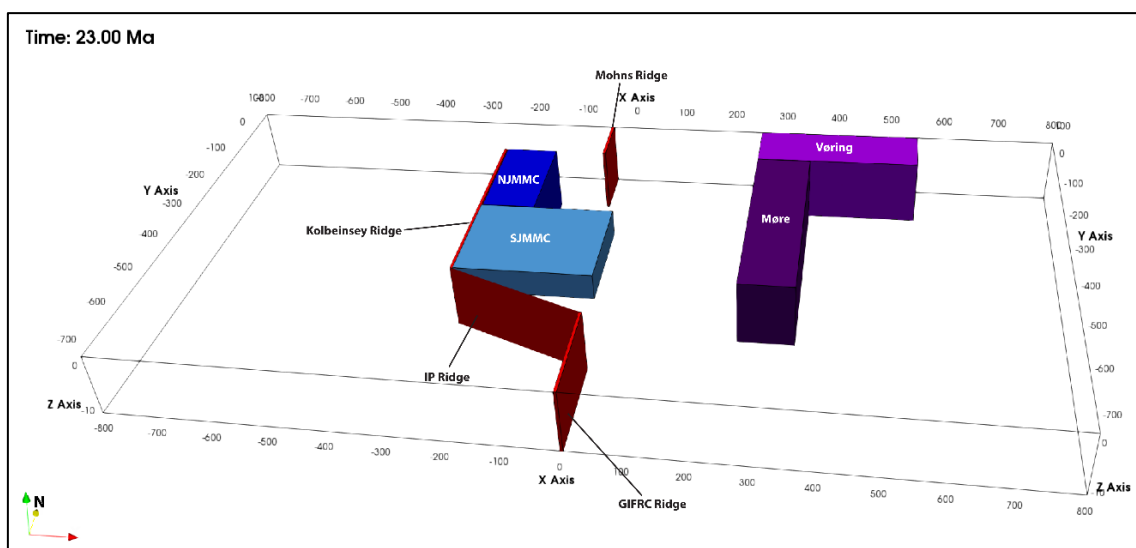

Figure 36. *Setup of Model 2 at the start of Stage 3 around 23 Ma showing the positions of the JMMC and Vøring and Møre basins with respect to the active ridges. The JMMC moves eastwards due to the generation of oceanic lithosphere at the Kolbeinsey Ridge during this stage.*

The JMMC moves eastwards as oceanic lithosphere is formed at the KR. As a result, the MR traverses the northern edge of the JMMC. The JMMC is heated from the northern and western edges by the MR and KR, respectively. It later cools down as it moves away from the influence of the spreading centres. The predicted present-day thermal structure has returned to background values in most of the interior of the JMMC with remnants of the ridge thermal input only present at the north-western edge (Figure 37). Maturity increases dramatically where the JMMC is in contact with the KR (Figure 38). Deviations of maturity levels w.r.t. to background values (ΔVR = 0.1 % Ro) covers all of the NJMMC during this stage. There is a minor perturbation in maturity levels at the south-western corner and western edge of the SJMMC. The perturbation extends ~60 km from the eastern edge of the SJMMC showing a slight reduction in extent as compared to the other stages.
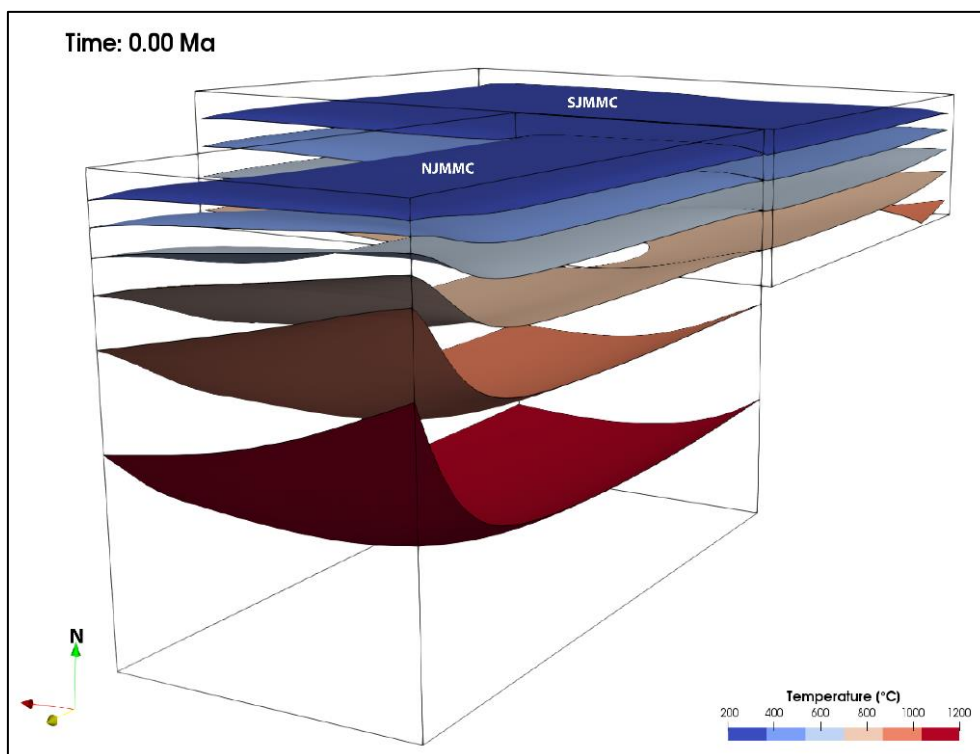
Figure 37. *Thermal structure of the JMMC at the end of Stage 3 at present day. Temperature isotherms in the interior have returned to background values with elevated values present only at the north-western edge. The ridges are not shown for visual clarity.*
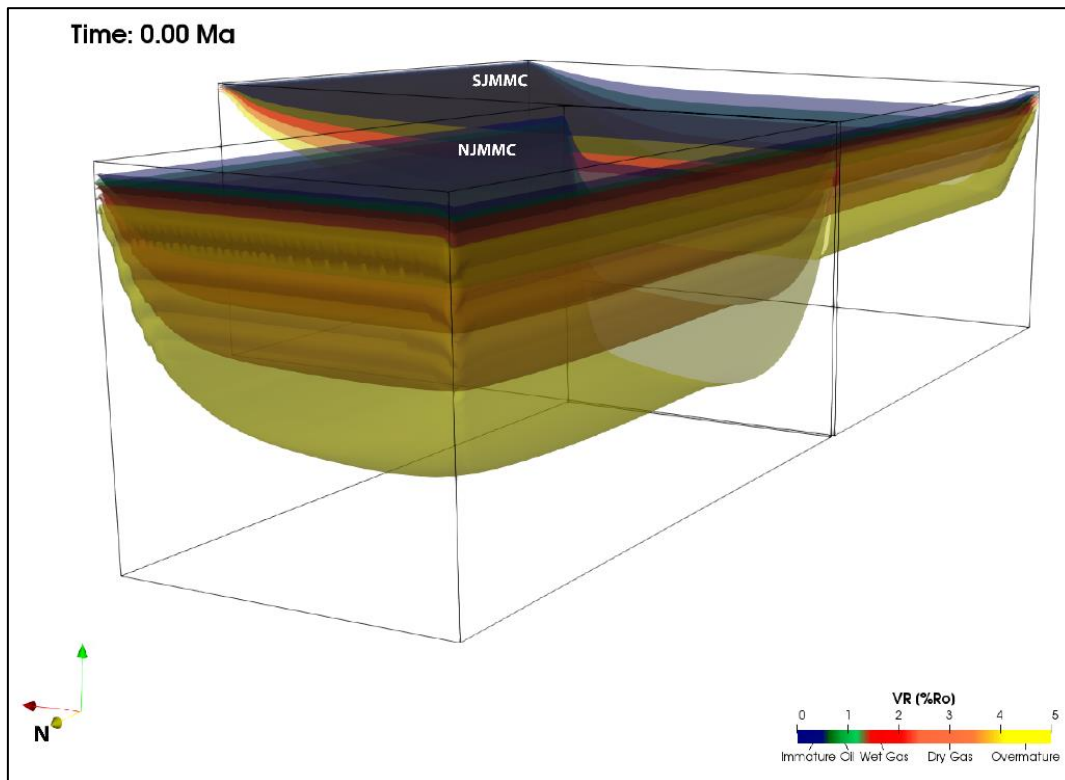
Figure 38. *Thermal maturity of the JMMC at the end of Stage 3 at present day. Maturity levels increase rapidly at the western JMMC margin due to the KR. The ridges are not shown for visual clarity.*

Heat flow values in the JMMC increase as it is heated by the KR from the western edge (see Figure 39). The NJMMC also receives heat from the MR as it passes by along the northern edge in the opposite direction from previous stages. Heat flow values reduce once the JMMC moves away from the spreading centres. Present-day heat flow values in the NJMMC reach a maximum of ~90 mW/m² in the north-western corner and decrease towards the south-eastern corner. The maximum value in the SJMMC is found in the south-western corner and is lower (~71 mW/m²) than the maximum in the NJMMC. Values decrease to background values towards the north-eastern corner.
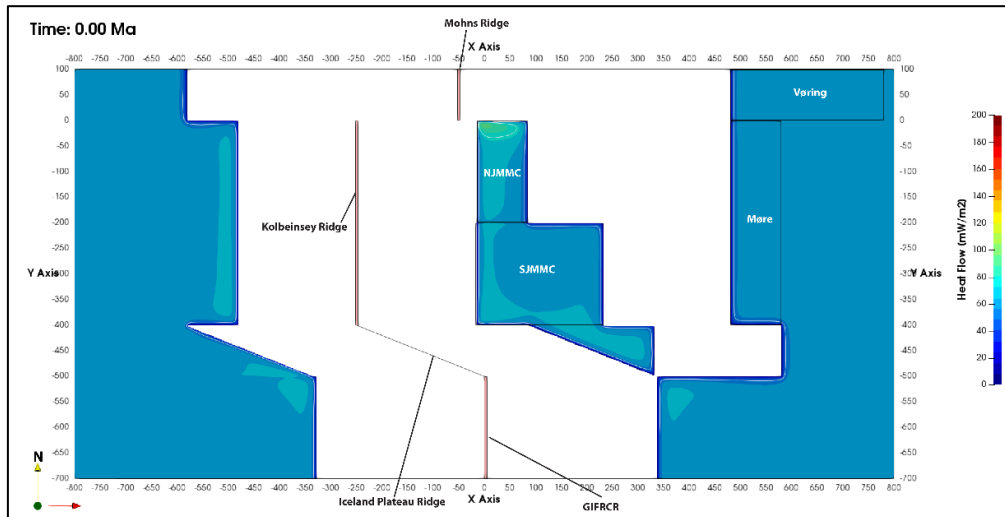
Figure 39. *Heat flow within the JMMC and the relative positions of the MR, KR, IPR and GIFRCR at the end of Stage 3 at present day. Contour values are between 50 and 200 mW/m² in steps of 25 mW/m².*

The entire western edge of the JMMC experiences (relative) uplift as it is heated by the KR (Figure 40). The northern edge of NJMMC experiences additional uplift due to the MR. The amount of uplift reduces as the JMMC moves away from the ridges and cools. The present-day uplift predicted by the model in the NJMMC is ~1200 m at the north-western edge and reduces down to ~150 m at the south-eastern edge. The present-day subsidence in the SJMMC is smallest at the south-western edge (around -2800 m) and largest in the northern part (around -3600 m). Note that the model does not take into account basin infill and erosion. Therefore, the prediction of uplift or subsidence should be realized as general tilt directions for the JMMC and not taken as absolute values.
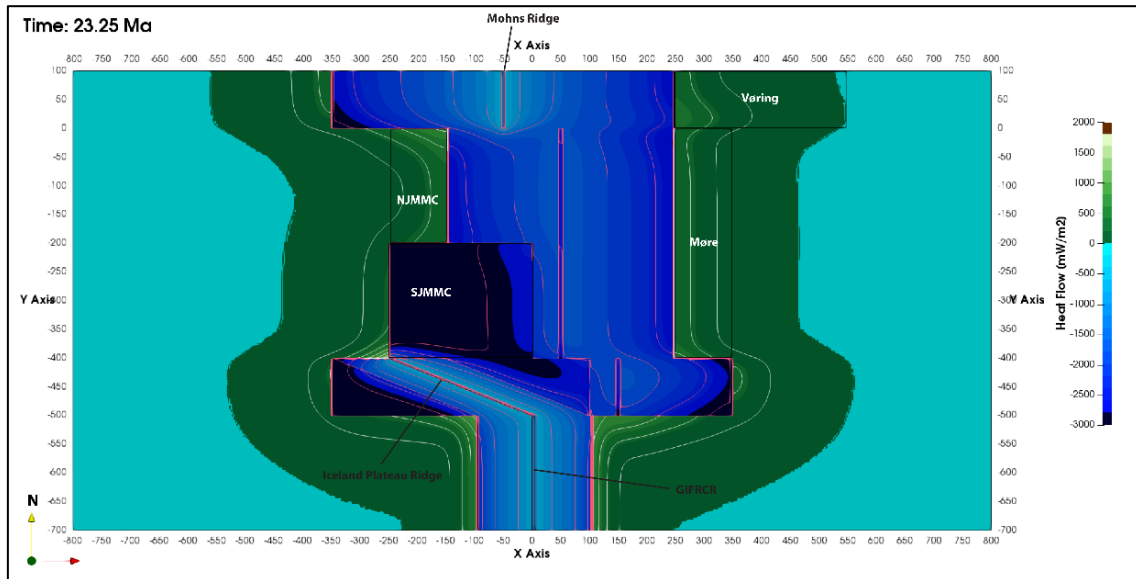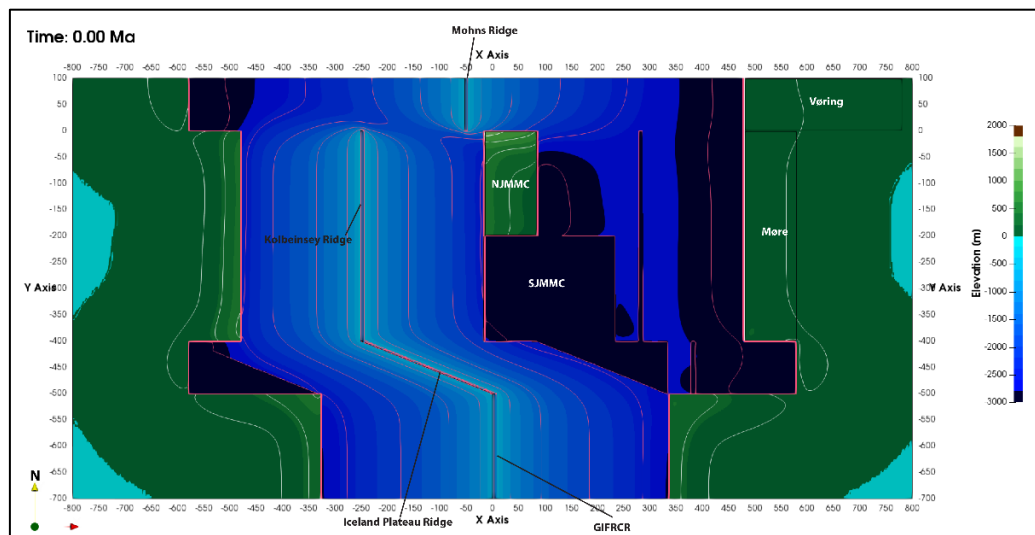

Figure 40. *Uplift within the JMMC and the relative positions of the MR, KR, IPR and GIFRCR at the end of Stage 2 at present day. Contour values for uplift are between 200 and 1600 m in steps of 200 m with an additional contour at 50 m. Contour values for subsidence are between -500 and -3000 m with an interval of -500 m.*

5.3   Model 3 (Reduced Rifting)

The reduced rifting model (see 4.2.3) is sub-divided into three stages defined by the initiation of spreading at the different ridges. The model iteration stages are listed in section 4.1.

5.3.1   Stage 1: 53 to 33 Ma

Initialization of the thermal structure and lithosphere geometry is the same as in the reference model (Figure 26). The AR and MR are active spreading centres during the first stage. The MR spreads symmetrically with a half-spreading rate of 1 cm/yr. The northern part of the AR in contact with the NJMMC spreads symmetrically with a half-spreading rate of 1 cm/yr. while the southern part of the AR in contact with the SJMMC spreads asymmetrically with half-spreading rate of 1 and 0.25 cm/yr. towards the east and west, respectively. The MR is centred 50 km west of model centre and extends 100 km south from the northern edge of the box. The southern tip of the MR initially lies at the north-western tip of the JMMC. The Vøring basin extends 300 km east of the MR and lies to the north of the JMMC. The AR is initially placed at the left flank of the JMMC and the Møre basin extends a further 100 km east of the AR and is 400 km long in the N-S direction. The northern and southern JMMC are, each, initially 100 km wide and 200 km long. The crust of the SJMMC is thinned from an initial thickness of 27 km to 20 km during this stage and is extended in the EW direction from an initial 100 km width to 250 km. The thinning and extension of the SJMMC per time step is done such that its western edge is always in line with that of the NJMMC.

The entire JMMC receives heat from the Ægir Ridge at its eastern edge, the influence of which decreases as the JMMC moves away and is abutted by increasingly colder and older oceanic lithosphere. The temperature in the SJMMC further increases as rifting progresses and hot mantle is brought up to shallower depths. The NJMMC also receives heat via its northern edge as it passes the Mohn´s Ridge. Maturity increases significantly and quickly to the maximum at the edges of the JMMC that are in contact with the hot ridge. Maturity of sediments inwards from the edges increases gradually as the thermal effects of the ridges propagates into the microcontinent. At the end of Stage 1, temperature isotherms at the eastern boundary of the NJMMC (AR influence) are almost flat due to the retreat of the AR by spreading while the isotherms are more uplifted towards the north-eastern edge of the NJMMC where the MR is closer (Figure 41). The isotherms of the SJMMC are relatively shallow compared with those in the NJMMC due to rifting which also results in somewhat increased temperatures at the boundary between the two regions of the JMMC.

Figure 41. *Thermal structure of the JMMC and the relative positions of the Mohn's and Ægir Ridges at the end of Stage 1 around 33.25 Ma.*
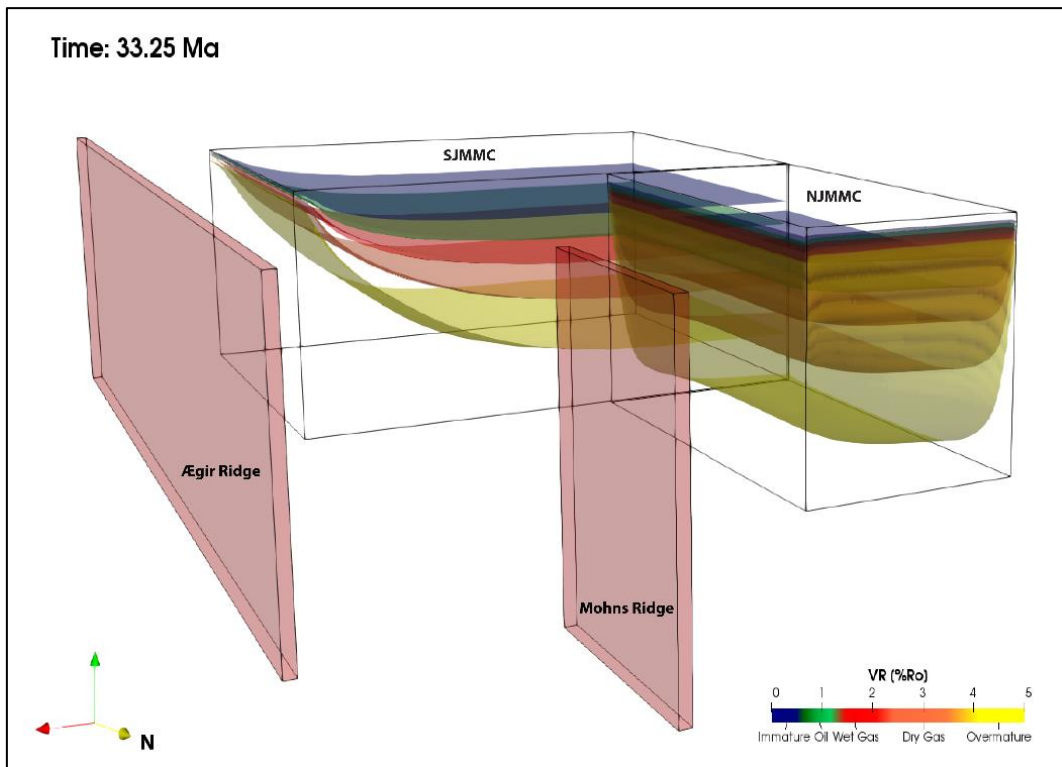
Figure 42. *Thermal maturity of the JMMC and the relative positions of the Mohn's and Ægir Ridges at the end of Stage 1 around 33.25 Ma. Maturity levels are highest at the eastern and northern boundaries through which heat from the ridges enters the JMMC. Additionally, the maturity isotherms are shallower in the SJMMC due to rifting.*

Thermal maturity concomitantly increases as temperature within the JMMC increases and follows the same pattern as the thermal input from the edges, i.e. highest maturity at the eastern and northern edges adjacent to the spreading centres at the end of Stage 1, with maturity levels falling back towards background levels towards the interior of the JMMC (Figure 42). Note that the maturity level in the SJMMC in this case is much higher due to heat input from rifting. Deviations of maturity levels w.r.t. to background values (ΔVR = 0.1 % Ro) in the NJMMC are observed ~60 km inwards from the eastern edge and the northern edge. The perturbation has also moved inwards from the southern edge of the NJMMC by ~20 km due to rifting in the SJMMC. The SJMMC shows a perturbation in maturity levels ~80 km away from the eastern edge. Note that maturity levels are calculated within the entire crustal section and not limited to the sediments.

Maximum heat flow values (~200 mW/m^2) occur within the continent close to the contact with the ridge where it is the hottest and spreads out away from there (Figure 43). Heat flow values decrease as the continent moves away from the spreading centres. An asymmetry develops in the regions with increased heat flow as they move away from the ridges during ocean spreading. The SJMMC shows heat flow values higher than the NJMMC due to rifting. An increase in heat flow (~75 mW/m^2) relative to the background value (59 mW/m^2) is observed in the region around the north-eastern corner of the NJMMC and in most of the SJMMC where it reaches a maximum of ~90 mW/m^2 at the end of Stage 1.

Figure 43. *Heat flow within the JMMC and the relative positions of the Mohn's and Ægir Ridges at the end of Stage 1 around 33.25 Ma. Contour values are between 50 and 200 mW/m^2 in steps of 25 mW/m^2.*

Maximum uplift (~2000 m) occurs within the continent close to the contact with the ridge where it is the hottest and spreads out away from there (Figure 44). Uplift decreases as the continents move away from the spreading centres and cool with an asymmetry developing in the uplifted continental lithosphere as they move away from the ridges during ocean spreading. The SJMMC subsides (max. ~1300 m) as it thins, bringing up hot mantle upwards

resulting in a dense lithospheric column relative to the initial continental configuration. The amount of subsidence is less than that in the previous reference model where rifting of the SJMMC results in a thinner crust. The eastern edge undergoes some uplift as heating by the Ægir Ridge is sufficient to counteract subsidence caused by rifting. Most of the NJMMC has experienced uplift by the end of Stage 1 except for a small region at the western edge.

Figure 44. *Uplift/subsidence within the JMMC and the relative positions of the Mohn's and Ægir Ridges at the end of Stage 1 around 33.25 Ma. Contour values for uplift are between 250 and 1750 m with a stepping of 250 m and an additional contour at 50 m. Contour values for subsidence are between -500 and -3000 m with a contour interval of -500 m.*

5.3.2   Stage 2: 33 to 23 Ma

The second stage is marked by the establishment of the IPR and GIFRCR with a half-spreading rate of 1 cm/yr. to the south of the JMMC and the simultaneous extinction of the Ægir ridge system (Figure 31). Rifting of the SJMMC ceases during this stage. The temperature within active spreading centres is 1333 °C. The GIFRCR is centred along the MR axis and extends 200 km north from the southern box edge with N-S orientation. The IPR extends diagonally from then south-western tip of the SJMMC to the northern tip of the GIFRCR diagonally splitting the Iceland Plateau.

The JMMC does not move with respect to the spreading centres during this stage. Only the SJMMC receives heat directly from the IPR from its south-western corner raising up isotherms in the region (Figure 45). The NJMMC receives some heat from its northern edge as relatively hot oceanic lithosphere formed at the Mohn's Ridge moves past it.

Maturity levels increase rapidly at and immediately around the south-western corner of SJMMC in contact with the northern tip of the IPR (Figure 46). Deviations of maturity levels w.r.t. to background values (ΔVR = 0.1 % Ro) move into the JMMC with time. This covers most of the NJMMC during this stage. There is a small perturbation in maturity levels at the south-

western corner of the JMMC. The perturbation extends ~75 km from the eastern edge of the SJMMC showing a slight reduction in extent as compared to Stage 1.
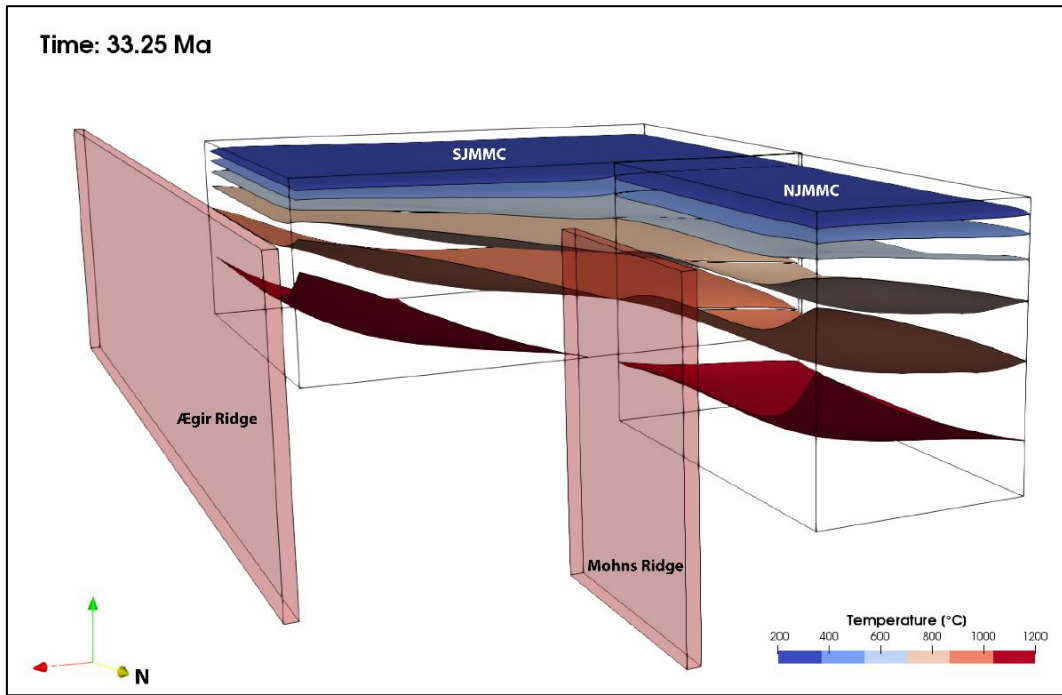

**Figure 45.** *Thermal structure of the JMMC and the relative positions of the Mohns and Iceland Plateau Ridges at the end of Stage 2 around 23.25 Ma. Temperature increases rapidly at the contact between the SJMMC and the IPR and the isotherms spread out from there. The GIFRCR is not shown for visual clarity.*
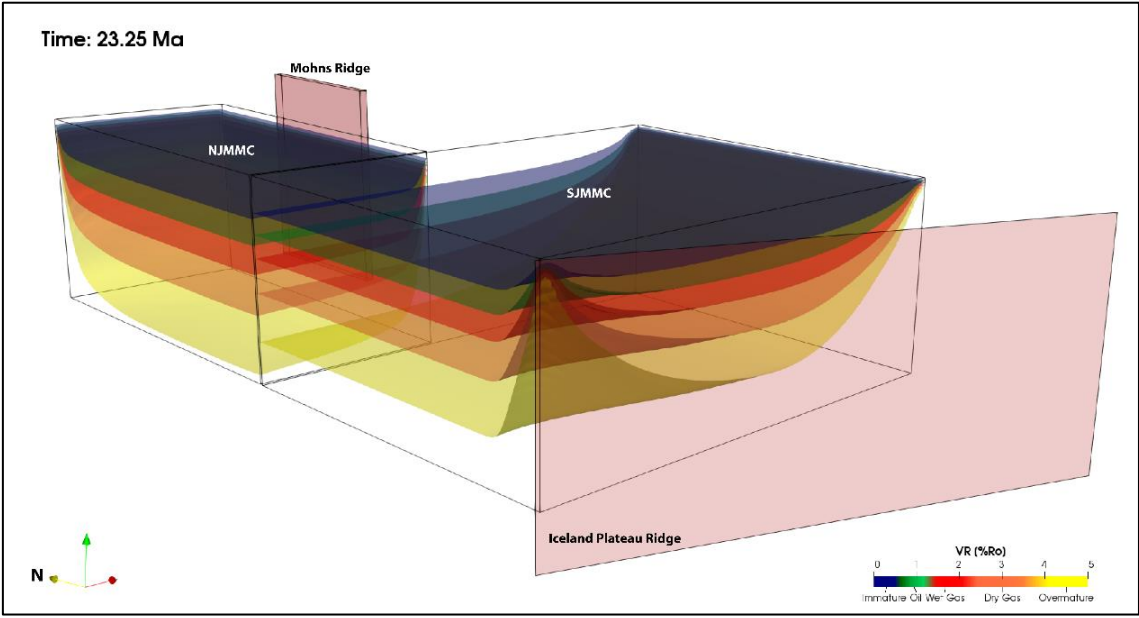
Figure 46. *Thermal maturity of the JMMC and the relative positions of the Mohn's and Iceland Plateau Ridges at the end of Stage 2 around 23.25 Ma. Maturity levels increase rapidly at the contact between the IPR and SJMMC and the region near it. The GIFRCR is not shown for visual clarity.*

Heat flow values in the NJMMC are slightly lower when compared to the previous stage but do not return to background values as it receives some heat from oceanic lithosphere generated by the MR (Figure 47). Maximum heat flow values are recorded at the north-eastern region and are only slightly higher (~69 mW/m^2) than the background value at the end of this stage. Heat flow values in most of the SJMMC decrease as it cools after rifting. Values close to the south-western corner increase due to heat input from the IPR but do not propagate significantly inwards due to the short time frame of this stage. Values of ~78 mW/m^2 are observed in the model close to the eastern edge.
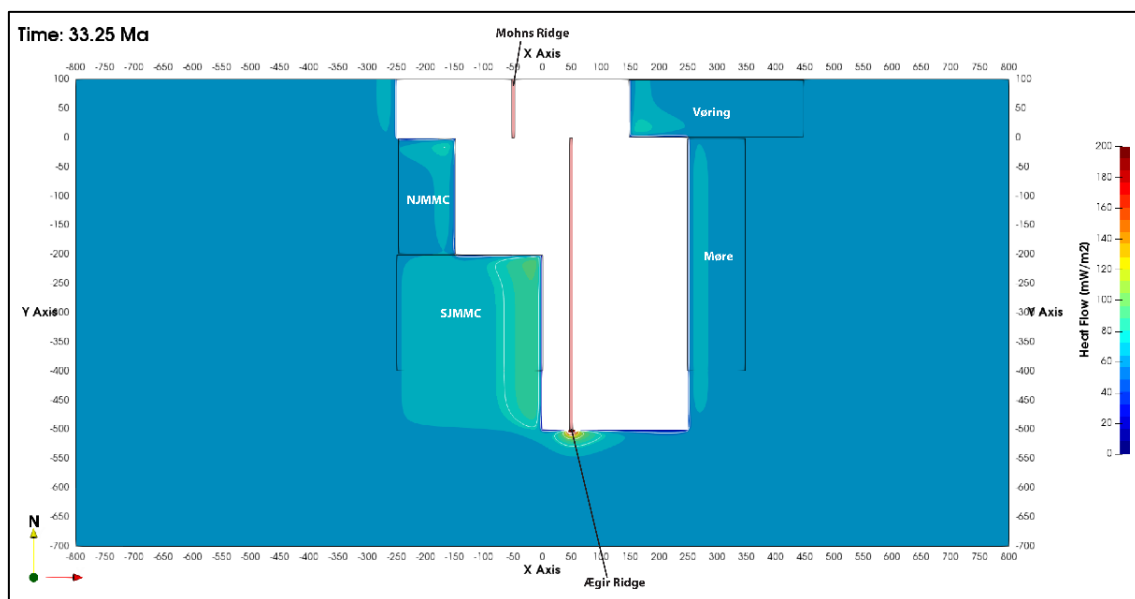

Figure 47. *Heat flow within the JMMC and the relative positions of the MR, IPR and GIFRCR at the end of Stage 2 around 23.25 Ma. Contour values are between 50 and 200 mW/m^2 in steps of 25 mW/m^2.*

The entire NJMMC has experienced uplift at the end of this stage with most of the region experiencing more than 50 m uplift (Figure 48). The highest amount of uplift (~800 m) is recorded at the north-eastern corner. Uplift decreases from east to west. The SJMMC subsides further as most of it cools during this stage. Only the south-western edge of the SJMMC records relative uplift as it heated by the IPR.
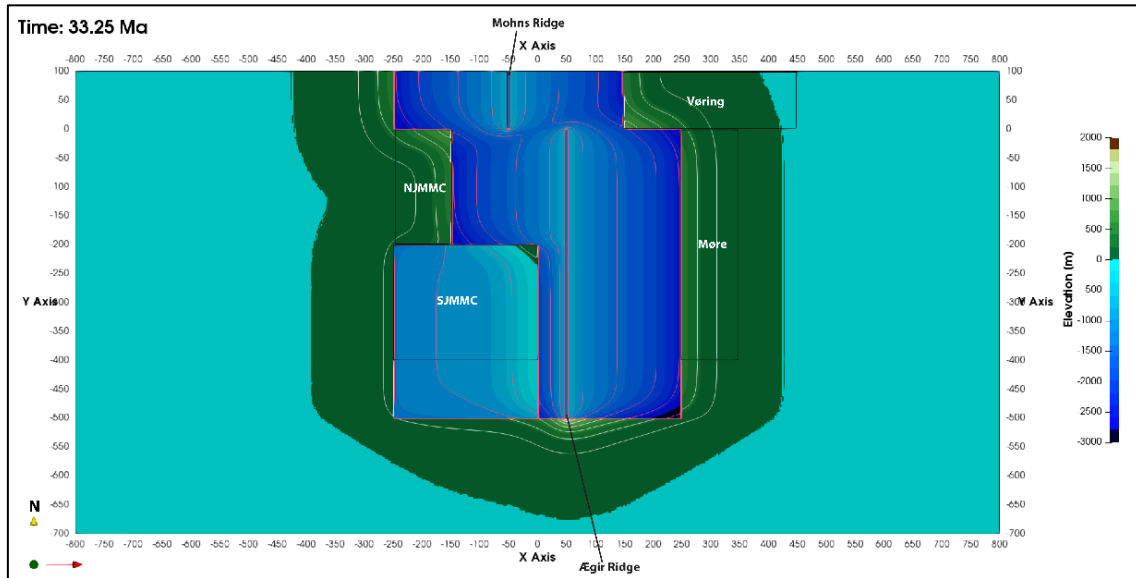
Figure 48. *Uplift/subsidence within the JMMC and the relative positions of the MR, IPR and GIFRCR at the end of Stage 2 around 23.25 Ma. Contour values for uplift are between 200 and 1600 m in steps of 200 m with an additional contour at 50 m. Contour values for subsidence are between -500 and -3000 m with a contour interval of -500 m.*

5.3.3   Stage 3: 23 to 0 Ma

The third and final stage is marked by the establishment of the Kolbeinsey Ridge with a half-spreading rate of 1 cm/yr. to the west of the JMMC which moves the microcontinent eastwards (Figure 36). The KR runs along the entire western margin of the JMMC and has N-S orientation.

The JMMC moves eastwards as oceanic lithosphere is formed at the KR. As a result, the MR traverses the northern edge of the JMMC. The JMMC is heated from the northern and western edge by the MR and KR, respectively. It later cools down as it moves away from the influence of the spreading centres. The predicted present-day thermal structure has returned to background values in most of the interior of the JMMC with remnants of the ridge thermal input only present at the north-western edge (Figure 49). Maturity increases dramatically where the JMMC is in contact with the KR (Figure 50). Deviations of maturity levels w.r.t. to background values (ΔVR = 0.1 % Ro) covers all of the NJMMC during this stage. Deviations of maturity levels extends by a few km into the SJMMC at the south-western corner and western edge. The perturbation extends ~70 km from the eastern edge of the SJMMC showing a slight reduction in extent as compared to the other stages.
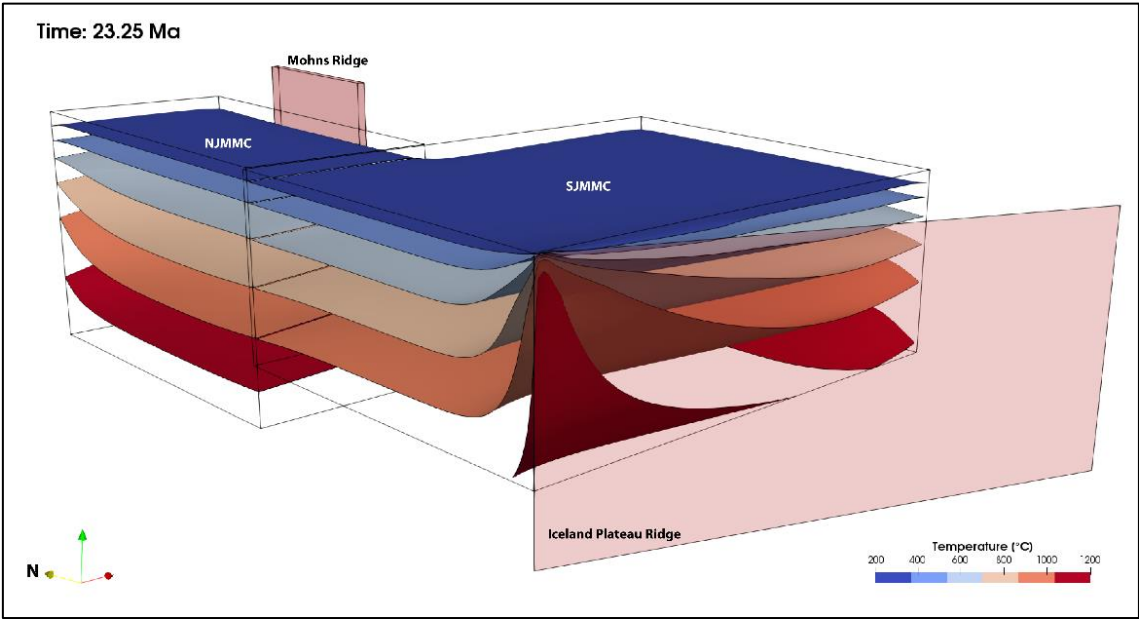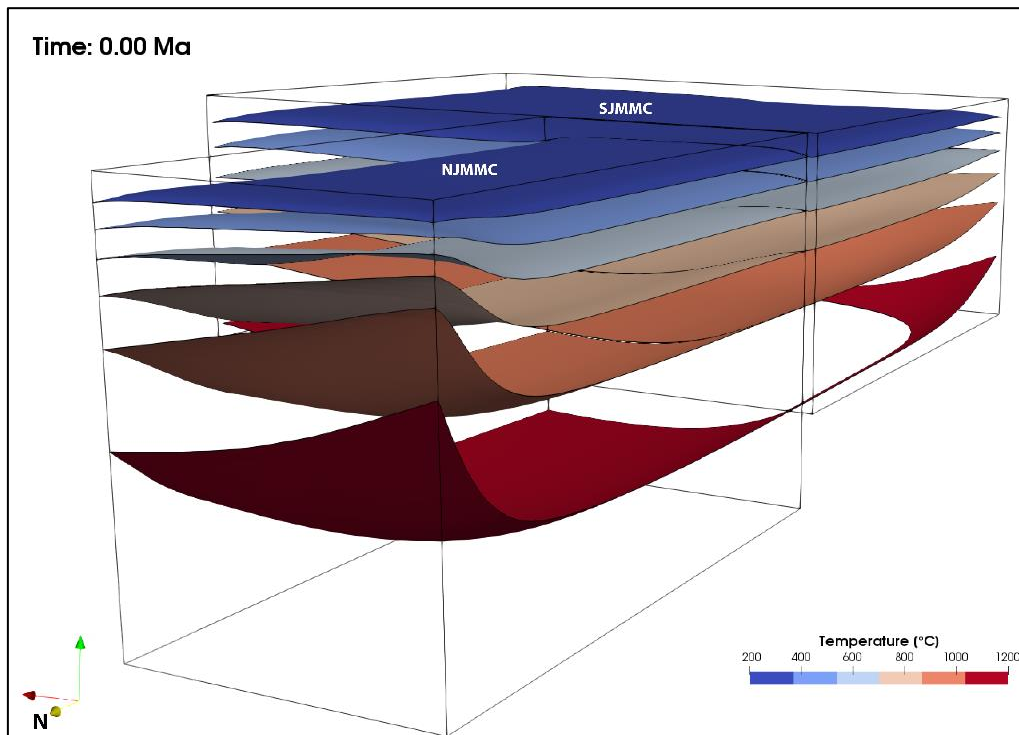
Figure 49. *Thermal structure of the JMMC at the end of Stage 3 at present day. Temperature isotherms in the interior have returned to background values with elevated values present only at the north-western edge. The ridges are not shown for visual clarity.*
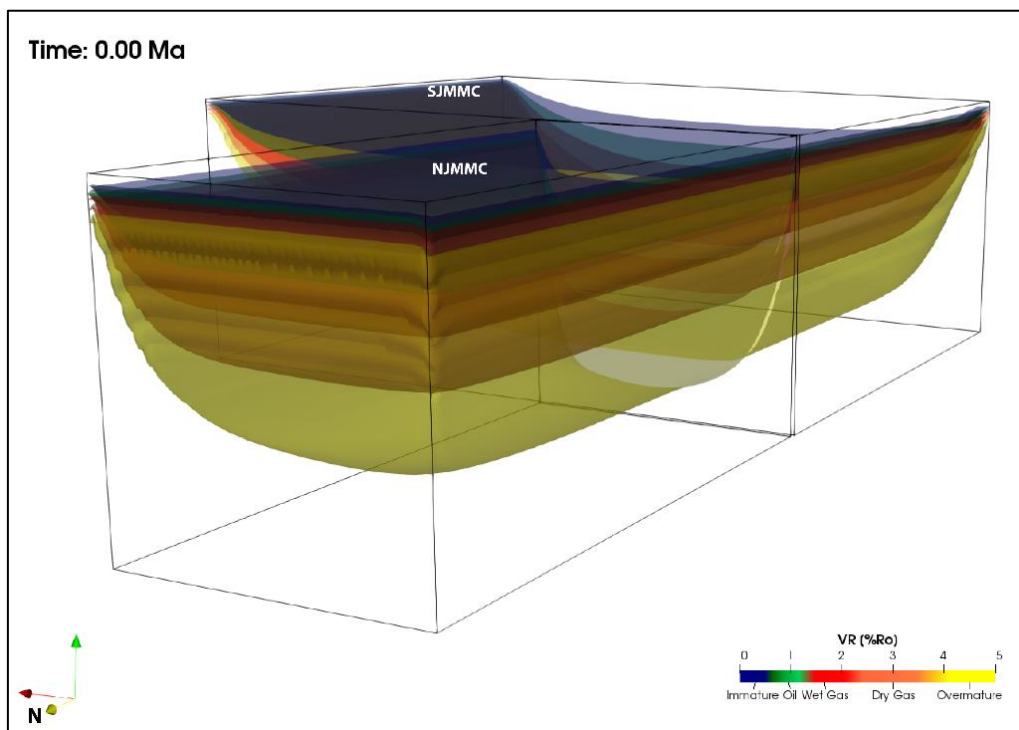
Figure 50. *Thermal maturity of the JMMC at the end of Stage 3 at present day. Maturity levels increases rapidly at the western JMMC margin due to the KR. The ridges are not shown for visual clarity.*

Heat flow values in the JMMC increase as it is heated by the KR from the western edge (see Figure 51). The NJMMC also receives heat from the MR as it passes by along the northern edge in the opposite direction from previous stages. Heat flow values reduce once the JMMC moves away from the spreading centres. Present-day heat flow values in the NJMMC reach a maximum of ~90 mW/m² in the north-western corner and decreases towards the south-eastern corner. The maximum value in the SJMMC is found in the south-western corner and is lower (~71 mW/m²) than the maximum in the NJMMC. Values decrease to background values towards the north-eastern corner.
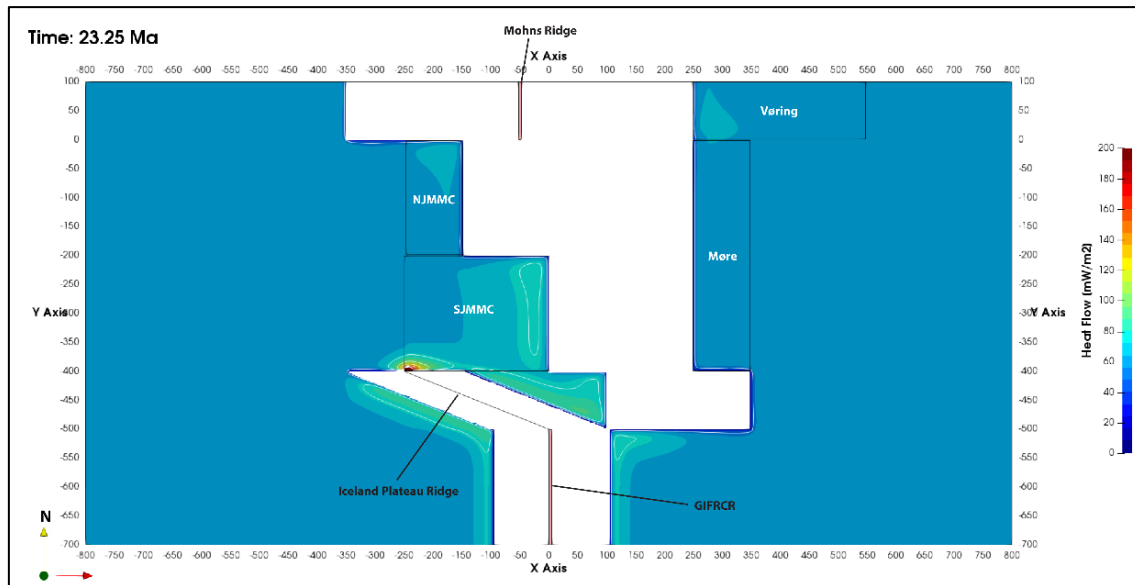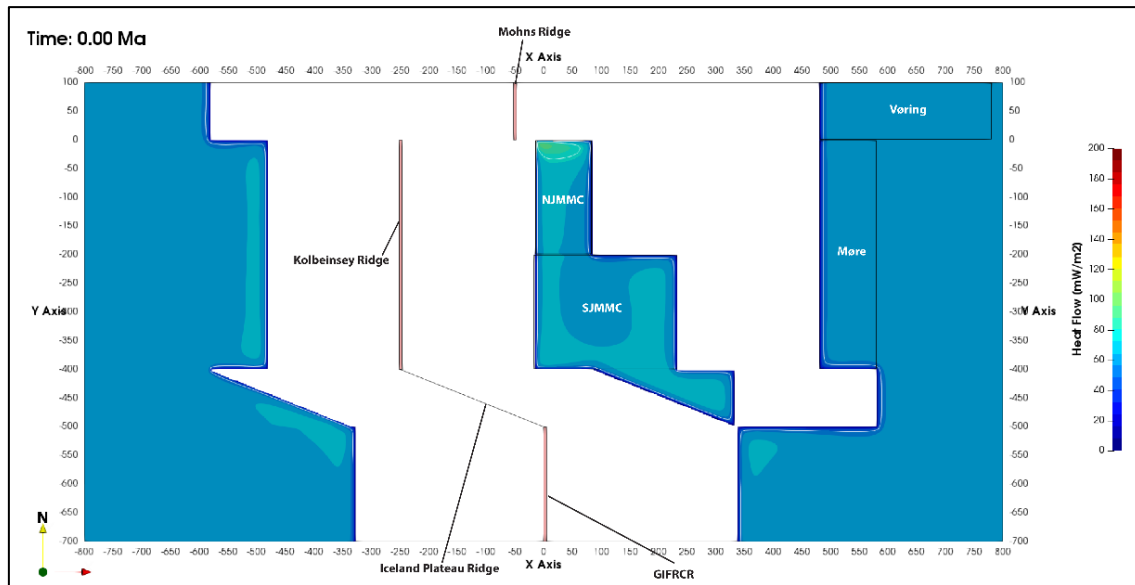

Figure 51. *Heat flow within the JMMC and the relative positions of the MR, KR, IPR and GIFRCR at the end of Stage 3 at present day. Contour values are between 50 and 200 mW/m² in steps of 25 mW/m².*

The entire western edge of the JMMC experiences (relative) uplift as it is heated by the KR (Figure 52). The northern edge of NJMMC experiences additional uplift due to the MR. The amount of uplift reduces as the JMMC moves away from the ridges and cools. The present-day uplift predicted by the model in the NJMMC is ~1100 m at the north-western edge and reduces down to ~110 m at the south-eastern edge. The present-day subsidence in the SJMMC is lowest at the south-western edge (~400 m) and highest in the northern part (~1250 m). Note that the model does not take into account basin infill and erosion. Therefore, the prediction of uplift or subsidence should be realized as general tilt directions for the JMMC and not taken as absolute values.
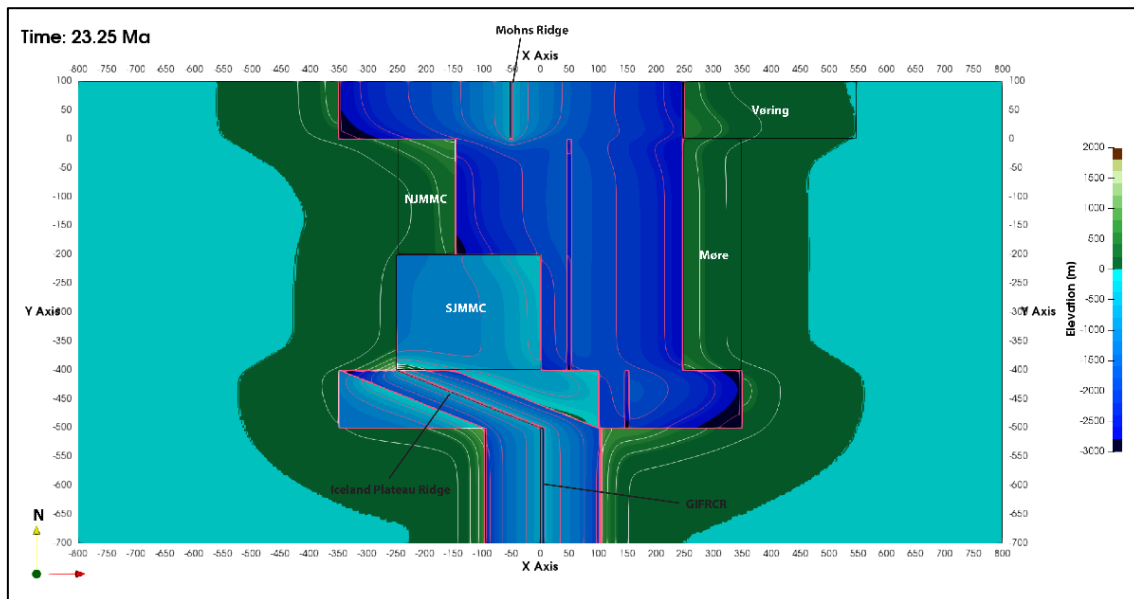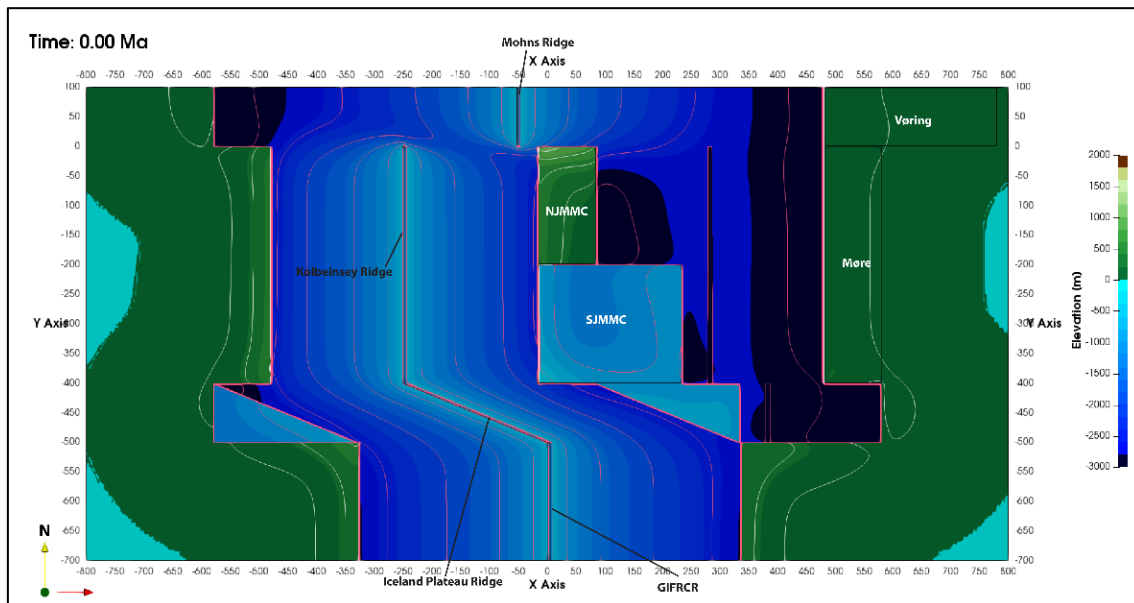
Figure 52. *Uplift within the JMMC and the relative positions of the MR, KR, IPR and GIFRCR at the end of Stage 3 at present day. Contour values for uplift are between 200 and 1600 m in steps of 200 m with an additional contour at 50 m. Contour values for subsidence are between -500 and -3000 m with a contour interval of -500 m.*

5.4 Model 4 (Increased Mantle Potential Temperature)

The increased mantle potential temperature model (see 4.2.4) addresses the final stage of the project´s calibration and is sub-divided into three stages defined by the initiation of spreading at the different ridges. This model considers the complex dual-breakup scenario and the possible influence of the Iceland plume.

5.4.1 Stage 0: 61 to 53 Ma

Initialization of the thermal structure and lithosphere geometry is the same as in the reference model. The model is run from 61 to 53 Ma during which the bottom boundary temperature is changed based on the mantle potential temperature curve and the thermal structure of the entire domain is calculated. The temperature in the lower part of the model (>80 km depth) increases due to relatively high bottom temperature but does not propagate to shallow depths during this stage.

5.4.2 Stage 1: 53 to 33 Ma

The first stage is marked by the establishment of the Ægir ridge system separating the mid-Norwegian Vøring and Møre basins from the Central East Greenland margin. The MR and AR are both active during this stage. The MR spreads symmetrically with a half-spreading rate of 1 cm/yr. The northern part of the AR in contact with the NJMMC spreads symmetrically with a half-spreading rate of 1 cm/yr. while the southern part of the AR in contact with the SJMMC spreads asymmetrically with half-spreading rate of 1 and 0.25 cm/yr. towards the east and west, respectively. The MR is centred 50 km west of model centre and extends 100 km south from the northern edge of the box. The southern tip of the MR initially lies at the north-western

tip of the JMMC. The Vøring basin extends 300 km east of the MR and lies to the north of the JMMC. The AR is initially placed at the left flank of the JMMC and the Møre basin extends a further 100 km east of the AR and is 400 km long in the N-S direction. The northern and southern JMMC are, each, initially 100 km wide and 200 km long. The crust of the SJMMC is thinned from an initial thickness of 27 km to ~11 km during this stage and is extended in the EW direction from an initial 100 km width to 250 km. The thinning and extension of the SJMMC per time step is done such that its western edge is always in line with that of the NJMMC.

Figure 53. *Thermal structure of the JMMC and the relative positions of the Mohn's and Ægir Ridges at the end of Stage 1 around 33.25 Ma.*
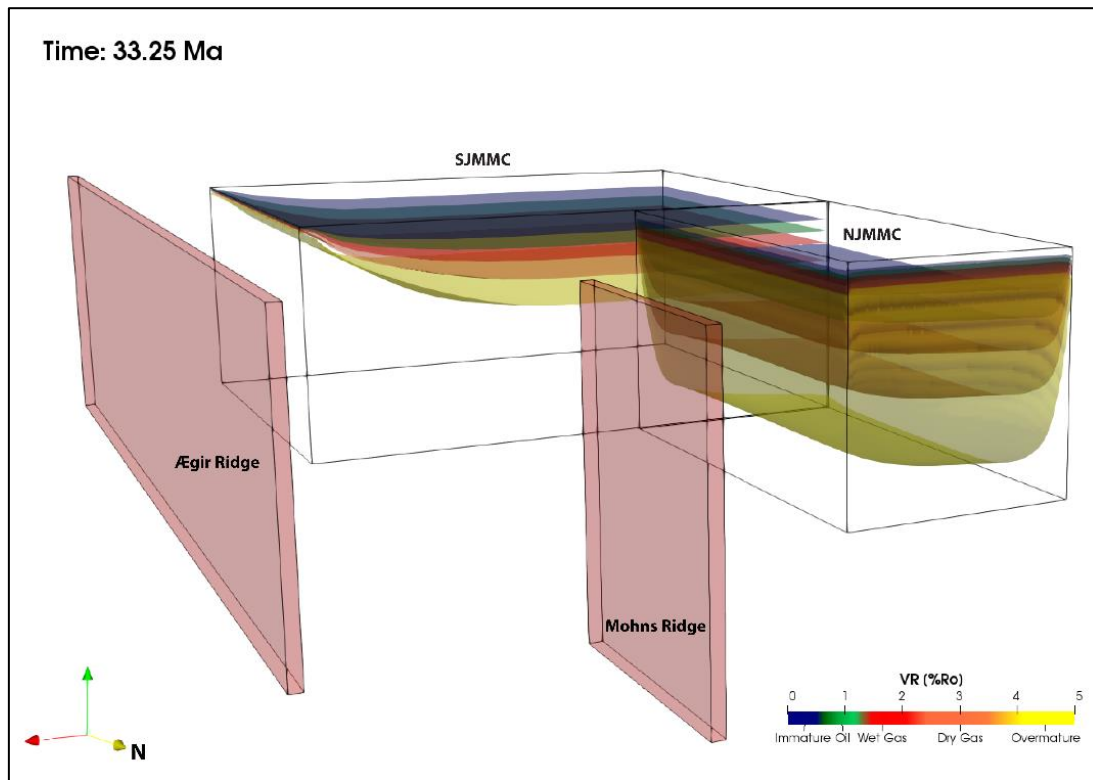
Figure 54. *Thermal maturity of the JMMC and the relative positions of the Mohn's and Ægir Ridges at the end of Stage 1 around 33.25 Ma. Maturity levels are highest at the eastern and northern boundaries through which heat from the ridges enters the JMMC. Additionally, the maturity isotherms are shallower in the SJMMC due to rifting.*

The entire JMMC receives heat from the Ægir Ridge at its eastern edge, the influence of which decreases as the JMMC moves away and is affected by increasingly colder and older oceanic lithosphere. The temperature in the SJMMC further increases as rifting progresses and hot mantle is brought up to shallower depths. The NJMMC also receives heat via its northern edge as it passes the Mohn's Ridge. Maturity increases significantly and quickly to the maximum at the edges of the JMMC that are in contact with the hot ridge. Maturity of sediments inwards from the edges increases gradually as the thermal effects of the ridges propagates into the microcontinent. At the end of Stage 1, temperature isotherms at the eastern boundary of the entire JMMC (AR influence) are almost flat due to the retreat of the AR by spreading while the isotherms are more uplifted towards the north-eastern edge of the NJMMC where the MR is closer (Figure 53). The isotherms are the SJMMC are much shallower than those in the NJMMC due to rifting which also results in somewhat increased temperatures at the boundary between the two regions of the JMMC.

Thermal maturity concomitantly increases as temperature within the JMMC increases and follows the same pattern as the thermal input from the edges, i.e. highest maturity is observed at the eastern and northern edges adjacent to the spreading centres at the end of Stage 1 with maturity levels falling back towards background levels towards the interior of the JMMC (Figure 54). Note that the maturity level in the SJMMC in this case is much higher due to heat input from rifting. Deviations of maturity levels w.r.t. to background values (ΔVR = 0.1 % Ro) in the NJMMC are observed ~60 km inwards from the eastern edge and the northern edge. The

perturbation has also moved inwards from the southern edge of the NJMMC by ~18 km due to rifting in the SJMMC. The SJMMC shows a perturbation in maturity levels ~65 km away from the eastern edge. Note that maturity levels are calculated within the entire crustal section and not limited to the sediments.

Maximum heat flow values (~200 mW/m²) occur within the continent close to the contact with the ridge where it is the hottest and spreads out away from there (Figure 55). Heat flow values decrease as the continent moves away from the spreading centres. An asymmetry develops in the regions with increased heat flow as they move away from the ridges during ocean spreading. The SJMMC shows heat flow values higher than the NJMMC due to rifting. An increase in heat flow (~75 mW/m²) relative to the background value (59 mW/m²) is observed in the region around the north-eastern corner of the NJMMC and in most of the SJMMC where it reaches a maximum of ~105 mW/m² at the end of Stage 1.

Note that since the reference column has a bottom temperature of 1333 °C, the entire continental lithosphere is uplifted because of variation in the bottom temperature. The amount of background uplift experienced at the end of Stage 1 is ~188 m. Maximum uplift (~2000 m) occurs within the continent close to the contact with the ridge, where it is the hottest, while the uplift decreases away from the ridge centre (Figure 56). Uplift decreases as the continents move away from the spreading centres and cool with an asymmetry developing in the uplifted continental lithosphere as they move away from the ridges during ocean spreading. The SJMMC subsides significantly (>3000 m) as it thins bringing up hot mantle upwards resulting in a dense lithospheric column relative to the initial continental configuration. Most of the NJMMC has experienced uplift by the end of Stage 1 except for a small region at the western edge.

Figure 55. *Heat flow within the JMMC and the relative positions of the Mohn's and Ægir Ridges at the end of Stage 1 around 33.25Ma. Contour values are between 50 and 200 mW/m² in steps of 25 mW/m².*
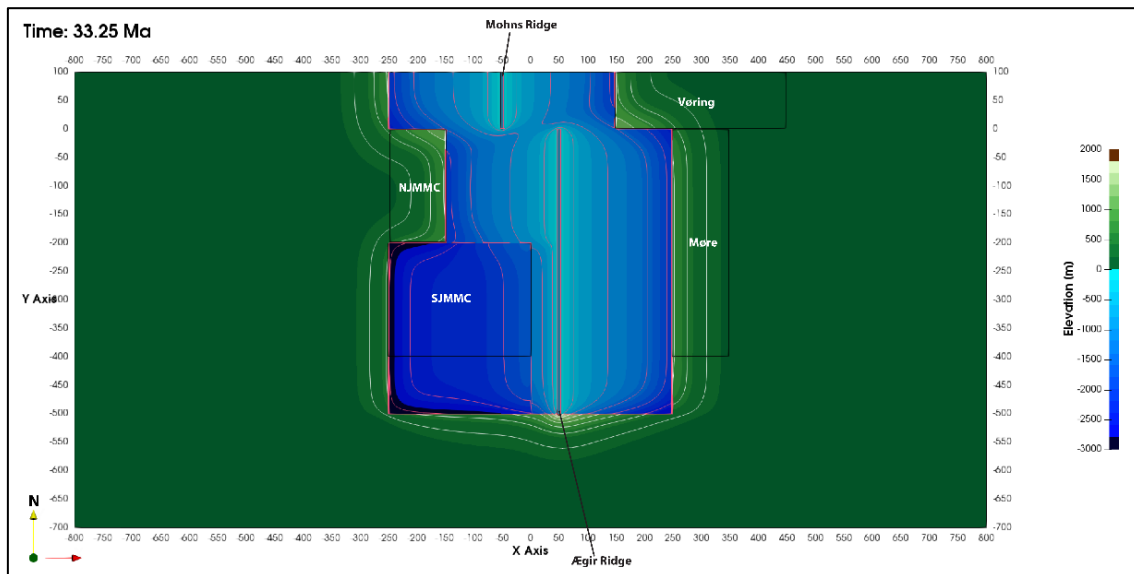
Figure 56. *Uplift/subsidence within the JMMC and the relative positions of the Mohn's and Ægir Ridges at the end of Stage 1 around 33.25Ma. Contour values for uplift are between 250 and 1750 m with a stepping of 250 m and an additional contour at 50 m. Contour values for subsidence are between -500 and -3000 m with a contour interval of -500 m.*

5.4.3 Stage 2: 33 to 23 Ma

The second stage is marked by the establishment of the IPR and GIFRCR with a half-spreading rate of 1 cm/yr. to the south of the JMMC and the simultaneous extinction of the Ægir ridge system (Figure 31). Rifting of the SJMMC ceases during this stage. The GIFRCR is centred along the MR axis and extends 200 km north from the southern box edge with N-S orientation. The IPR extends diagonally from then south-western tip of the SJMMC to the northern tip of the GIFRCR diagonally splitting the Iceland Plateau.

The JMMC does not move with respect to the spreading centres during this stage. Only the SJMMC receives heat directly from the IPR from its south-western corner bringing up isotherms in the region (Figure 57). The NJMMC receives some heat from its northern edge as relatively hot oceanic lithosphere formed at the Mohn's Ridge moves past it. Maturity levels increase rapidly at and immediately around the south-western corner of SJMMC in contact with the northern tip of the IPR (Figure 58). Deviations of maturity levels w.r.t. to background values (ΔVR = 0.1 % Ro) move into the JMMC with time. This covers most of the NJMMC during this stage. There is a small perturbation in maturity levels at the south-western corner of the JMMC. The perturbation extends ~62 km from the eastern edge of the SJMMC showing a slight reduction in extent as compared to Stage 1.

Heat flow values in the NJMMC are slightly lower when compared to the previous stage but do not return to background values as it receives some heat from oceanic lithosphere generated by the MR (Figure 59). Maximum heat flow values are recorded at the north-eastern region and are only slightly higher (~70 mW/m²) than the background value at the end of this stage. Heat flow values in most of the SJMMC decrease as it cools after rifting. Values close to the south-western corner increase due to heat input from the IPR but do not propagate

significantly inwards due to the short time frame of this stage. Values of ~84 mW/m² are recorded close to the eastern edge.
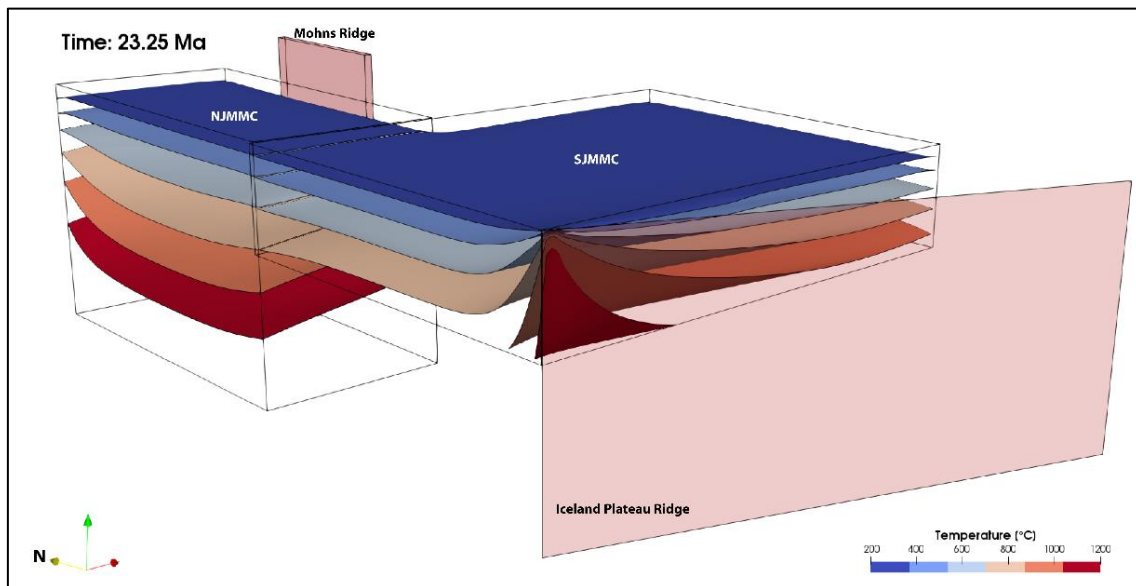
Figure 57. *Thermal structure of the JMMC and the relative positions of the Mohn's and Iceland Plateau Ridges at the end of Stage 2 around 23.25Ma. Temperature increases rapidly at the contact between the SJMMC and the IPR and the isotherms spread out from there. The GIFRCR is not shown for visual clarity.*
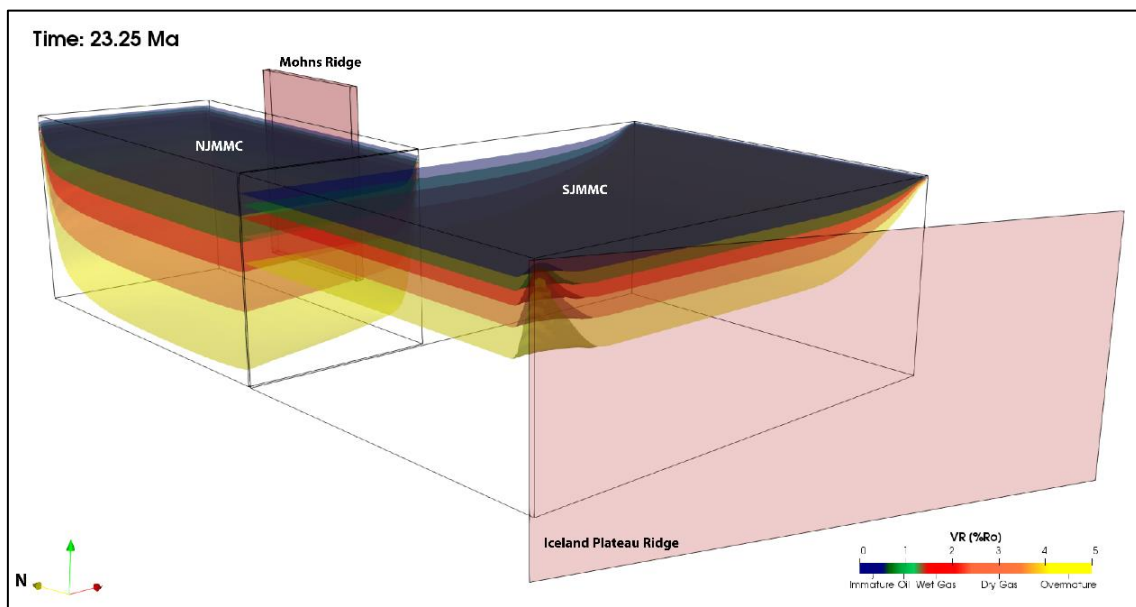
Figure 58. *Thermal maturity of the JMMC and the relative positions of the Mohn's and Iceland Plateau Ridges at the end of Stage 2 around 23.25Ma. Maturity levels increase rapidly at the contact between the IPR and SJMMC and the region near it. The GIFRCR is not shown for visual clarity.*
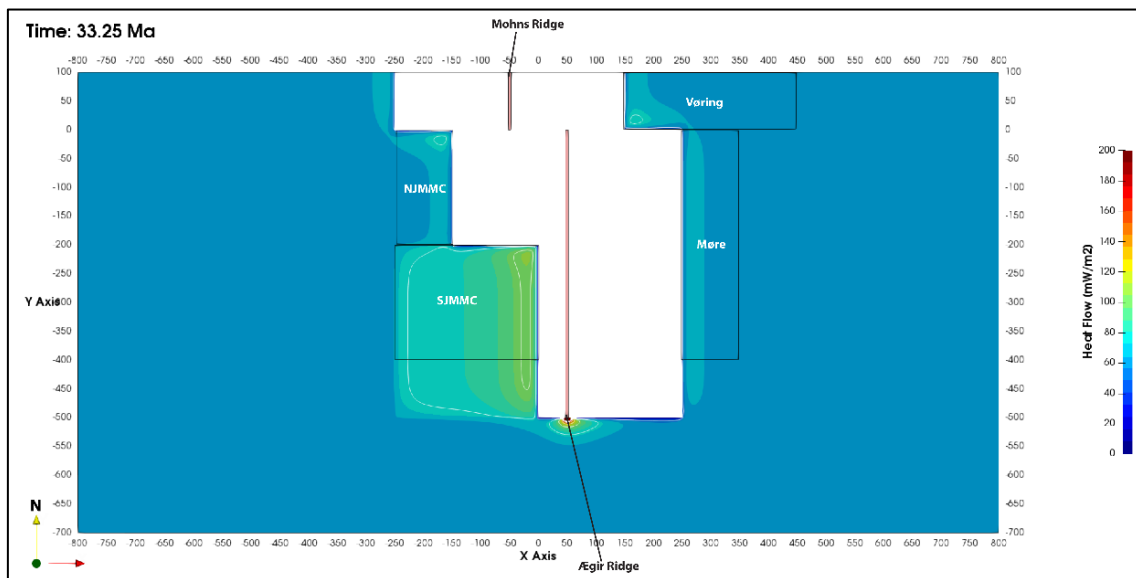
Figure 59. *Heat flow within the JMMC and the relative positions of the MR, IPR and GIFRCR at the end of Stage 2 around 23.25Ma. Contour values are between 50 and 200 mW/m² in steps of 25 mW/m².*

Note that since the reference column has a bottom temperature of 1333 °C the entire continental lithosphere is uplifted because of variation in the bottom temperature. The amount of background uplift experienced at the end of Stage 2 is ~196 m. The entire NJMMC has experienced uplift at the end of this stage with most of the region experiencing more than 200 m uplift (Figure 60). The highest amount of uplift (~1100 m) is recorded at the north-eastern corner. Uplift decreases from east to west. The SJMMC subsides further as most of it cools during this stage. Only the south-western edge of the SJMMC records relative uplift (w.r.t. the rest of the SJMMC) as it is heated by the IPR.

Figure 60. *Uplift/subsidence within the JMMC and the relative positions of the MR, IPR and GIFRCR at the end of Stage 2 around 23.25Ma. Contour values for uplift are between 200 and 1600 m in steps of 200 m with an additional contour at 50 m. Contour values for subsidence are between -500 and -3000 m with a contour interval of -500 m.*

5.4.4   Stage 3: 23 to 0 Ma

The third and final stage is marked by the establishment of the Kolbeinsey Ridge with a half-spreading rate of 1 cm/yr. to the west of the JMMC which moves the microcontinent eastwards (Figure 36). The KR runs along the entire western margin of the JMMC and has N-S orientation.

The JMMC moves eastwards as oceanic lithosphere is formed at the KR. As a result, the MR traverses the northern edge of the JMMC. The JMMC is heated from the northern and western edge by the MR and KR, respectively. It later cools down as it moves away from the influence of the spreading centres. The predicted present-day thermal structure has returned to background values in most of the interior of the JMMC with remnants of the ridge thermal input only present at the north-western edge (Figure 61). Maturity increases dramatically where the JMMC is in contact with the KR (Figure 62). Deviations of maturity levels w.r.t. to background values cover ($\Delta VR = 0.1$ % Ro) all of the NJMMC during this stage. There is a minor perturbation in maturity levels at the south-western corner and western edge of the SJMMC. The perturbation extends ~60 km from the eastern edge of the SJMMC showing a slight reduction in extent as compared to the other stages.
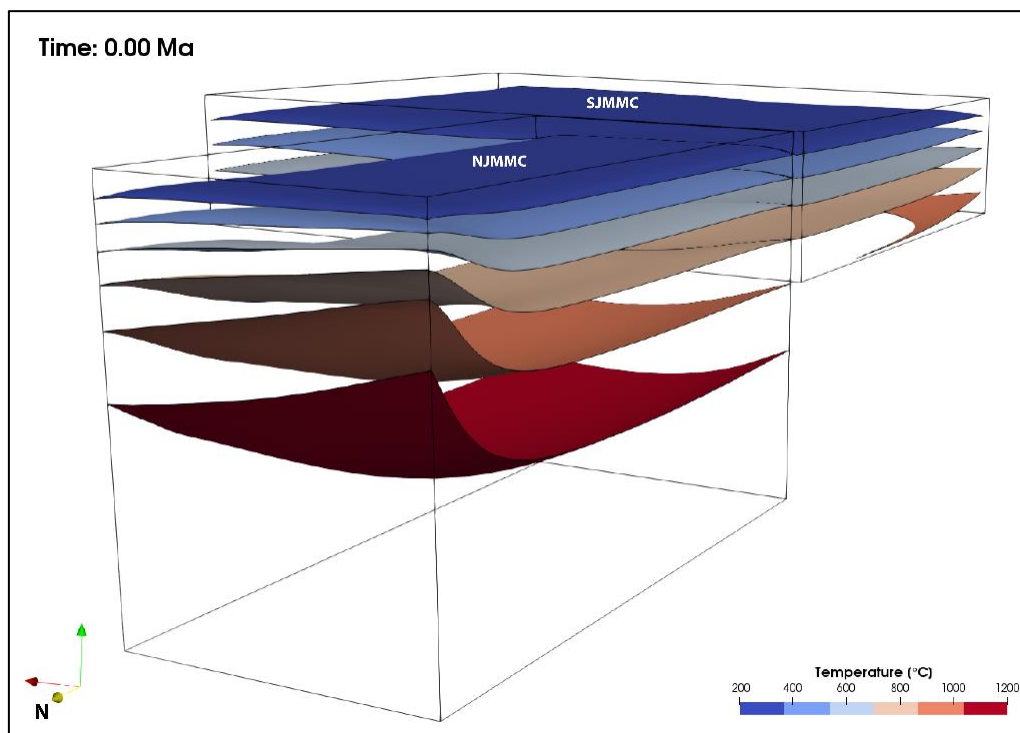
Figure 61. *Thermal structure of the JMMC at the end of Stage 3 at the present. Temperature isotherms in the interior have returned to background values with elevated values present only at the north-western edge. The ridges are not shown for visual clarity.*
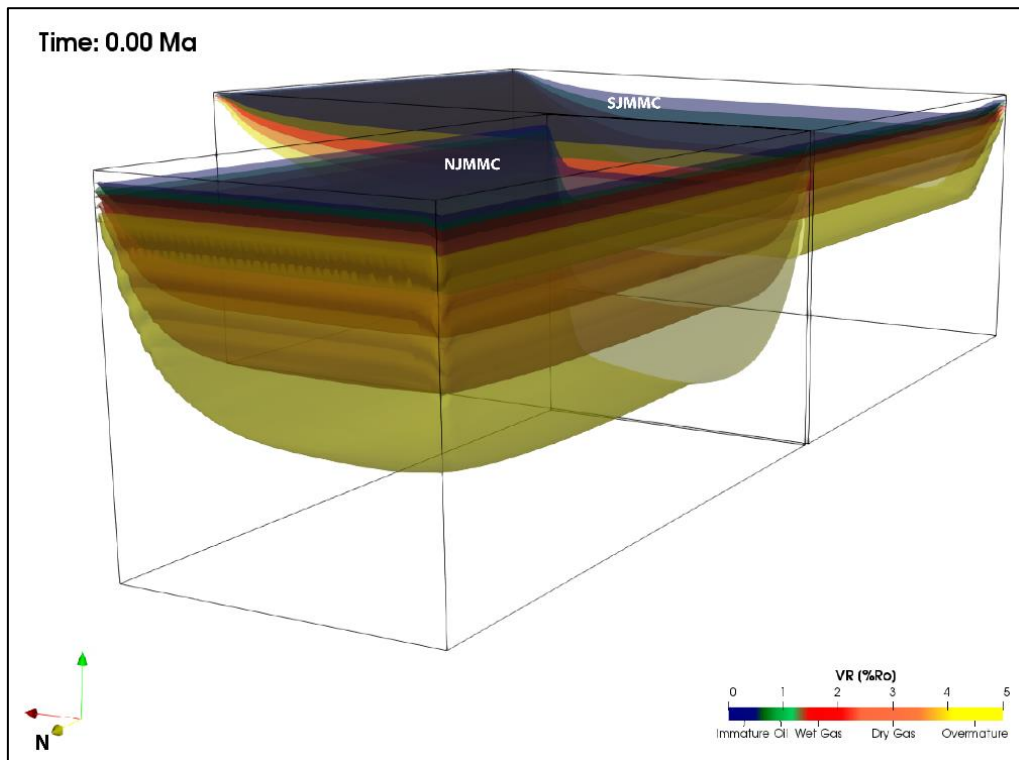
Figure 62. *Thermal maturity of the JMMC at the end of Stage 3 at the present. Maturity levels increase rapidly at the western JMMC margin due to the KR. The ridges are not shown for visual clarity. Note that only the upper 10 km of the JMMC is shown with vertical exaggeration.*

Heat flow values in the JMMC increase as it is heated by the KR from the western edge (see Figure 63). The NJMMC also receives heat from the MR as it passes by along the northern edge in the opposite direction from previous stages. Heat flow values reduce once the JMMC moves away from the spreading centres. Present-day heat flow values in the NJMMC reach a maximum of ~92 mW/m² in the north-western corner and decreases towards the south-eastern corner. The maximum value in the SJMMC is found in the south-western corner and is lower (~73 mW/m²) than the maximum in the NJMMC. Values decrease to background values towards the north-eastern corner.
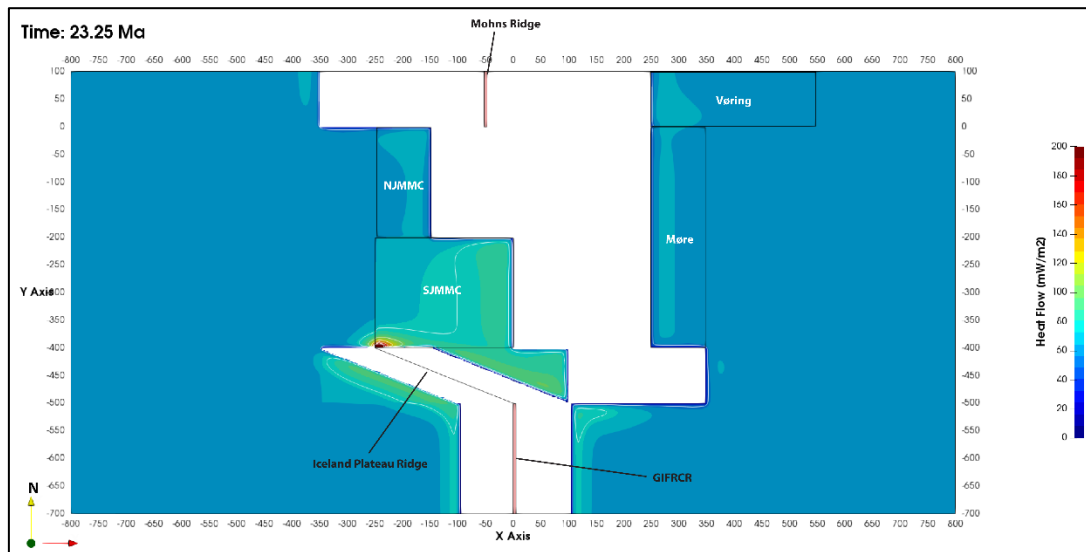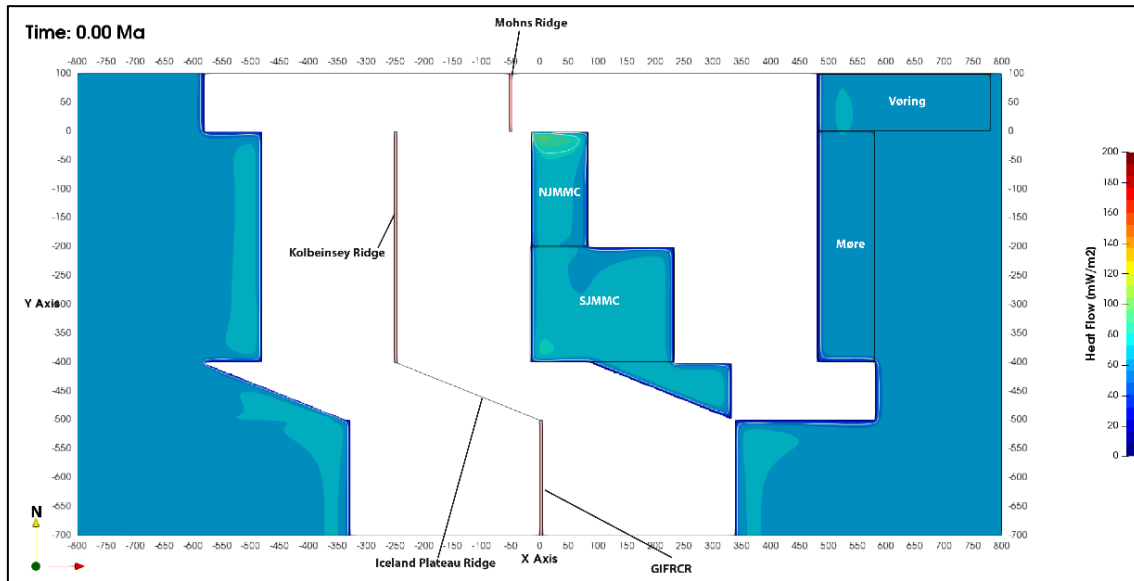
Figure 63. *Heat flow within the JMMC and the relative positions of the MR, KR, IPR and GIFRCR at the end of Stage 3 at the present. Contour values are between 50 and 200 mW/m² in steps of 25 mW/m².*

Note that since the reference column has a bottom temperature of 1333 °C the entire continental lithosphere is uplifted because of variation in the bottom temperature. The amount of background uplift experienced at the end of Stage 3 is ~175 m. The entire western edge of the JMMC experiences (relative) uplift as it is heated by the KR (Figure 64). The northern edge of NJMMC experiences additional uplift due to the MR. The amount of uplift reduces as the JMMC moves away from the ridges and cools. The present-day uplift predicted by the model in the NJMMC is ~1300 m at the north-western edge and reduces down to ~350 m at the south-eastern edge. The present-day subsidence in the SJMMC is lowest at the south-western edge (~2500 m) and highest in the northern part (~3250 m). Note that the model does not take into account basin infill and erosion. Therefore, the prediction of uplift or subsidence should be realized as general tilt directions for the JMMC and not taken as absolute values.
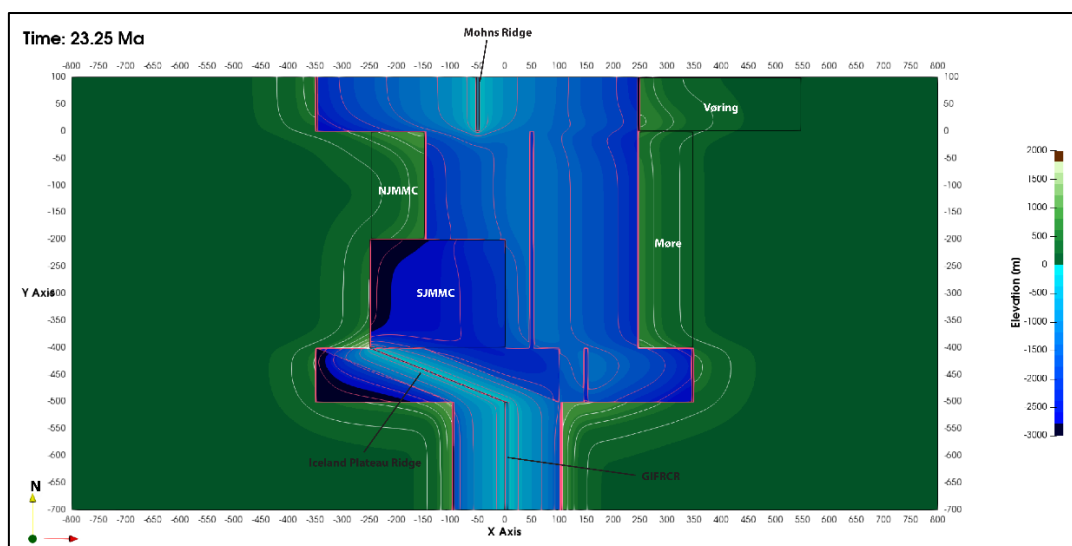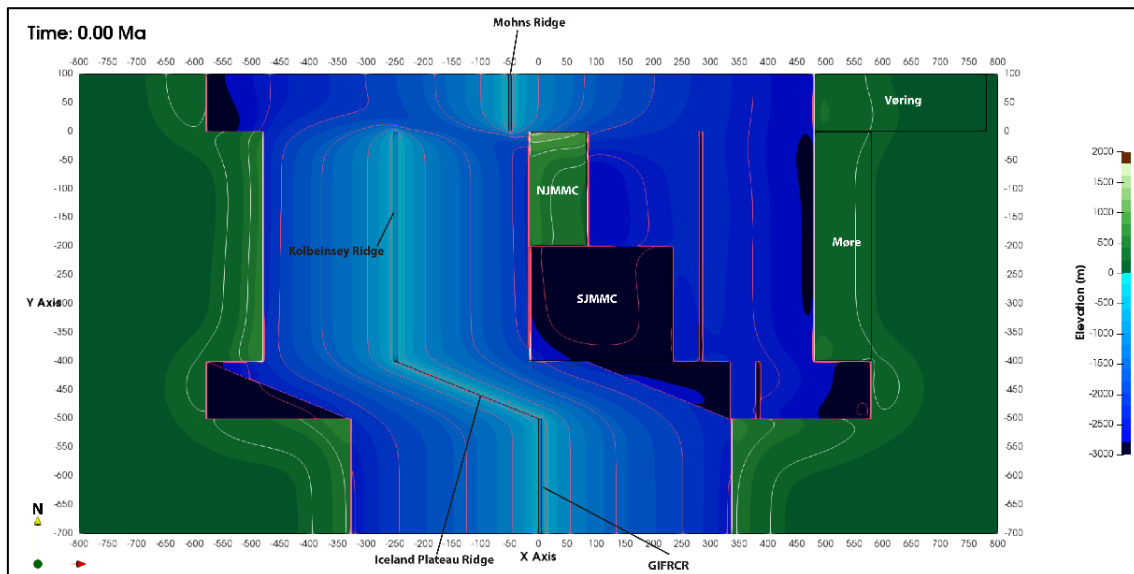
Figure 64. *Uplift within the JMMC and the relative positions of the MR, KR, IPR and GIFRCR at the end of Stage 2 at the present. Contour values for uplift are between 200 and 1600 m in steps of 200 m with an additional contour at 50 m. Contour values for subsidence are between -500 and -3000 m with a contour interval of -500 m.*

6 Discussion

The first model presented in this report is used as proof of concept and ignores the geometrical and structural complexity of the Jan Mayen microcontinent and the adjacent spreading centres, with no rifting of the SJMMC and symmetric spreading centres aligned along an N-S direction. Therefore, although it provides a useful starting point to understand the overall system, it cannot be directly compared with the other more complex models.

The second model is presented as the reference model, which builds upon the first model while capturing the asymmetrical spreading of the Ægir Ridge and simultaneous rifting of the SJMMC. Additionally, the IPR spreading centre diagonally splits the Icelandic Plateau south of the SJMMC.

The third and fourth models explore the thermal effects of reduced rifting of the SJMMC and increased mantle potential temperature as a result of an impinging plume on the JMMC, respectively.

6.1 Uplift and subsidence

Uplift and subsidence in the models is calculated based on the principle of local isostasy, i.e. how much heavier or lighter the lithosphere column is relative to a reference column. A lighter column is buoyant and results in uplift while a heavier column will sink and result in subsidence. Any extra increase in temperature relative to the reference configuration will result in a reduction of density and, therefore cause uplift. On the other hand, rifting of the

SJMMC results in relatively heavy mantle taking up most of the column and will result in overall subsidence in spite of the increased temperature relative to the reference configuration.

The absolute present-day values for uplift or subsidence obtained from the last three models cannot be directly compared to each other since the reference configuration is not the same (second vs. fourth models) or different final configurations for the SJMMC is implemented (second vs. third models). However, the relative uplift obtained from the various models can be correlated.

The NJMMC has experienced maximum modelled uplift at the north-western corner with values decreasing towards the southeast. The maximum and minimum values of uplift in the NJMMC are slightly different for the different models but the variation between them for any of the models is similar (~1000 m). Similarly, the SJMMC in the different models shows the same trend in subsidence values with the minimum value recorded at the south-western edge and the maximum value towards the centre of the northern part. The difference in these values is again similar (~800 m). This suggests that the internal variation of topography may be largely controlled by thermal input from the ridges. However, in order to accurately determine the extent of uplift/subsidence in the region, a basin model that accounts for sedimentation in conjunction with rifting is required.

6.2 Heat flow

Although the different models include different processes that affect the thermal input into the JMMC, the present-day heat flow pattern in the JMMC does not differ significantly between them. The highest values (~90 mW/m^2) are modelled in the north-western part of the NJMMC due to relatively recent passage of the MR, while the maximum heat flow values in the SJMMC are lower (~70 mW/m^2), as modelled in the south-western region. The maximum present-day heat flow values obtained from the second and third model are identical while the fourth model shows slightly elevated values (couple of mW/m^2), albeit not significantly.

The most obvious difference between the models is observed in the heat flow pattern in the SJMMC. The values decrease from the south-western edge (~71 mW/m^2) towards the north-eastern region (~60 mW/m^2) in the reference model while the model with reduced rifting predicts slightly higher values also along the eastern edge of the SJMMC (~65 mW/m^2). The relatively, hotter model which includes mantle plume effects shows slightly increased values over almost the entire SJMMC (~65 mW/m^2) with the maximum at the south-western corner (~73 mW/m^2).

The predicted present-day decrease in heat flow values from maxima in the north-western and south-western parts of the NJMMC and SJMMC, respectively, towards the central and eastern regions are also observed in measured data from the region (Rey et al., 2003) (Figure 5). It is important to note, in relation to the increased mantle temperature model, that upwelling of the increased temperature mantle into the rift zones was not incorporated into the model due partly to the complexities of integration and associated time, and partly due to the large associated uncertainties of heat-flow with dynamic temperature profiles in simultaneously upwelling and melting mantle. The implies that model 4 represents a minimum net influence of increased mantle temperatures based on the increased mantle T_P boundary condition and highlights the potential for greater thermal influences within these rift zones, which may be incorporated in future modelling.

6.3   Thermal maturity

While the different models predict relatively similar present-day heat flow patterns, large variations are observed in the heat flow values in the SJMMC that result from the amount of rifting modelled there. These variations subside with time after rifting ceases resulting in the relatively similar present-day values. However, this variation of thermal evolution in time is captured by the thermal maturity (vitrinite reflectance) of sediments, which is a function of time and temperature.

One of the most important processes, besides direct heat input from spreading centres, which controls maturation and hydrocarbon generation, is rifting of continental lithosphere and is observed in the second and third models that undergo different amounts of crustal thinning.

The depths of the oil and gas windows in the NJMMC, which does not undergo rifting, are the same in all three models at ~1800 and 4000 m, respectively. On the other hand, reduced rifting in the SJMMC in the third model significantly increases the oil and gas window depths, from 1000 and 2000 m to 1600 and 3500 m, respectively.

Additionally, rifting is usually associated with sedimentation which further complicates the thermal input into the system due to blanketing effects (Theissen and Rüpke, 2010). This suggests that a full basin model that treats rift events and sedimentation while also honouring the present-day stratigraphy is required to accurately determine hydrocarbon generation in the JMMC.

Lastly, in volcanic margins such as the region explored here, emplacement of intrusive bodies within the sedimentary succession can locally either enhance or degrade petroleum generation (Aarnes, 2010, 2015; Iyer et al., 2018). Igneous intrusions in otherwise relatively immature sediments can jump-start maturation and hydrocarbon generation due to additional heat input. On the other hand, the presence of an igneous intrusion close to a prospect may degrade oil that may be potentially present there to gas. Besides, such intrusions may change local flow dynamics resulting in the transport and venting of generated hydrocarbons (Iyer et al., 2013; 2017). Such processes operate on much smaller temporal and spatial scales and cannot be captured by large basin- and geodynamic-scale models.

7 Conclusions

The project's main goal was to develop heat-flow, uplift, and maturity models for the Jan Mayen microcontinent (JMMC) for the time of the Northeast Atlantic breakup and the forming of the North Atlantic igneous province (NAIP), through the separation of the microcontinent area from the East Greenland margin. The models serve as a basic tool for future frontier basin maturity modelling and hydrocarbon system predictions for the JMMC, specifically the northern Dreki exploration area.

Estimated thermal uplift history during breakup (Figure 7) and rifting was reviewed in relation to evidence from reflection seismic interpretation and known onshore areas. This, in comparison to the modelled uplift events (Jones et al., 2012) during the main phases of NAIP volcanism, indicated the pulsing of the proto-Icelandic plume also effects frequency and magnitude of the regions of uplift and igneous activity. The JMMC uplift model indicates approximately a 1000 m uplift for the northern block (NJMMC) and approximately 800 m for the southern ridge block (SJMMC), which compares well with the large regional model uplift by Jones et al. (2012).

Selected rifting events were compared to the geo-chronological reconstructions, which guided the selection of the thermal model stages and segmentations to compute the best case JMMC thermal model history. A simplified version of the latest high-resolution tectonostratigraphic model of the JMMC was used as a model base for three distinct phases that were taken into considerations:

(1) *the initial breakup phase ca. 53-33.25 Ma with the Ægir ridge system;*

(2) *the rift transition phase ca. 33.25-23.25 Ma with the active Iceland plateau rifts IPR);
and*

(3) *the final breakup phase ca. 23.25-present21 Ma and the establishing of the Kolbeinsey Ridge.*

The complexity of the model geometry was gradually increased in phases to assure that the model parameter calculations and iterations function properly. The phases were separated into four models:

(1) *base orthogonal model – simple spreading scenario and geometry;*

(2) *oblique spreading of the IPR, asymmetric spreading of the Ægir ridge and rifting of the SJMMC;*

(3) *oblique spreading of the IPR, asymmetric spreading of the Ægir ridge and reduced rifting of the SJMMC (variation in crustal thickness); and*

(4) *oblique spreading of the IPR, asymmetric spreading of the Ægir ridge and rifting of the SJMMC and variable mantle potential temperature (Tp).*

The thermal evolution of the JMMC is complex and results largely from the interaction between ridge and rifting processes. Relatively similar present-day heat flow and topographical patterns are obtained from the different models as the processes affecting them are the same. These similarities are also due to the fact that the JMMC is presently removed

from active spreading centres and rift processes. However, our models show significant differences in the thermal evolution of the two JMMC blocks.

The northern and southern blocks of the JMMC have very different thermal histories as only the southern block is affected by rifting. The models predict maximum uplift and heat-flow values at the north-western corner of the northern block close to the still active Jan Mayen igneous centre with values decreasing towards the southeast along the main Jan Mayen Ridge. This pattern emerges due to exposure and movement of the Northern block with respect to the Ægir, Mohns and Kolbeinsey Ridges. The southern block, which primarily represents the Dreki area, shows a relative increase in topography and heat-flow towards the IPR from minimum values in the north-central part of the SJMMC and is influenced by the Ægir, IP and Kolbeinsey Ridges. Both suggest that for both sub-regions modelled internal variation of topography may be largely controlled by thermal input from the ridges and that it may not just be due to regional tectonic processes and changes in sea level. This had been noted by a high resolution sequence stratigraphy mapping study as well (Blischke et al., 2018).

Increased hydrocarbon maturation occurs towards the northern, western and eastern edges of the NJMMC due to the influence of the Mohns, Kolbeinsey and Ægir Ridges, respectively, with values returning to background values towards the centre of the block where the depths of the oil and gas windows are ~1800 and 4000m, respectively. A small perturbation in maturity levels with respect to background is observed in the entire NJMMC. Hydrocarbon maturity in the SJMMC is not only affected by heat input from the ridges but also by significant rifting. The thermal effects of ridge processes do not extend toward the centre of the SJMMC. However, rifting of the SJMMC moves the oil and gas windows to relatively shallower depths between 1000 and 3500m depending on the rift intensity. Consequently, the models predict that the central Jan Mayen Ridge area is least effected by igneous activity, and more likely to have hydrocarbons preserved in the southern central area of the northern block (NJMMC) just north of the Dreki area. Rifting processes in the southern block (SJMMC) would need to be more accurately modelled to determine hydrocarbon potential there.

A complete risk analysis of the prospect areas within the Dreki license areas would require further transect and intrusion models in addition to the large-scale geodynamic models presented there.

8 Future work steps necessary

The models presented here form the basis for further, more detailed basin and intrusive models (phase 3 of the original project proposal not funded by the IHCRF).

- ✓ *Detailed transect model defining the hydrocarbon maturation process for the main hydrocarbon target exploration area for the microcontinent that would include traditional basin model of prospect area transects and sill/intrusion impact models.*

The modelling process is of fundamental importance for the accurate appraisal of the JMMC maturation history, and additional funding options have to be discussed and obtained, as further modelling treats rift events and sedimentation while also honouring the present-day stratigraphy.

Thus, the actual application of the phase 2 model to the detailed transect JMMC model would better determine hydrocarbon generation in the JMMC. Additionally, since this is a volcanic margin domain, models resolving the emplacement of intrusive bodies within the sedimentary succession would further enhance our knowledge of hydrocarbon generation potential at the prospect-scale.

Such a modelling process would involve known hydrocarbon areas, such as the Jameson Land basin on the western margin of the JMMC, the Vøring shelf margin to the north, the Møre shelf margin to the east, and the Faroe-Shetland basin area to the south of the JMMC in order to facilitate comparison to their pre-breakup hydrocarbon history (Figure 1).

Specifically, the Vøring escarpment area with its 3D seismic reflection data coverage and well mapped base basalt unconformity, serves as a good analogue for the JMMC region. The availability of comprehensive maturation data, along with examples of sills and their thermal aureoles intersected by boreholes, makes the Vøring margin an ideal region for sill maturation modelling and the perfect basis for developing Phase 3 of the JMMC project. Associated research, including state of the art sill maturation modelling, has been developed by Geomodelling Solutions (Iyer et al., 2017).

Table 5. *Project continuation time table suggestion.*

Year	2018		2019	
Quarter	3	4	1	2
PHASE 3: VMAPP modelling application				
Prospect areas transects selection	X			
Build of traditional basin model		X		
Build of sill/intrusion impact models			X	
Reporting				X

Establishing a full modelling setup would also relate to additional work, addressing the western volcanic margin that has to be accounted for along the western JMMC boundary up to the area of the southern JM basin, (Blischke et al., 2016; 2018). This area is of importance as it is very close to some of the main prospect areas being investigated within the western region of the Dreki licensing area.

As can be seen above, some fundamental questions are still open but could be addressed by a detailed phase 3 continuation project (Table 5), which would include tertiary maturation modelling by incorporating the thermal impacts of smaller but extensive intrusive bodies (dykes and sills) already identified within the JMMC structures. These maturation results would be a key input in any risk analysis assessment for the Dreki area.

9 List of abbreviations

ÆR	-	Ægir MOR
CEG	-	Central East Greenland
EJMFZ	-	East Jan Mayen Fracture Zone
EVZ	-	East Iceland Volcanic Zone
GIFRC	-	Greenland–Iceland–Faroe Ridge Complex
GIR	-	Greenland–Iceland Ridge;
FI	-	Faroe Islands
IFFZ	-	Iceland–Faroe Fracture Zone
IFR	-	Iceland–Faroe Ridge
JMI	-	Jan Mayen Island Volcanic Complex
JMMC	-	Jan Mayen microcontinent
KR	-	Kolbeinsey MOR
MB	-	Møre Basin
MIB	-	Mid-Iceland Volcanic Belt
MOR	-	Mid-Oceanic Ridge
MR	-	Mohn's MOR
NAIP	-	North Atlantic igneous province
NJMMC	-	Northern Jan Mayen microcontinent segment
NVZ	-	North Iceland Volcanic Zone
RR	-	Reykjanes MOR
RVB	-	Reykjanes Volcanic Belt
SDR	-	Seaward dipping reflectors
SISZ	-	South Iceland Seismic Zone
SJMMC	-	Southern Jan Mayen microcontinent segment
SRC	-	Jan Mayen Southern Ridge Complex
SVB	-	Snæfellsnes Volcanic Belt
TFZ	-	Tjörnes Fracture Zone
VB	-	Vøring Basin
VR	-	Vitrinite reflection
WJMFZ	-	West Jan Mayen Fracture Zone
WVZ	-	West Iceland Volcanic Zone
ÖVB	-	Öræfajökull Volcanic Belt

10 References

Aarnes, I. (2010). *Sill emplacement and contact metamorphism in sedimentary basins. Local processes with global implications*. [Ph.D.]: University of Oslo, 181 p.

Aarnes, I., Planke, S., Trulsvik, M. and Svensen, H. (2015). Contact metamorphism and thermogenic gas generation in the Vøring and Møre basins, offshore Norway, during the Paleocene–Eocene thermal maximum. *Journal of the Geological Society*, *172 (5)*, 588, doi:10.1144/jgs2014-098.

Bjarnason, I.T. & Schmeling H. (2009). The lithosphere and asthenosphere of the Iceland hotspot from surface waves. *Geophysical Journal International, Volume 178, Issue 1*, 1 July 2009, Pages 394–418, https://doi.org/10.1111/j.1365-246X.2009.04155.x.

Blischke, A. & Erlendsson, Ö. (2014). *CRUSMID-3D – NORDMIN. Status report 2014*. Iceland GeoSurvey, ÍSOR-2014/056. 33 p.

Blischke, A., Arnarson, T.S. & Gunnarsson, K. (2011). The structural history of the Jan Mayen Micro-Continent (JMMC) and its role during the rift jump between the Aegir to the Kolbeinsey Ridge, paper presented at *The Polar Petroleum Potential Conference and Exhibition, American Association of Petroleum Geologists, Halifax, Nova Scotia, Canada, August 30– September 2, 2011.*

Blischke, A., Gaina, C., Hopper, J.R., Péron-Pinvidic, G., Brandsdóttir, B., Guarnieri, P., Erlendsson, Ö. and K. Gunnarsson (2016). The Jan Mayen microcontinent: an update of its architecture, structural development and role during the transition from the Ægir Ridge to the mid-oceanic Kolbeinsey Ridge. *Geological Society, London, Special Publication*s, 447, first published on September 8, 2016, doi:10.1144/SP447.5.

Blischke, A., Stoker, M.S., Ólavsdóttir, J., Brandsdóttir, B., Peron-Pinvidic, G. & Japsen, P. (2018). *The Cenozoic stratigraphy of the Jan Mayen Micro-Continent from breakup to present time.* EGU2018-10483 - EGU General Assembly 2018, Vienna.

Brandsdóttir, B., Hooft, E., Mjelde, R. & Murai, Y. (2015). Origin and evolution of the Kolbeinsey Ridge and Iceland Plateau, N-Atlantic. *Geochemistry, Geophysics, Geosystems 16*, 612–634.

Doré, A.G., Lundin, E.R., Jensen, L.N., Birkeland, Ø., Eliassen, P.E. & Fichler, C. (1999). Principal tectonic events in the evolution of the northwest European Atlantic margin. In: Fleet, A.J., & Boldy, S.A. R (eds.) *Petroleum Geology of Northwest Europe: Proceedings of the 5th Conference.* The Geological Society, London, 41–61.

Einarsson, P. (2008). Plate boundaries, rifts and transforms in Iceland. *Jökull, 58*, 35–58.

Foulger, G.R. and Anderson, D.L. (2005). A cool model for the Iceland hotspot. *Journal of Volcanology and Geothermal Research, 141(1)*, 1–22.

Funck, T., Hopper, J.R., Faittah, R.A., Blischke, A., Ebbing, J., Erlendsson, Ö., Gaina, C., et al. (2014). Chapter 6: Crustal Structure. IN: Hopper, J. R., Funck, T., Stoker, T., Arting, U., Peron-Pinvidic, G., Doornebal, H., and C. Gaina, (eds.) *Tectonostratigraphic Atlas of the North-East Atlantic region*, 340 pp., GEUS, Copenhagen, Denmark, ISBN 978-87-7871-378-0.

Gadd, S. & Scrutton, R. (1997). An integrated thermomechanical model for transform continental margin evolution. *Geo-Marine Letters, February 1997, Volume 17, Issue 1*, 21–30.

Gaina, C., Gernigon, L. & Ball, P. (2009). Palaeocene-Recent plate boundaries in the NE Atlantic and the formation of the Jan Mayen microcontinent. *Journal of the Geological Society, London, 166(4)*, 601–616, doi: 10.1144/0016-76492008-112.

Gaina, G., Nasuti, A., Kimbell, G.S. and Blischke, A. (2017). *Break-up and seafloor spreading domains in the NE Atlantic.* Geological Society, London, Special Publications, 447, first published on February 3, 2017, doi:10.1144/SP447.12.

Geissler, W.H., Gaina, C., Hopper, J.R., Funck, T., Blischke, A., Arting, U., Horni, J.Á., Péron-Pinvidic, G. and Abdelmalak, M.M. (2016). Seismic volcanostratigraphy of the NE Greenland continental margin. *Geological Society, London, Special Publications, 447*, first published on December 14, 2016, doi:10.1144/SP447.11.

Gernigon, L., Blischke, A., Nasuti, A. & Sand, M. (2015). Conjugate volcanic rifted margins, seafloor spreading, and microcontinent: insights from new high-resolution aeromagnetic surveys in the Norway Basin. *Tectonics, 34*, 907–933.

Gernigon, L., Gaina, C., Olesen, O., Ball, P., Peron-Pinvidic, G. & Yamasaki, T. (2012). The Norway Basin revisited: from continental breakup to spreading ridge extinction. *Marine and Petroleum Geology, 35*, 1–19.

Gunnarsson, K., Sand, M. & Gudlaugsson, S.T. (1989). *Geology and Hydrocarbon Potential of the Jan Mayen Ridge.* Orkustofnun, OS-98014, report, 143 pp., 5 appendices incl. 9 maps Reykjavík and Norwegian Petroleum Directorate, Stavanger, OD-89-91, 156 pp.

Harðarson, B., Fitton, J. & Hjartarson, Á. (2008). Tertiary volcanism in Iceland. *Jökull, Vol. 58*, 161–178.

Hartley, R.A., Roberts, G.G., White, N. and Richardson, C. (2011). Transient convective uplift of an ancient buried landscape. *Nature Geoscience, 4(8)*, 562–565, doi: 10.1038/ngeo1191.

Herzberg, C. & Asimow, P. D. (2015). PRIMELT3 MEGA.XLSM software for primary magma calculation: Peridotite primary magma MgO contents from the liquidus to the solidus. *Geochemistry, Geophysics, Geosystems 16*, 563–578.

Herzberg, C. & Gazel, E. (2009). Petrological evidence for secular cooling in mantle plumes. *Nature 458*, 619–623.

Hjartarson, Á., Erlendsson, Ö. & Blischke, A. (2017). The Greenland–Iceland–Faroe Ridge Complex. *Geological Society, London, Special Publications, 447*, first published on February 3, 2017, doi:10.1144/SP447.14.

Hole, M.J. and Millett, J.M. (2016). Controls of mantle potential temperature and lithospheric thickness on magmatism in the North Atlantic Igneous Province. *Journal of Petrology, 57 (2)*, 417-436, dx.doi.org/10.1093/petrology/egw014.

Hole, M. J., Millett, J. M., Rogers, N. W. & Jolley, D. W. (2015). Rifting and mafic magmatism in the Hebridean basins. *Journal of the Geological Society, London 172*, 218–236.

Holbrook, W.S. and Kelemen, P.B. (1993). Large igneous province on the US Atlantic margin and implications for magmatism during continental breakup. *Nature 364*, 433–436 (29 July 1993), doi:10.1038/364433a0.

Holbrook, W.S., Larsen, H.C., Korenaga, J., Dahl-Jensen, T., Reid, I.D., Kelemen, P.B., Hopper, J.R., Kent, G.M., Lizzarralde, D., Berstein, S. and Detrick, R.S. (2001). Mantle structure and active upwelling during continental breakup in the North Atlantic. *Earth and Planetary Science Letters 190*, 251–266.

Hopper, J.R., Funck, T., Stocker, M., Árting, U., Peron-Pinvidic, G., Doornenbal, H. and Gaina, C. (2014). *NAGTEC Atlas: Tectonostratigraphic Atlas of the North-East Atlantic Region*, Geological Survey of Denmark and Greenland, Copenhagen, Denmark.

á Horni, J., Hopper, J.R., Blischke, A., Geissler, W., Judge, M., McDermott, K., Erlendsson, Ö., Stewart, M. & Árting, U. (2017). Regional Distribution of Volcanism within the North Atlantic Igneous Province. *Geological Society, London, Special Publications, 447*, 18, http://dx.doi.org/10.1144/SP447.18.

Iyer, K., Rüpke, L., and Galerne, C. Y. (2013). Modeling fluid flow in sedimentary basins with sill intrusions: Implications for hydrothermal venting and climate change: *Geochemistry, Geophysics, Geosystems, v. 14, no. 12*, 5244–5262.

Iyer, K., Schmid, D.W., Planke, S., and Millett, J. (2017). Modelling hydrothermal venting in volcanic sedimentary basins: Impact on hydrocarbon maturation and paleoclimate. *Earth and Planetary Science Letters 467* (2017) 30–42, http://dx.doi.org/10.1016/j.epsl.2017.03.023.

Iyer, K., Svensen, H., and Schmid, D. W. (2018). SILLi 1.0: a 1-D numerical tool quantifying the thermal effects of sill intrusions: *Geosci. Model Dev., v. 11, no. 1*, 43–60.

Japsen, P., Green, P.F., Bonow, J.M., Nielsen, T.F.D. and Chalmers, J.A. (2014). From volcanic plains to glaciated peaks: Burial, uplift and exhumation history of southern East Greenland after opening of the NE Atlantic. *Global and Planetary Change 116* (2014) 91–114.

Johansen, J.M. (1992). *Modellering av det magnetiske anomalifeltet over Jan Mayen Ryggen.* Cand. scient. thesis, University of Oslo, 139 p.

Jones, A.G., Fullea, J., Evans, R.L. & Muller, M.R. (2012). Water in cratonic lithosphere: Calibrating laboratory-determined models of electrical conductivity of mantle minerals using geophysical and petrological observations, *Geochem. Geophys. Geosyst., 13*, Q06010, doi:10.1029/2012GC004055.

Larsen, L.M., Pedersen A.K., Søorensen E.V., Watt W.S. and Duncan R.A. (2013). Stratigraphy and age of the Eocene Igtertiva Formation basalts, alkaline pebbles and sediments of the Kap Dalton Group in the graben at Kap Dalton, East Greenland. *Bulletin of the Geological Society of Denmark 61*, 1–18.

Larsen, L.M., Pedersen, A.K., Tegner, T. and Duncan, R.A. (2014). *Eocene to Miocene igneous activity in NE Greenland: northward younging of magmatism along the East Greenland margin.* Lithos, in press., doi: 10.1144/jgs2013-118.

Lawver, L. & Müller, D. (1994). Iceland hotspot track. *Geology 22.* 311–314. 10.1130/0091-7613(1994).

Lundin, E., & Doré, A.G. (2002). Mid-Cenozoic post-breakup deformation in the 'passive' margins bordering the Norwegian–Greenland Sea. *Marine and petroleum geology, 19(1)*, 79–93. doi: 10.1016/s0264-8172(01)00046-0.

Millett, J.M. (2014*). Geochemical stratigraphy and correlation within the Faroe Islands Basalt Group with developments in the analysis of Large Igneous Province deposits from well data.* Unpublished PhD thesis, University of Aberdeen.

Millett, J.M., Hole, M.J., Jolley, D.W., Schofield, N. and Campbell, E. (2015). Frontier exploration and the North Atlantic Igneous Province: new insights from a 2.6 km offshore volcanic sequence in the NE Faroe–Shetland Basin. *Journal of the Geological Society, 173(2),* 320–336.

Morgan, W.J. (1971). Convection Plumes in the Lower Mantle. *Nature volume 230*, 42–43 (05 March 1971), doi:10.1038/230042a0.

Nadin, P.A., Kusznir, N.J., and Cheadle, M.J. (1997). Early Tertiary plume uplift of the North Sea and Faeroe-Shetland Basins. *Earth and Planetary Science Letters, 148*, 109–127.

Parnell-Turner, R., White, N., Henstock, T., Murton, B., Maclennan, J. and Jones, S.M. (2014). A continuous 55-million-year record of transient mantle plume activity beneath Iceland. *Nature Geoscience, 7(12)*, 914–919.

Passey, S. R. & Jolley, D. W. (2009). A revised lithostratigraphic nomenclature for the Palaeogene Faroe Islands Basalt Group, NE Atlantic Ocean. *Earth and Environmental Science Transactions of the Royal Society of Edinburgh 99*, 127–158.

Peron-Pinvidic, G., Gernigon, L., Gaina, C. & Ball, P. (2012a). Insights from the Jan Mayen system in the Norwegian-Greenland Sea - I: mapping of a microcontinent. *Geophysical Journal International, 191*, 385–412.

Peron-Pinvidic, G., Gernigon, L., Gaina, C. & Ball, P. (2012b). Insights from the Jan Mayen system in the Norwegian-Greenland Sea - II: architecture of a microcontinent. *Geophysical Journal International, 191*, 413–435.

Putirka, K. D. (2009). A Consensus on Mantle Potential Temperatures? *American Geophysical Union, Fall Meeting 2009*, abstract id. V21F-01.

Rey, S., Eldholm, O., and Planke, S. (2003). Formation of the Jan Mayen microcontinent, the Norwegian Sea, in *Proceedings AGU Fall Meeting Abstracts 2003.*

Rickers, F., Fichtner, A. & Trampert, J. (2013). The Iceland–Jan Mayen plume system and its impact on mantle dynamics in the North Atlantic region: Evidence from full-waveform inversion. *Earth and Planetary Science Letters, Volume 367*, 39–51, ISSN 0012-821X, https://doi.org/10.1016/j.epsl.2013.02.022.

Rudge, J.F., Champion, M.E.S., White, N., McKenzie, D. and Lovell, B. (2008). A plume model of transient diachronous uplift at the Earth's surface. *Earth and Planetary Science Letters, 267(1–2)*, 146–160, doi: 10.1016/j.epsi.2007.11.040.

Saunders, A.D., Fitton, J.G., Kerr, A.C., Norry, M.J. & Kent, R.W. (1997). The North Atlantic Igneous Province. In: Mahoney, J.J. & Coffin, M.F. (eds.) Large Igneous Provinces. *American Geophysical Union, Geophysical Monographs, 100, 45–94.*

Saunders, A.D., Jones, S.M., Morgan, L.A., Pierce, K.L., Widdowson, M. and Xu, Y.G. (2007). Regional uplift associated with continental large igneous provinces: The roles of mantle plumes and the lithosphere. *Chemical Geology 241*, 282–318.

Schmid, D.W., Iyer, K., Dabrowski, M. and Hartz, E.H. (2017). Thermal Effects at Continent-Ocean Transform Margins: A 3D Perspective, Geochemistry, Geophysics, Geosystems.

Scott, R.A., Ramsey, L.A., Jones, S.M., Sinclair, S. & Pickles, C.S. (2005), Development of the Jan Mayen microcontinent by linked propagation and retreat of spreading ridges. In: Onshore-Offshore Relationships on the North Atlantic Margin, in Norwegian Petroleum Society Conference, edited by B. T. G. W. e. al., 69–82, *Norwegian Petroleum Society Special Publications*, doi: 10.1016/S0928-8937(05)80044-X.

Sundvor, E., Eldholm, O., Gladczenko, T.P. & Planke S. (2000). Norwegian-Greenland Sea thermal field. *Journal of the Geological Society (167)*, 397–410.

Svellingen, W. & Pedersen, R. (2003). Jan Mayen: A result of ridge-transform-micro-continent interaction. *Geophysical Research Abstracts, 5*, 12993.

Talwani, M. & Eldholm, O. (1977). Evolution of the Norwegian-Greenland Sea. *Geological Society of America Bulletin, 88*, 969–999.

Theissen, S. & Rüpke, L. (2010). Feedbacks of sedimentation on crustal heat flow: New insights from the Vøring basin, Norwegian Sea: *Basin Research, v. 22, no. 6*, 976–990.

Tissot, B.P. & Welte, D.H. (1984). Petroleum Formation and Occurrence, 2 ed.: New York, Springer-Verlag, 699 p.

Torsvik T.H., Amundsen, H.E.F, Trønnes, R.G., Doubrovine, P.V., Gaina, C., Kusznir N.J., Steinberger, B., Corfu, F., Ashwal, L.D., Griffin, W.L., Werner, S.C. and Jamtveit, B. (2015). Continental crust beneath southeast Iceland. *Proceedings of the National Academy of Sciences 112, E1818-E1827*.

Torsvik, T. H., Mosar, J. and Eide, E.A. (2001). Cretaceous-Tertiary geodynamics: a North Atlantic exercise. *Geophysical Journal International, 146(3)*, 850–866.

Vogt, P.R., Anderson, C.N., Bracey, D.R. and Schneider, E.M. (1970). North Atlantic Magnetic Smooth Zones. *Journal of Geophysical Research, 75*, 3955–3968.

White, R. S. (1997). Rift-plume interaction in the North Atlantic. *Philosophical Transactions of the Royal Society of London, Series A, 355(1723)*, 319–339.

Appendix 1: Original project proposal, including the phase 3 hydrocarbon maturation modelling estimate of the JMMC.

Appendix 2: Geomodelling Solutions – final model runs <u>(includes model run video files imbedded in pptx-file</u>)